

**Polysiloxanes with Luminescent Molecular Probes:
Synthesis, Characterization and Application of Ordered and
Non-Ordered Structures**



**Polysiloxane mit molekularen Lumineszenz-Sonden:
Synthese, Charakterisierung und Anwendung von
geordneten und ungeordneten Strukturen**

DISSERTATION

der Fakultät für Chemie und Pharmazie
der Eberhard-Karls-Universität Tübingen

zur Erlangung des Grades eines Doktors
der Naturwissenschaften

2001

vorgelegt von

Elisabeth Holder

Tag der mündlichen Prüfung:

03. Dezember 2001

Dekan:

Prof. Dr. H. Probst

1. Berichterstatter:

Prof. Dr. E. Lindner

2. Berichterstatter:

Prof. Dr. Dr. h. c. J. Strähle

Meiner Familie

Die vorliegende Arbeit wurde am
Institut für Anorganische Chemie II der
Eberhard–Karls–Universität Tübingen
unter der Leitung von
Herrn Professor Dr. rer. nat. Ekkehard Lindner
angefertigt.

Meinem Doktorvater,
Herrn Prof. Dr. Ekkehard Lindner,
danke ich herzlich für die Themenstellung,
für die Bereitstellung ausgezeichneter Arbeitsbedingungen,
für wertvolle Anregungen und Diskussionen
sowie sein stetes Interesse an dieser Arbeit.

Mein besonderer Dank gilt:

Herrn Prof. Dr. D. Oelkrug für die in allen Bereichen freundschaftliche Zusammenarbeit und Unterstützung, sowie vielen hilfreichen Anregungen und Diskussionen. Herrn Dr. H.–J. Egelhaaf für viele Diskussionen und die erfolgreiche und gute Zusammenarbeit. Den Herren Dr. Larry Lürer und Dipl.–Chem. Jens Christian Weber für unzählige Hilfestellungen, allen anderen Oelis für viele Schlüsseldienste.

Herrn Prof. Dr. Hermann A. Mayer für viele hilfreiche Diskussionen in NMR– und chemischen Fragen, sowie für die Unterstützung und seinem Beitrag zum Gelingen dieser Arbeit.

Herrn Prof. Dr. K. Albert, Dr. Stefan Bachmann und Renata Rabelo–Schaefer für die erfolgreiche und gute Zusammenarbeit sowie die Unterstützung.

Herrn Prof. Dr. V. Schurig, Frau Dr. Gabriele Trapp (geb. Schötz) und Herrn Dr. Oliver Trapp für Ideen, Anregungen, Diskussionen und die erfolgreiche und gute Zusammenarbeit sowie die Unterstützung.

Herrn Prof. Dr. J. R. Lakowicz and Petr Herman für den Zugang am Center of Fluorescence in Baltimore, sowie Mary Rosenfeld für Unterstützung und unzählige Hilfestellungen.

Prof. Dr. P. C. Schmidt und A. Brenn für die BET Messungen und Unterstützung in BET Fragen.

Herrn Dr. M. Kaspar für QCM-Messungen, Frau Elke Nadler für die Aufnahme unzähliger SEM's.

Meinem ehemaligen Kollegen Dr. Markus Schmid für die problemlose Vermittlung von XRD Messungen bei der BASF AG Ludwigshafen.

Meinen Kollegen Dr. Stefan Brugger und Dr. Ulf Kehrer sowie Frau Heike Dorn und Frau Angelika Ehmman für die Vermessung vieler schwieriger Festkörper und Hochauflösungs-NMR-Proben.

Dem "Koordinator" Dr. Klaus Eichele möchte ich für seine freundschaftliche Diskussionsbereitschaft und seine vielen Hilfestellungen bezüglich aller GK-Interphasen Fragen danken.

Frau Roswitha Conrad, Frau Barbara Saller, Frau Elwine Oster, Herrn Wolfgang Bock, Herrn Peter Wegener, Herrn Dr. Hans-Dieter Ebert, sowie allen technischen und wissenschaftlichen Angestellten, die zum Gelingen dieser Arbeit beigetragen haben.

Allen Kollegen aus dem GK-Interphasen für Hilfestellungen und Diskussionen und die gute Zusammenarbeit.

Den Herren Mitassistenten Dipl.-Chem. Michael Walker und Dr. Wolfgang Wischert, für die sehr schöne Zusammenarbeit während den E-Kursrunden, sowie allen anderen Assistenten des Anorganik-Praktikums für die gute Zusammenarbeit.

Meinen Kollegen im Labor 8M05 Frau Dr. Monika Förster, den Herren Dipl.-Chem. Thomas Salesch, Dr. Joachim Wald, Dr. Robert Veigel, sowie M. Sc. Samer Al-Gharabli und Dr. Zhong-Lin Lu für viele unvergessliche und lustige Momente, die hilfreiche Unterstützung in chemischen Fragen und die vielen, wenn auch nicht immer freiwilligen Diskussionen und das geduldige Ertragen meiner noch ausreifungsbedürftigen Gesangeskünste. Ich übe weiter!

Herrn Dr. Stefan Brugger, den ehemaligen Kollegen Dr. Markus Mohr, Dr. Wolfram Wielandt, Dr. Robert Veigel, Dr. Joachim Wald und Dr. Markus Schmid für viele Diskussionen, Hilfestellungen und Anregungen in allen chemischen Fragen, die maßgeblich zum Gelingen dieser Arbeit beigetragen haben.

Den Computerfachherrs Dr. Frank Höhn und Dipl.–Chem. Michael Henes für ihr stets offenes Ohr und prompte Hilfe.

Allen Kollegen des Anorganischen Institutes für Kollegialität und das gute Arbeitsklima und den vielen unvergesslichen Momenten im Computer– und Kaffeeraum.

Herrn Dr. Marcus Bauser und allen Mitarbeiter/innen seines Teams für die schöne und lustige Zeit bei der Bayer AG, Pharma Research in Wuppertal–Elberfeld.

Meiner Familie und allen meinen Freunden gebührt besonderer Dank, da sie mich während der gesamten "Entstehungszeit" dieser Arbeit besonders unterstützt, er– und getragen haben und so besonders zum Gelingen beigetragen haben.

1.INTRODUCTION	1
2.GENERAL SECTION	7
2.1 Synthesis, Characterization, and Fluorescence Spectroscopic Mobility	
Studies of Fluorene Labeled Inorganic–Organic Hybrid Polymers	7
2.1.1 Introduction	7
2.1.2 Results	12
2.1.2.1 Synthesis of the T–Silyl Functionalized Fluorene 3	12
2.1.2.2 Synthesis of the Polymeric Fluorenes	13
2.1.2.3 Fluorescence Spectroscopic Investigations	15
2.1.2.3.1 Fluorescence and Fluorescence Excitation Spectra of 3	15
2.1.2.3.2 Fluorescence Decay Curves of 3	17
2.1.2.3.3 Steady State Measurements of Fluorescence Anisotropy	19
2.1.2.3.4 Time Resolved Measurements of Fluorescence Anisotropy	22
2.1.2.3.5 Investigation of the Translational Mobility by Exciplex Formation Between Triethylamine and Fluorene in 7	25
2.1.3 Discussion	29
2.1.3.1 Rotational Mobility of Fluorene and 7	29
2.1.3.2 Translational Mobility of 7 and TEA	32
2.1.4 Conclusion	33
2.2 Synthesis and Enantiomer Separation of a Modified Tris(2,2′–bipyridine)ruthenium(II) Complex	36
2.2.1 Introduction	36
2.2.2 Results and Discussion	38

2.2.2.1	Synthesis of the Modified Tris(2,2'-bipyridine)ruthenium(II) Complex 11	38
2.2.2.2	Electrokinetic Chromatography of Complex 11	40
2.2.3	Conclusion	42
2.3	Synthesis, Characterization, and Luminescence Spectroscopic Accessibility Studies of Tris(2,2'-bipyridine)ruthenium(II)-Labeled Inorganic-Organic Hybrid Polymers	43
2.3.1	Introduction	43
2.3.2	Results	52
2.3.2.1	Synthesis of the T-Silyl Functionalized Tris(2,2'-bipyridine)ruthenium(II) Complex 12	52
2.3.2.2	Synthesis of the Polymeric Tris(2,2'-bipyridine)- ruthenium(II) Complexes 18-22	52
2.3.2.3	Scanning Electron Micrographs	55
2.3.2.4	Luminescence Spectroscopic Investigations	56
2.3.2.4.1	Luminescence and Luminescence Excitation Spectra of 11	56
2.3.2.4.2	Kinetic Analysis of Luminescence Decay Curves	60
2.3.2.4.3	Luminescence Decay Curves of 11 and 18-22 without Quencher	63
2.3.2.4.4	Luminescence Decay Curves of 11 and 18-22 in the Presence of Oxygen	64
2.3.2.4.5	Luminescence Decay Curves of 11 and 18-22 in the Presence of Anthracene as Quenching Substrate	70
2.3.3	Conclusion	75

2.4	Novel Mesoporous Stationary Phases Incorporating Anthracene as Interaction Centers and their Application in HPLC	77
2.4.1	Introduction	77
2.4.2	Results	78
2.4.3	Conclusion	85
2.5	Sol–Gel Process on Surfaces for the Application as Chemical Sensors in Liquid Phase	86
2.5.1	Sol–Gel Layers on Sensors for Liquid Phase	86
2.5.2	Preparation of Sol–Gel Layers on Gold and Silicon Surfaces	88
2.5.2.1	Sol–Gel Layers on Gold Surfaces	88
2.5.2.2	Sol–Gel Layers on Silicon Surfaces	89
2.5.3	Characterization of the Sol–Gel Polymer Modified Surfaces	90
	3.EXPERIMENTAL SECTION	99
3.1	Fluorescence Measurements	99
3.2	Electrokinetic Chromatography	103
3.3	Luminescence Measurements	104
3.4	Syntheses	106
3.5	Preparation of the Compounds	108
3.5.1	6–(9H–Fluorenyl)hexyltrimethoxysilane 3	108
3.5.2	Sol–Gel Processing of 3 with Different Co–condensation Agents – General Procedure	109
3.5.2.1	Preparation of the Polysiloxane 7	110

3.5.2.2	Preparation of the Polysiloxane 8	111
3.5.2.3	Preparation of the Polysiloxane 9	111
3.5.2.4	Preparation of the Polysiloxane 10	112
3.5.3	5-(4-Hydroxybutyl)-5'-methyl-2,2'-bipyridine (11a)	112
3.5.4	<i>cis</i> -(bpy) ₂ RuCl ₂ · 2 H ₂ O (11b)	114
3.5.5	Spaced Ruthenium(II) Complex 11	115
3.5.6	Preparation of Complex 12	116
3.5.7	Sol-Gel Processing of 12 with Different Co-condensation Agents – General Procedure	117
3.5.7.1	Preparation of the Polysiloxane 18	118
3.5.7.2	Preparation of the Polysiloxane 19	119
3.5.7.3	Preparation of the Polysiloxane 20	119
3.5.7.4	Preparation of the Polysiloxane 21	120
3.5.7.5	Preparation of the Polysiloxane 22	120
3.5.8	N-2-anthracenyl-N'-[3-(triethoxysilyl)propyl]urea 23	121
3.5.8.1	Modified Silica Gel 24	122
3.5.9	Sol-Gel Processing of 23 with Different Concentrations of Co-condensation Agent – General Procedure	122
3.5.9.1	Mesoporous Polysiloxane 25	123
3.5.9.2	Mesoporous Polysiloxane 26	123
4.	REFERENCES	125
5.	SUMMARY	138

Abbreviations and Definitions

A	Amplitude
Å	Ångström (10^{-10}m)
AFM	Atomic Force Microscope
BaP	Benzo[<i>a</i>]pyrene
BET	Brunauer–Emmett–Teller (Determination of Surfaces by Adsorption of Nitrogen)
bge	Background Electrolyte
BJH	Barrett–Joyner–Halenda
c	Concentration
CDCl_3	Chloroform
CE	Capillary Electrophoresis
CEC	Capillary Electro Chromatography
CMPA	Chiral Mobile Phase Additive
COSY	Correlation Spectroscopy
CP	Cross–Polarization
CSP	Chiral Stationary Phases
Cy	Cyclohexane
D	D Type Silicon Atom (Two Oxygen Neighbors)
<i>D</i>	Diffusion Constant

DCM	Dichloromethane
2D	Two-Dimensional
DNA	Desoxyribonucleinacid
EA	Elemental analyses
EI	Electron Ionisation (Mass Spectroscopy)
EKC	Electrokinetic Chromatography
Et ₂ O	Diethyl Ether
EtOH	Ethanol
FAB	Fast Atom Bombardment (Mass Spectroscopy)
FD	Field Desorption (Mass Spectroscopy)
Fn	Functionality
G	Grams
GC	Gas Chromatography
h	Hour
HMQC	Heteronuclear Multiple Quantum Coherence
H ₂ O	Water
HPLC	High Pressure Liquid Chromatography
Hz	Hertz
I	Intensity
i	Number of Si–O–Si Bonds in D Silyl Species (i=0–2)
IR	Infrared

K	Kelvin
k	Rate Constant
k_q	Rate Constant of Quenching Process
kHz	Kilohertz
kV	Kilovolt
M	Molarity
MAS	Magic–Angle Spinning
MeOH	Methanol
MEKC	Micellar Electrokinetic Chromatography
MHz	Megahertz
min	Minute
ml	Milliliter
MLCT	Metal Ligand Charge Transfer
mmol	Millimol
mM	Millimol
MS	Mass Spectroscopy
ms	Millisecond
m	Number of Si–O–Si Bonds in T Silyl Species (m=0–3)
N	Mean Plate Number
\bar{N}	Average Mean Plate Number
NMR	Nuclear Magnetic Resonance Spectroscopy

nm	Nanometer
ns	Nanosecond
O ₂	Dioxygen
OTCE	Open Tubular Capillary Electro Chromatography
PAH	Polyaromatic Hydrocarbon
PhPh	Phenanthro[3,4-c]phenanthrene
PMMA	Polymethylmethacrylate
ppm	Parts per Million
ps	Pico Second
Q	Q Type Silicon Atom (Four Oxygen Neighbors)
QCM	Quartz Crystal Microbalance
\bar{R}	Mean Distance
r ₀	Steady State Anisotropy
R _c	Critical Distance
R _s	Resolution
r _{ss}	Steady State Fluorescence Anisotropy
Ru	Ruthenium
S	Substrate
s	Second
SEM	Scanning Electron Microscopy
SFC	Supercritical Fluid Chromatography

SRM 869a	Shape Selectivity Test Mixture Consisting of 1,2–3,4–5,6–7,8–Tetrabenzonaphthalene (TBN), Phenanthro[3,4–c]phenanthrene (PhPh), and Benzo[<i>a</i>]pyrene (BaP) in Acetonitrile
T	T Type Silicon Atom (Three Oxygen Neighbors)
T	Temperature
TBN	1,2–3,4–5,6–7,8–Tetrabenzonaphthalene
TEA	Tetraethylamin
TEOS	Tetraethoxysilane
TMEDA	Tetramethylethyldiamine
t_r	Migration Time
TMS	Tetramethylsilane
THF	Tetrahydrofuran
UV/VIS	Ultraviolett, Visible
w_h	Respective Peak Width at Half Height
XRD	X–Ray Diffraction

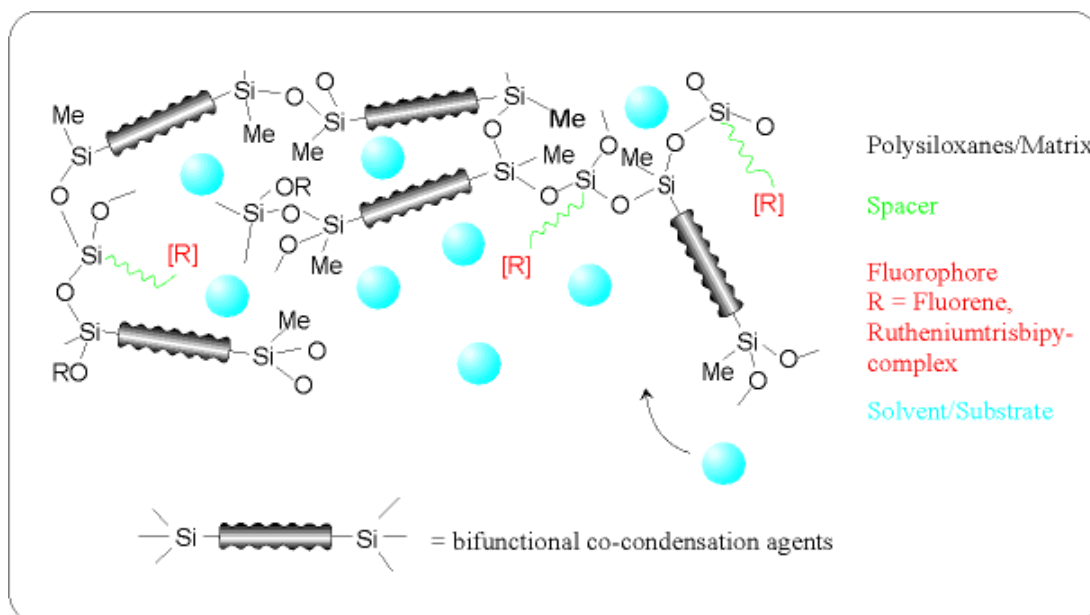
Greek letters:

α	Selectivity
δ	Chemical Shift
μ	Mikro
μl	Microliter
μm	Micrometer
ν	Frequency
$\tilde{\nu}$	Wave Number
λ	Wave Length
η	Viscosity
χ^2	Durbin–Watson Parameter
τ_F	Mean Fluorescence Decay Time
τ_R	Mean Rotational Correlation Time
Δ	Change
Δ, Λ	Different Enantiomers of the Tris(2,2'-bipyridine)- ruthenium(II) Complex

1. Introduction

One of the most important advantages of homogeneous catalysis is the possibility to control conversions and selectivity towards the desired products. The ambition to transfer these properties to supported catalysts has not been achieved in a satisfactory way. The known problems of leaching of the catalysts from the polymer backbone have not been solved yet.¹ In addition, the knowledge about the nature of reactive centers is mostly empirical. A considerable improvement of the benefits in the combination of homogeneous and heterogeneous catalysis was obtained by introducing the concept of the interphase, which is derived from reversed phase chromatography.²⁻⁴

Interphases are systems in which a stationary phase and a mobile component penetrate each other on a molecular level without forming a homogeneous phase (Scheme 1). In an ideal interphase the reactive centers remain highly mobile and simulate properties of a solution. Simple recovery of catalysts by filtration and a control of activity and selectivity are guaranteed, the leaching is largely reduced, and the reactivity can be modified by the employment of copolymers.⁵



Scheme 1. Schematic representation of an Interphase.

The sol-gel process⁶ (Scheme 2) is a versatile method capable to generate chemically and thermally inert inorganic-organic hybrid polymers with excellent swelling abilities and high accessibility for even large substrates such as e.g. anthracene. If transition metal complexes are provided with T-silyl functionalities they can be subjected to a sol-gel process to yield stationary phases.⁷ They consist of an inert polysiloxane matrix (widely modifiable by the selection of monomeric silanes), a flexible spacer (PEG, alkyl chains, combined alkyl-phenyl systems) and a reactive center (ligand or a reactive center).



Scheme 2. Main steps of the sol–gel process.

The mobile phase is a gaseous, liquid or dissolved reactant or simply a solvent. The matrix located transition metal complexes are securely incorporated into the hybrid polymer and sufficient swelling allows the accessibility of the reactive centers.

T–functionalized silanes of the type Fn–Si(OMe)_3 serve for the generation of stationary phases, which were subjected to the sol–gel process with or without co–condensation agents.^{6–11} The functional group Fn generally represents either a ligand or a complex distributed statistically across the entire carrier matrix.

Co–condensation agents are taking over the task of control the density and distance of the reactive centers, the polarity of the matrix, and eventually avoid leaching.^{6,10,12,13} They are the components which modulate the stationary phase in type (e.g. TiO_2 , polysiloxane, organic polymer or inorganic–organic hybrid polymer) and mobility from rigid to highly mobile and are responsible for the porosity and swelling ability of the materials.

Frequently applied co-condensation agents are siloxanes such as $\text{Si}(\text{OEt})_4$ (**Q⁰**),¹⁴⁻¹⁶ $\text{RSi}(\text{OMe})_3$ (**T⁰**),^{14,15} or $\text{Me}_2\text{Si}(\text{OMe})_2$ (**D⁰**).^{14,15,17} Although the copolymers with D-groups reveal the desired high mobility in interphases, they have the disadvantage to be washed out during the sol-gel process. However, Q type copolymers are characterized by complementary properties. They are rigidly anchored within the matrix and hence cannot be washed out, but they are lacking of the necessary mobility and accessibility. By employing D-functionalized silanes of the type $\text{R}(\text{MeO})_2\text{Si}(\text{CH})_z\text{Si}(\text{OMe})_2\text{R}$ (**D⁰-C_z-D⁰**) recently the combination of the advantages of D and Q co-condensing agents was successful. The resulting copolymers revealed an optimum of cross-linkage and swelling abilities and cannot be washed out of the polymer matrix.¹⁸⁻²² Similar results can be achieved by the use of the alternative co-condensation agent $(\text{MeO})_3\text{Si}(\text{CH})_z\text{Si}(\text{OMe})_3$ (**T⁰-C_z-T⁰**).

As the non-ordered polymers described above are of completely amorphous nature X-ray crystal structural analysis is not applicable to characterize their structures. The main tool to investigate, characterize and quantify the inorganic-organic hybrid polymers is solid-state NMR spectroscopy, also elemental analyses,

infrared spectroscopy, scanning electron microscopy, BET measurements, or UV/VIS spectroscopy.

This tool is as well available for ordered sol-gel polymers but they can also be characterized by XRD-measurements to reveal their ordered structures.

The edge of sol-gel materials is the high range of variations which can be attained by the use of several silane monomers and the variation of the reactive center. The density of active centers is easily assessable. Another advantage is the easy covalent attachment of the fluorophores. In order to analyze the mobility and accessibility of fluorophores covalently attached to the polymer in very low concentrations fluorescence spectroscopy is a powerful tool. The method is profitably used to get new informations about the microenvironment of the fluorophores. It is thus helpful to find polymers with favorable characteristics for catalysis in interphases where small concentrations of catalysts are used and high mobility and accessibility of the catalyst is necessary. The influence of the polymer backbone and the behavior of the fluorophores can be noticed. In this thesis the behavior of covalently attached fluorene in different non-ordered sol-gel polymers is discussed investigating the rotational mobility.

The precursor molecule of a luminescent ruthenium complex was synthesized and separated into its enantiomers, further modification reveals a covalently attachable luminescent ruthenium complex which gives a more detailed prediction of non-ordered sol-gel polymers concerning the translational mobility of oxygen and anthracene by the reduced metal complex luminescence.

The synthesis in the presence of template molecules reveals ordered sol-gel polymers and they are synthesized for application in HPLC.

A further characterization of sol-gel modified silicon and gold surfaces was carried out by the use of several microscopic techniques and QCM measurements in liquid and gaseous phase. QCM measurements in the gaseous phase allow a classification of the sol-gel materials on the surface concerning solvent affinity of these materials. These measurements can be used for some sensing applications as well as for the design of polymer backbones fitting for the respective reactive center embedded into the sol-gel polymers for catalysis or solid phase synthesis.

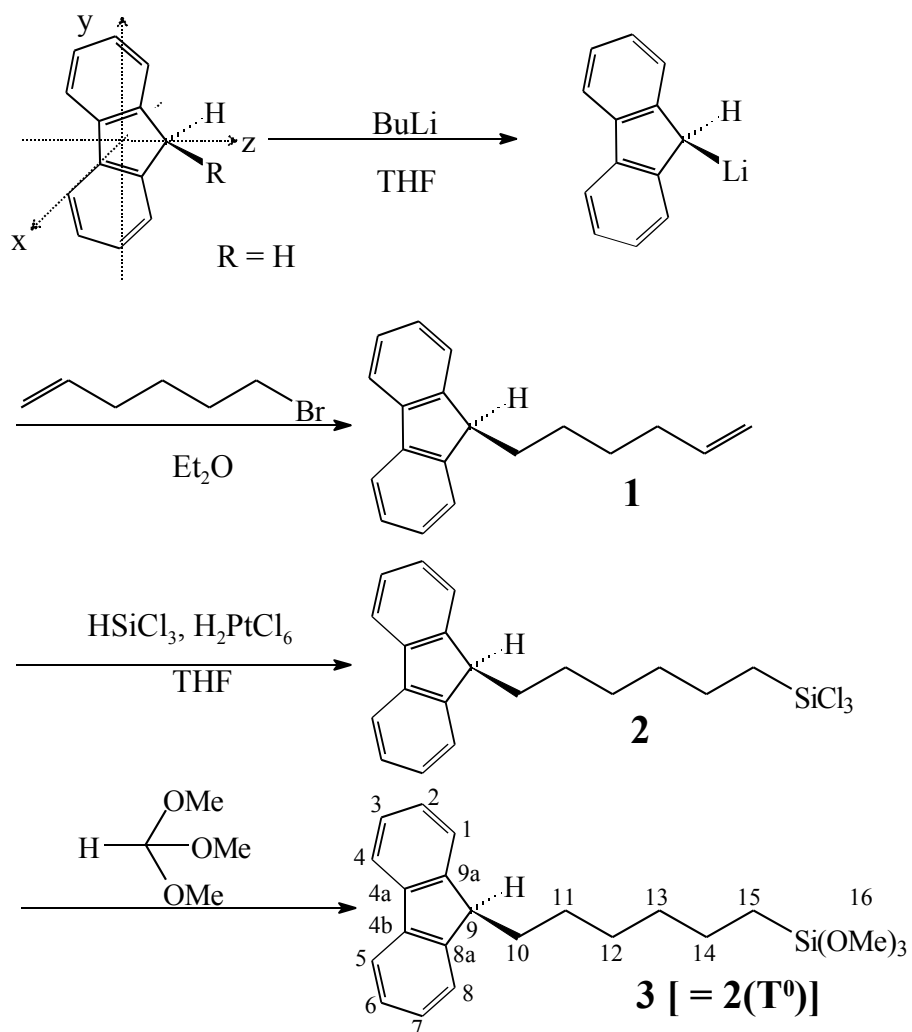
2. General Section

2.1 Synthesis, Characterization, and Fluorescence Spectroscopic Mobility Studies of Fluorene Labeled Inorganic–Organic Hybrid Polymers

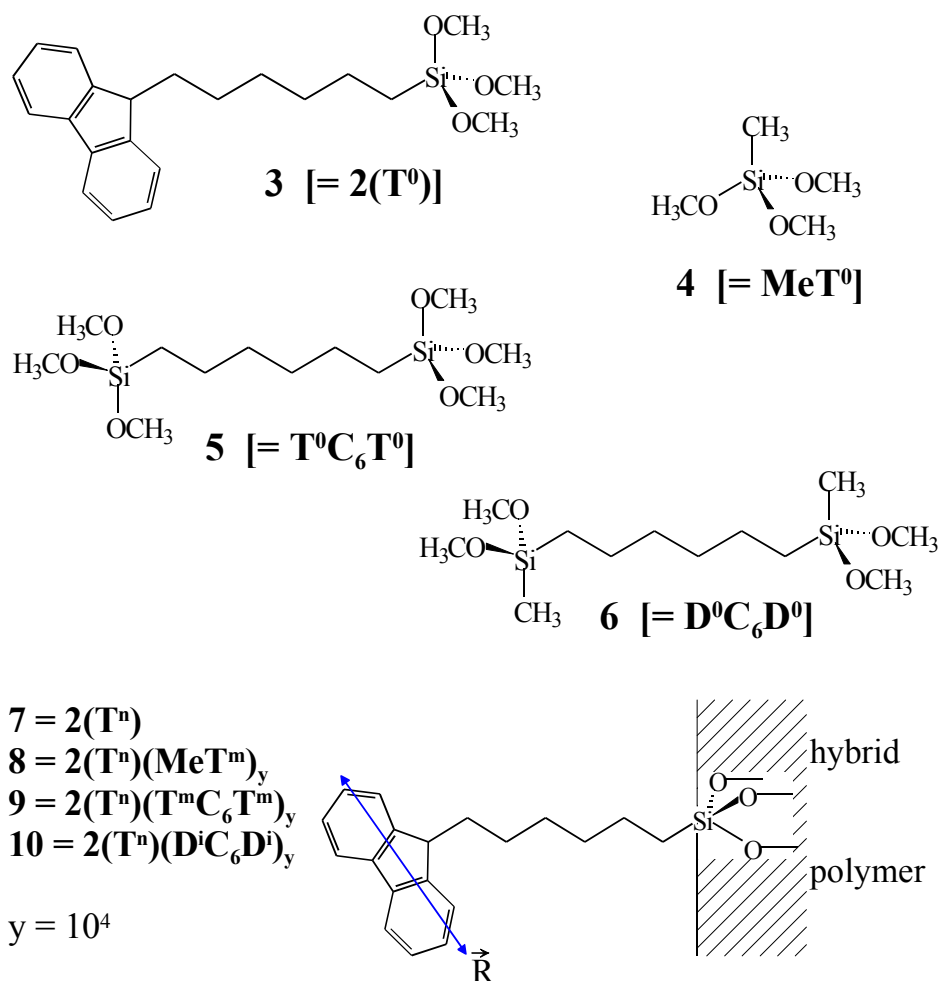
2.1.1 Introduction

Sol–gel processed polysiloxanes are widely investigated as potential supports for reporter molecules in chemical sensors.^{23,24} However, only little use has been made of sol–gel processed polymeric materials as supports for catalytically active transition metal complexes.^{5,25} Upon swelling of the polymer in appropriate solvents, an interphase is formed, where solid and liquid phase interpenetrate on the molecular level without forming a homogeneous solution. Ideally, these materials combine the convenient handling of solids with the molecular dispersity of the active sites encountered in homogeneous solutions. Real samples suffer from several problems, among which chemical stability and accessibility of the active centers are the most serious ones. Decomposition of the matrix is reduced by increasing the cross–linking of the polymer, i.e., by using tri– (T) or quater– (Q) functionalized silanes. Leaching of the active centers is impeded by

covalently binding them to the matrix via long-chain T-silyl functionalized spacers and by the employment of polyfunctionalized ligands. However, by increasing the cross-linking of the material, the swelling of the polymer in liquids is reduced, which leads to diffusion problems and greatly diminished accessibility of the active centers for reactant molecules dissolved in the liquid phase. A possible approach to resolve this dilemma is to employ hybrid polymers instead of pure polysiloxanes. In these hybrid polymers, which are employed by our group as solid supports for tethered transition metals complex catalysts, the functionalized silanes **3** [= **2(T⁰)**] (Schemes 3 and 4) are subjected to the sol-gel process together with the co-condensation agents **4** [= **Me-T⁰**], **5** [= **T⁰-C₆-T⁰**], and **6** [= **D⁰-C₆-D⁰**] (Scheme 4). The siloxane groups provide the desired degree of cross-linking, while the organic substituents of the co-condensation agents are supposed to enhance the swelling ability of the hybrid polymers.



Scheme 3. Synthesis of the sol-gel polymerizable fluorene **3**.



\vec{R} = transition dipole moment

T = T type silicon atom (three oxygen neighbors)

D = D type silicon atom (two oxygen neighbors)

n, m, i = number of Si-O-Si bonds (n = 0-3; m = 0-3; i = 0-2)

y = molar ratio of co-condensate and $2(\text{T}^n)$

Scheme 4. Sol-gel process with different co-condensation agents.

Optimization of stationary phases requires quantification of the accessibility of the active centers bound to the matrix and of the diffusional mobility of reactants dissolved in the liquid phase. A variety of spectroscopic techniques, including NMR and UV/VIS spectroscopy, has been applied for this purpose. NMR spectroscopy provides mainly information on the polymeric matrix and highly concentrated active centers.^{9,18} For the investigation of species present in the interphase at low concentrations, the highly sensitive UV/VIS fluorescence spectroscopy is more appropriate. Ample use has been made of fluorescent probes to characterize the microenvironment in sol-gel processed materials.²⁶⁻³⁹ The vast majority of these publications deals with probe molecules sequestered within the matrix, while only few studies employ covalently attached probes.⁴⁰⁻⁵²

In this work, fluorene is attached covalently to organic-inorganic hybrid polymers as a fluorescent model compound for matrix bound active centers. We are thus able to investigate quantitatively the mobility in the interphase by fluorescence spectroscopic methods. The rotational mobility of the fluorene labels is probed by steady-state and time-resolved fluorescence depolarization. The translational mobility of low

molecular weight species dissolved in the mobile component is probed by the kinetics of exciplex formation between fluorene and triethylamine. These experiments provide a detailed picture of the factors affecting the accessibility of matrix bound active centers by molecules dissolved in the mobile phase. The insight thus gained will be useful in the synthesis of new hybrid catalysts with improved turn over rates.

2.1.2 Results

2.1.2.1 Synthesis of the T-Silyl Functionalized Fluorene 3

To bind fluorene in 9-position to a hydrocarbon spacer with a terminal T-silyl function, it is derivatized with butyl lithium to the corresponding lithium compound (Scheme 3). Subsequently follows a coupling reaction with 1-bromo-5-hexene to give the unsaturated intermediate **1**.⁵³ In the presence of H_2PtCl_6 as catalyst a hydrosilylation reaction takes place between **1** and HSiCl_3 to give the trichlorosilane **2** which is immediately transformed to **3** with trimethyl orthoformate. After column chromatographic purification **3** represents a yellow oil which is sensitive to moisture and dissolves readily in organic solvents of medium polarity. The composition of **3** was verified by its EI mass

spectrum showing the expected molecular peak. Analytical data are summarized in the Experimental Section.

2.1.2.2 Synthesis of the Polymeric Fluorenes

Stationary phases containing fluorene have to be investigated by fluorescence spectroscopy in a highly diluted form. Therefore the sol-gel process of **3** was carried out in the presence of high amounts ($1:10^4$) of the mono- and bifunctional co-condensation agents **4**, **5**, and **6** (Scheme 4) influencing the properties of the resulting polymeric materials essentially. For reasons of comparison also the fluorene **3** without any co-condensation agent was subjected to a sol-gel procedure. The properties of sol-gel processed materials strongly depend on the applied reaction conditions such as concentration of the starting materials, amount and type of solvent, temperature, reaction time, drying conditions of the wet gel, and type of catalyst. To ensure the same reaction kinetics for the synthesis of each polymer as a prerequisite for comparable results, the adherence to uniform reaction conditions has to be maintained during the entire hydrolysis and polycondensation procedure.^{5,8,53} Methanol was added during the sol-gel process to homogenize the reaction

mixture. Ammonia (**7**, **8**, **9**) and hydrogen chloride (**10**) were appropriate catalysts, which do not interfere with fluorene.¹⁴

The ^1H and $^{13}\text{C}\{^1\text{H}\}$ NMR spectra of the polymer **7** (suspension in CDCl_3) reveal broadened ^1H and ^{13}C resonances, respectively. However, the pattern of these ^1H and ^{13}C signals is similar to that of the respective high resolution ^1H and $^{13}\text{C}\{^1\text{H}\}$ NMR spectra of the monomeric precursor **3** which is an evidence that fluorene remained intact during the sol-gel process.

The ^{29}Si and ^{13}C CP/MAS NMR spectra of the polymeric materials **8**, **10**, and **9** ($\gamma = 10^4$) are dominated by the polymeric parts **Me-T^m**, **Dⁱ-C₆-Dⁱ**, and **T^m-C₆-T^m**. Hence no ^{29}Si signals for the Tⁿ functions of **7** are observed. The ^{29}Si CP/MAS NMR spectrum of **8** is characterized by two resonances of different intensity which are assigned to T² (small) and T³ (intensive) silyl species. In the case of **10** two signals are observed for D¹ silyl groups, probably because of diastereotopic effects. An intense signal occurs for the completely hydrolyzed D² functions. The ^{29}Si CP/MAS NMR spectrum of **9** shows all resonances for T⁰⁻, T¹⁻, T²⁻, and T³⁻ silyl groups. Obviously also non-cross linked T-silyl species are present in the polymer. Both spectra are similar to those of the pure hybrid polymers **Dⁱ-C₆-Dⁱ** and **T^m-C₆-T^m** which were reported

recently.^{14,18} The ^{13}C CP/MAS NMR spectra of the stationary phases **8**, **10**, and **9** show resonances at δ 50.0 which are attributed to the carbon atoms of silicon bound methoxy groups. This is consistent with an incomplete hydrolysis and thus a reduced cross linkage of the polymers. Because of steric effects the fraction of non-hydrolyzed methoxy residues is higher in the case of the polymer **9**. However, the concentration of residual methoxy groups is rather small, because hydrolysis and condensation of the materials must be fairly complete as is obvious from the similarity of experimental elemental analysis data and the values calculated for fully reacted materials.

2.1.2.3 Fluorescence Spectroscopic Investigations

2.1.2.3.1 Fluorescence and Fluorescence Excitation Spectra of **3**

Figure 1 presents the UV/VIS absorption and fluorescence spectra of **3** in solution. The vibrationally structured low-energetic absorption band is assigned to the $A \rightarrow L_a$ transition,⁵⁴ while the strong and structureless absorption band at 38500 cm^{-1} is assigned to the $A \rightarrow B_b$ transition.⁵⁴ Upon binding **3** to the hybrid polysiloxanes, fluorescence and fluorescence excitation spectra do

not change noticeably (see Figure 2). No aggregation of the fluorophores is observable in the spectra.

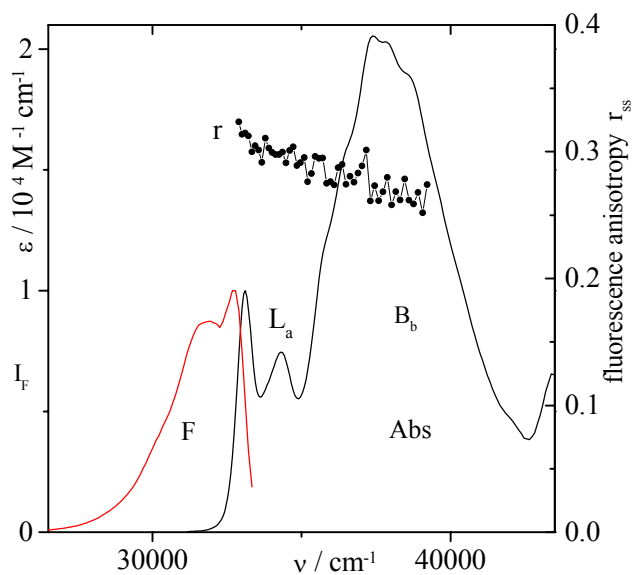


Figure 1. Absorption (Abs), fluorescence (F) and fluorescence anisotropy spectra (r) of **3** in PMMA glass.

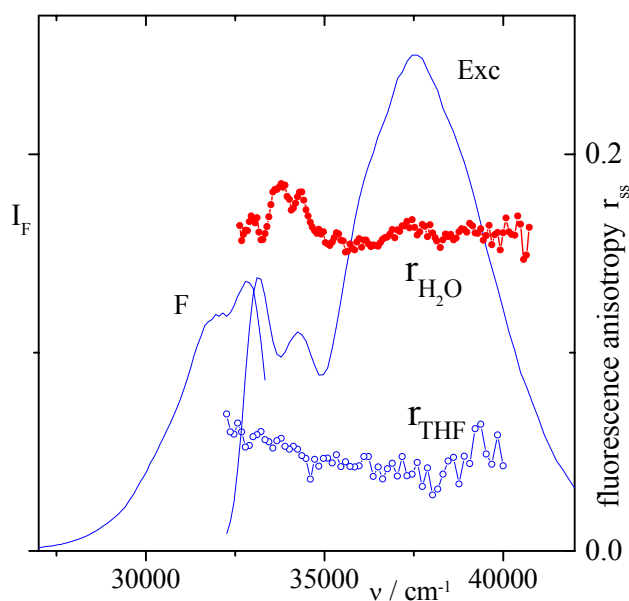


Figure 2. Fluorescence and fluorescence excitation spectra of **10** in THF as well as the anisotropy spectra of **10** in water and in THF. The maximum at 34000 cm^{-1} in the anisotropy spectrum in water is due to the Raman peak of water.

2.1.2.3.2 Fluorescence Decay Curves of **3**

The fluorescence decay curves of **3** dissolved homogeneously in low viscous solutions are single exponential with decay times of $\tau_F \approx 6\text{ ns}$ (Table 1). Only in dichloromethane, the fluorescence lifetime is reduced to $\tau_F \approx 3\text{ ns}$, indicating that this liquid partially quenches the excited singlet state of **3**, due to the heavy atom

Table 1. Mean fluorescence decay time $\langle\tau_F\rangle$ of **3** in homogeneous solutions and of the polysiloxane hybrid polymers suspended in different liquids

$\langle\tau_F\rangle/\text{ns}$	Cy	THF	DCM	MeOH
Solution ^a	6.4	6.0	3.6	6.5
8 ^b	6.0	5.3	4.0	6.2
9 ^b	6.0	5.5	4.2	6.2
10 ^b	6.0	5.6	4.3	6.2

^a The values in solution are obtained from exponential fits to the decay curves.

^b The values in the polysiloxane matrices are calculated by eq. (1), inserting the data obtained from biexponential fits.

effect of chlorine. For suspensions of the fluorene-labeled polysiloxanes in all investigated solvents, slightly non-exponential decay curves are observed. This type of decay curve is best described by narrow distributions of decay times, but can also be fitted by sums of two exponentials without loss of accuracy. The deviation from exponentiality implies that the fluctuations of the microenvironment of the fluorophores are slow on the time scale of fluorene fluorescence. The mean fluorescence decay times of the fluorene labeled polymer suspended in, e.g., cyclohexane, THF, and

methanol are close to the values obtained for the corresponding homogeneous solutions of **3** (Table 1). The decay curves of suspensions of the polymers in dichloromethane show two clearly distinct lifetime components of $\tau_F \approx 5$ ns and $\tau_F \approx 3$ ns of about equal weight, which result in mean decay times which are significantly longer than those of **3** in dichloromethane solution (Table 1). The existence of the long lifetime component indicates that a considerable fraction of the matrix bound probes is quenched less than in bulk solution, and thus is partly protected from dichloromethane by the matrix.^{55,56}

2.1.2.3.3 Steady State Measurements of Fluorescence Anisotropy

Fluorene, for which $R = H$ (see Scheme 3), belongs to the point group C_{2v} , and both of the transitions corresponding to the L_b - and B_b -bands are of $A_1 \rightarrow B_2$ type in terms of symmetry. Hence, the transitions are polarized along the molecular y -axis.^{30,57} Upon introduction of an alkyl group for R , as in **3**, the local symmetry of the π -electron system is hardly affected and consequently the orientation of the transition dipole moments remains practically unchanged. The fluorescence anisotropy excitation spectrum of **3** embedded in a rigid

polymethylmethacrylate (PMMA) resin (Figure 1) shows a steady-state anisotropy of $r_0 \approx 0.30$ for the lowest energy transition. The steady state fluorescence anisotropy decreases with decreasing excitation wavelength due to increased light scattering by the PMMA matrix.

In homogeneous solutions of **3** in low viscosity solvents, the steady state fluorescence anisotropy, r_{ss} , is not significantly different from zero. Upon binding **3** to the polymer matrix, much higher values of r_{ss} are obtained. In Figure 2, the fluorescence anisotropy excitation spectra of **10** in THF and water are shown as typical examples. By inserting r into eq. (1)

$$\langle \tau_R \rangle \approx \frac{\langle \tau_F \rangle}{\frac{r_0}{r_{ss}} - 1} \quad (1)$$

which is valid for small deviations of fluorescence decay curves from exponentiality, the mean rotational correlation time, $\langle \tau_R \rangle$, is obtained. As the mean fluorescence decay times, $\langle \tau_F \rangle$, are similar for all solvents (except for dichloromethane), the steady-state values of r already give a rough measure of the mobility of the probe. The values of $\langle \tau_R \rangle$ for matrix bound **7**, calculated by eq. (16), are about one to two orders of magnitude larger than the

value of $\langle \tau_R \rangle \approx 30$ ps, obtained for fluorene in solution (Table 2). A more detailed picture of the microenvironment of the probe can be obtained by time-resolved measurements of the fluorescence anisotropy.

Table 2. Steady state fluorescence anisotropies, r_{ss} , and mean rotational correlation times, $\langle \tau_R \rangle$, of fluorene-labeled polysiloxane hybrid polymers suspended in different liquids

$\langle \tau_F \rangle / \text{ns}$		Cy	Et ₂ O	THF	DCM	MeOH	H ₂ O
8	r_{ss}	0.14	0.005	0.005	0.025	0.06	0.12
	$\langle \tau_R \rangle / \text{ns}^a$	3.8	0.07	0.08	0.30	1.20	3.20
9	r_{ss}	0.06	0.025	0.02	0.025	0.06	0.11
	$\langle \tau_R \rangle / \text{ns}^a$	1.2	0.45	0.30	0.30	1.20	2.80
10	r_{ss}	0.14	0.045	0.045	0.08	0.13	0.16
	$\langle \tau_R \rangle / \text{ns}^a$	3.8	0.90	0.80	1.20	3.50	4.50

^a The values of $\langle \tau_R \rangle$ are calculated by eq. (3) from steady state fluorescence anisotropies, r_{ss} , and mean fluorescence decay times, $\langle \tau_F \rangle$.

2.1.2.3.4 Time Resolved Measurements of Fluorescence Anisotropy

Figure 3 shows typical decay traces of fluorescence anisotropy after pulsed laser excitation of the samples. The fluorescence anisotropy decay of fluorene dissolved in THF is faster than the instrument response time of $\tau = 70$ ps. For matrix bound **7**, strongly non-exponential fluorescence anisotropy decay curves are obtained. Fitting them to sums of three exponentials yields correlation times, which fall into three distinctly different time ranges, namely $\tau_{R1} = 100 - 200$ ps, $\tau_{R2} = 1 - 3$ ns, and $\tau_{R3} = 10 - 50$ ns. No residual anisotropies are obtained from fitting the decay curves in the accessible time range ($0 \text{ ns} < t < 15 \text{ ns}$). Even the fastest component, τ_{R1} , is significantly slower than the anisotropy decay of fluorene in homogeneous solution, due to the reduced mobility of the probe molecules. The mobility is affected by both the type of the polysiloxane matrix and the liquid in which the polymer is suspended. Figure 4 gives a graphic representation of

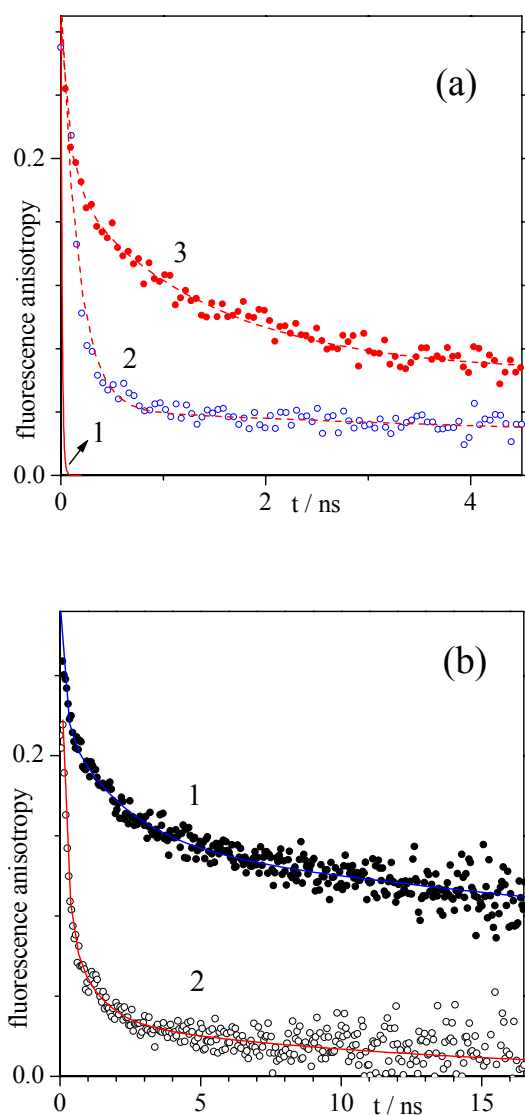


Figure 3. Theoretical fluorescence anisotropy decay curve of fluorene in THF (curve 1 in Figure 3a), calculated from the data of ref. 33 by eq. (2), and examples of experimental fluorescence anisotropy decay traces after pulsed laser excitation ($\lambda_{\text{ex}} = 295 \text{ nm}$, $\Delta t = 10 \text{ ps}$ fwhm). **(a)** **9** (2) and **10** (3) suspended in THF. **(b)** **8** suspended in cyclohexane (1) and in dichloromethane (2). Points – experimental data, lines – three-exponential fits.

the amplitudes of the three components of τ_R for the three

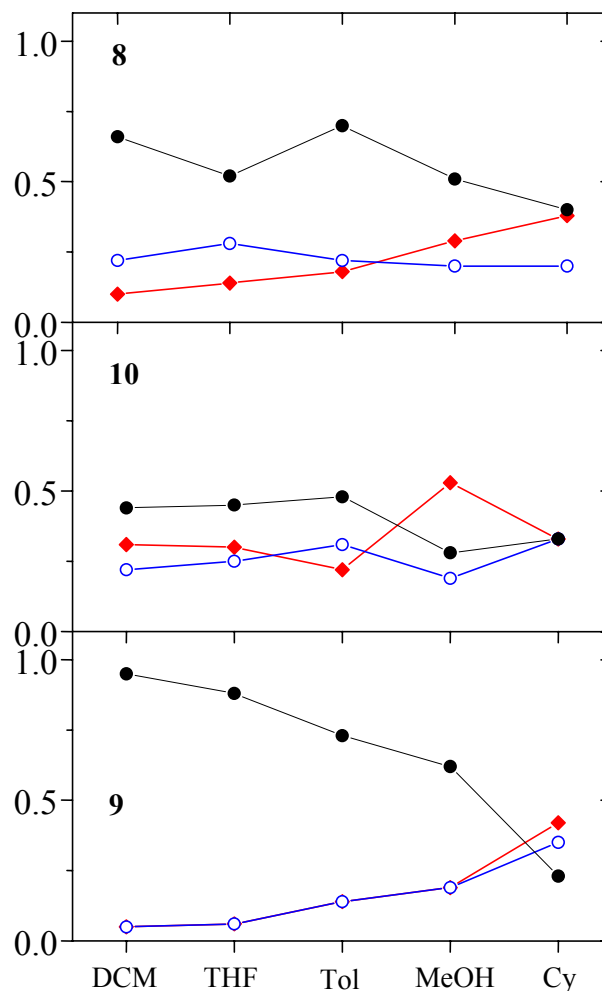


Figure 4. Relative amplitudes of the three components of the fluorescence anisotropy decays for the hybrid polymers in different liquids. Points: short component ($\tau_{R1} = 0.1\text{--}0.2$ ns), open circles: medium component ($\tau_{R2} = 1.0\text{--}3.0$ ns), diamonds: long component ($\tau_{R3} = 10\text{--}50$ ns). In DCM – dichloromethane, THF – tetrahydrofuran, Tol – toluene, MeOH – methanol, and CH –cyclohexane.

polymers suspended in different liquids. For **9**, a clear trend of the amplitudes with the suspending solvent is observable. In dichloromethane and in THF the short component, τ_{R1} , is dominating, indicating a high mobility of the fluorophore. In cyclohexane, almost no contribution of the short component is left, which is due to strongly hindered motions of the probe molecule. In **10**, the contribution of the short component is small in all solvents, corresponding to solvent independent low mobility of the fluorophore. In the case of **8**, an intermediate situation is found.

2.1.2.3.5 Investigation of the Translational Mobility by Exciplex Formation Between Triethylamine and Fluorene in 7

The translational mobility of low molecular weight species dissolved in the mobile component is available from the analysis of bimolecular processes such as exciplex formation. Upon electronic excitation, fluorene forms an exciplex with triethylamine (TEA).⁵⁸ This holds also true for fluorene in **7**. These exciplexes exhibit structureless fluorescence spectra (Figure 5), which are red-shifted against the emission of molecular fluorene. The spectral position of the exciplex band shifts to longer wavelengths with increasing

polarity of the environment, due to the large dipole moment of the exciplex of $\mu = 13$ D.⁵⁸ In homogeneous solutions of fluorene in mixtures of TEA and *n*-hexane, the maximum of the exciplex

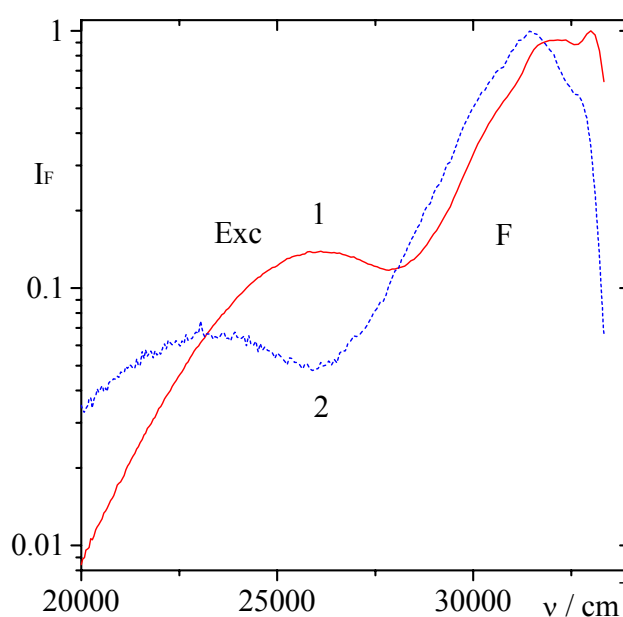


Figure 5. Fluorescence spectra of the system fluorene / triethylamine (TEA). (1) solution of fluorene (10^{-5} M) and TEA (0.1 M) in *n*-hexane. (2) Suspension of **10** in 1 M solution of TEA in THF. Excitation wavelength $\lambda_{ex} = 280$ nm. F – Fluorene fluorescence, Exc – Exciplex fluorescence.

emission is found at $\tilde{\nu}_{max} \approx 26000$ cm^{-1} . In suspensions of **10** in THF/TEA mixtures, the emission maximum is shifted to $\tilde{\nu}_{max} \approx 23000$ cm^{-1} , indicating that the exciplex is at least partially solvated by THF.

For suspensions of the hybrid polymers in dichloromethane, THF, diethyl ether, and toluene sufficient amounts of exciplex are formed, whereas in methanol and cyclohexane no significant exciplex formation is observed. Figure 6 shows the fluorescence decay curves of a suspension of **10** in a diethyl ether/TEA mixture. In this example, the mean fluorescence decay time of **7** is reduced to $\bar{\tau}_F = 4.5$ ns, against $\bar{\tau}_F = 6.0$ ns before addition of TEA. The time-resolved intensity trace of the exciplex fluorescence reveals two rising components, one of which is instantaneous on the time scale of our experiment. The instantaneous component is due to "static" exciplexes, which are formed upon excitation of ground state aggregates of **7** and TEA. The slow rising component has a rise time of $\tau_F = 3.5$ ns. Considering the inhomogeneity of the sample and the non-exponentiality of the decay traces, this rise time may be regarded as being approximately equal to the decay time of **7** and is thus ascribed to the dynamic formation of the

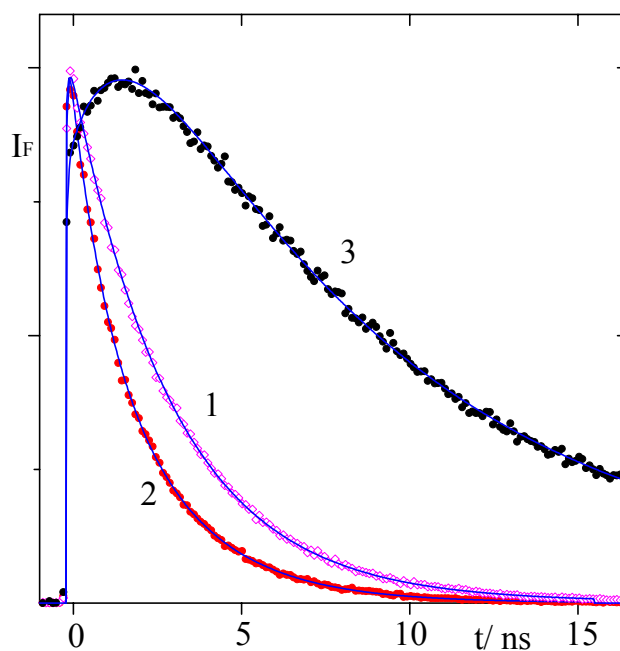


Figure 6. Fluorescence decay curves of suspensions of **10** in diethyl ether after pulsed laser excitation (laser pulse width $\Delta t = 10$ ps fwhm). (1) fluorene fluorescence without TEA. (2) fluorene fluorescence for $c_{TEA} = 1$ M. (3) exciplex fluorescence for $c_{TEA} = 1$ M. Excitation wavelength $\lambda = 290$ nm, detection of fluorene and exciplex fluorescence at $\lambda = 340$ nm and $\lambda = 410$ nm, respectively.

exciplex. The decaying component of the exciplex trace, with $\tau_F = 16.3$ ns, is assigned to the deactivation of the exciplex to the ground state complex.

2.1.3 Discussion

2.1.3.1 Rotational Mobility of Fluorene and 7

In the case of fluorene in bulk solutions, i.e. $R = H$ (see Scheme 3), fluorescence will be depolarized by rotational diffusion around the principal x- and z-axes, as the transition dipole moment of emission is oriented parallel to the principal y-axis of rotation to a good approximation. These two diffusional motions result in a biexponential decay of the fluorescence anisotropy⁵⁹

$$r(t) = \frac{1}{5} \left[1 + \frac{2D_y - D_x - D_z}{2\Delta} \right] \cdot e^{-(6\bar{D}-2\Delta)t} + \frac{1}{5} \left[1 - \frac{2D_y - D_x - D_z}{2\Delta} \right] \cdot e^{-(6\bar{D}+2\Delta)t}$$

$$= A_1 \cdot e^{-t/\tau_{R1}} + A_2 \cdot e^{-t/\tau_{R2}}$$
(2)

where $\bar{D} = \frac{D_x + D_y + D_z}{3}$ and $\Delta = \sqrt{D_x^2 + D_y^2 + D_z^2 - D_x D_y - D_y D_z - D_z D_x}$

The rotational diffusion constants of fluorene in $CDCl_3$ at $T = 310$ K have been determined by T_1 relaxation measurements of ^{13}C NMR signals as $D_x = 2.8 \cdot 10^{10} \text{ s}^{-1}$, $D_y = 2.1 \cdot 10^{10} \text{ s}^{-1}$, and $D_z = 0.73 \cdot 10^{10} \text{ s}^{-1}$.⁶⁰ These values are in agreement with results obtained by depolarized Raman scattering, which yield $C = 27 \text{ ps} \cdot (\text{mPa} \cdot \text{s})^{-1}$ for the viscosity dependent part of the rotational correlation time, $\tau_R = C + \tau_0$.⁶¹ Inserting the diffusion

constants D_x , D_y , and D_z into eq. (2) yields the theoretical fluorescence anisotropy decay curve of fluorene in CDCl_3 shown in Figure 3a. The rotational correlation times and their respective amplitudes are calculated as $\tau_{R1} = 13.4$ ps ($A_1 = 0.24$) and $\tau_{R2} = 6.8$ ps ($A_2 = 0.16$). Very similar parameters are expected for fluorene in THF at $T = 293$ K, because the viscosity of THF at $T = 293$ K ($\eta = 0.48$ mPa · s) is practically identical to that of CHCl_3 at $T = 310$ K ($\eta = 0.47$ mPa · s).⁶² Thus, the theoretical decay curve of fluorene in THF cannot be obtained experimentally with our setup, due to its limited time resolution.

When the fluorophore is attached to the hybrid polymer matrix, the mobility of the fluorene moiety is strongly reduced by the alkyl spacer and by the geometry of the environment, resulting in slow and strongly non-exponential fluorescence anisotropy decay curves. Although the inhomogeneity of the environment leads to a broad distribution of rotational correlation times, three significantly different ranges of correlation times are obtained, which can tentatively be assigned to characteristic motions of the fluorophore. Each of these motions may be associated with a specific site of the probe molecules.²⁶ The short correlation time component of

$\tau_R = 100 - 200$ ps is ascribed to fast, practically unimpeded motions of the fluorophore. The most important of these motions is fast rotation of the fluorene moiety around the C₉-C₁₀-bond of the alkyl spacer (see Schemes 3 and 4). This motion is only weakly hindered if the pores in the polymer matrix are large compared to the fluorophore size. According to eq. (2) and similar treatments described in refs.,⁶³⁻⁶⁵ this rotation leads to a single exponential decay

$$r(t) = 0.1 + 0.3 \cdot e^{-4D'_z t} \quad (3)$$

which does not decay to zero, even for infinitely long times after the laser pulse. The diffusion coefficient, D'_z , for rotation around the C₉-C₁₀ bond, adopts values in the range $0.6 \cdot 10^9 \text{ s}^{-1} \leq D'_z \leq 2.5 \cdot 10^9 \text{ s}^{-1}$. Motions of larger segments of the alkyl spacers, with correlation times in the medium time range of 1–3 ns, eventually lead to complete depolarization, because they make the whole solid angle accessible to the transition dipole moment. As these motions involve different conformations of the alkyl spacers, they require relatively large free volumes. The long correlation time components of $\tau_R > 10$ ns comprise motions which are slow compared to the fluorescence lifetime of **7** of

$\tau_F \approx 5 - 6$ ns and correspond to almost complete immobilization of the fluorophore caused by very small free volumes or strongly attractive interactions between **7** and the polymeric backbone.

2.1.3.2 Translational Mobility of **7** and TEA

For suspensions of the hybrid polymers in dichloromethane and diethyl ether the rate constants of formation; k_{MD} , of the exciplexes are calculated by eq. (4) from the dynamic portion of the quenching of fluorene fluorescence

$$k_{MD} = \left(\frac{1}{\tau_F} - \frac{1}{\tau_F^0} \right) \frac{1}{c_{TEA}} \quad (4)$$

where τ_F and τ_F^0 are the fluorescence decay times of fluorene at the given concentration of TEA, c_{TEA} , and without TEA, respectively. The results summarized in Table 3 are obtained under the assumption that the concentration of TEA in the polymer is the same as in the bulk solution. They must be considered as mean values, from which considerable deviations may occur in different regions of the polymer.²⁶ The rate constants, k_{MD} , in the interphases are reduced by an order of magnitude against the values in homogeneous solutions. The latter are known to be close

to the diffusion limit, e.g., $k_{MD} = 1.1 \cdot 10^9 \text{ M}^{-1}\text{s}^{-1}$ has been obtained in cyclohexane.⁵⁸ It is thus inferred that the translational mobility in the three hybrid polymers under investigation is greatly reduced compared to that observed in bulk solution. The translational mobility decreases by a factor of two in the series **8** \geq **9** > **10** (Table 3).

Table 3. Rate constants k_{MD} of exciplex formation between **7** and triethylamine in the hybrid polymers, suspended in dichloromethane and in diethyl ether^a

polymer	in dichloromethane	in diethyl ether
	$k_{MD}/10^8 \text{ M}^{-1} \cdot \text{s}^{-1}$	$k_{MD}/10^8 \text{ M}^{-1} \cdot \text{s}^{-1}$
8	2.4	2.3
9	2.1	1.8
10	1.4	1.1

^a The values of k_{MD} are calculated by eq. (6).

2.1.4 Conclusion

The fluorescence spectroscopic investigations of rotational and translational mobility in organic–inorganic hybrid polymers show clearly that both, the rotational mobility of the matrix bound

active centers and the translational mobility of low molecular weight species dissolved in the liquid phase are reduced by one to two orders of magnitude compared to homogeneous solutions. Obviously, diffusion processes in the interphase are appreciably hindered by the polymer matrix. This observation is in agreement with the small swelling volumes of the polymers in liquids. The largest diffusion coefficients are obtained in dichloromethane, THF and diethyl ether, in which the swelling volumes reach almost 10% of the original volumes. In all other solvents, in which no swelling of the polymers is measurable, the diffusion coefficients are significantly smaller. In polar liquids, the mobility of the probe molecules is further reduced due to their low solubility in these solvents, which leads to adsorption of the probe molecules to the polymer backbone.

In all liquids, the translational and rotational diffusion coefficients found in **8** and **9** are significantly larger than those obtained in **10**. As swelling does not substantially increase the free volumes of the materials, this dependence of mobility on the type of material is probably due to the inherently larger pore volumes of materials based on co-condensation agents with T-silyl groups compared to those built from co-condensation agents carrying

D-silyl groups. It is known that in materials which are prepared from monomers with D-silyl functions less rigid pore structures are formed than in materials consisting of monomers with T-silyl functions. Actually, the BET surface area for **9** exceeds that of **10** by a factor of almost twenty. However, the extremely small BET surface area found for **8** does not fit into this concept. The non-polar nature of **7** may offer a possible explanation for the high mobilities observed in both T-silyl based materials compared to those found in the D-silyl based polymer. The relatively polar silanes, mainly those with T-silyl functions, tend to avoid the vicinity of **7** during the sol-gel process, thus forming pores large enough to allow unimpeded diffusional motions of the fluorene moiety. As D-silyl functions do not form rigid pore structures, only pores formed by T-silyl moieties are persistent. The pores caused by this template effect^{54,55} do not show up in the BET measurements because the mole fraction of **7** is only 10^{-4} .

In order to reach the goal of combining high chemical stability of the interphases with solution-like accessibility of the active centers, the swelling capability of the polysiloxane backbone has to be improved appreciably, e.g. by introducing phenyl groups into the organic parts of the co-condensation agents. An

alternative approach is the synthesis of highly micro- or mesoporous materials, making use of the template effect.^{66,67}

2.2 Synthesis and Enantiomer Separation of a Modified Tris(2,2'-bipyridine)ruthenium(II) Complex

2.2.1 Introduction

Enantioselective chromatography (GC, SFC, HPLC)⁶⁸⁻⁷⁰ and capillary electrophoretic methods (CE, EKC, MEKC, OTCE, CEC)⁷¹⁻⁷⁶ employing chiral stationary phases (CSP) or chiral mobile phase additives (CMPA) are an effective tool for the separation of enantiomeric mixtures. Due to its high efficiency, capillary electrophoretic methods have become increasingly important for the separation of pharmaceutical products, biological samples and other charged and uncharged chiral compounds in recent years. CE methods have the advantage of easily changing the separation conditions by varying the type and concentration of the background electrolyte (bge) or the type of chiral mobile phase additive (CMPA). A large variety of CMPAs such as cyclodextrins, proteins, antibiotics, polysaccharides, cholic acids and supramolecular structures, are commonly employed for the separation of chiral compounds.⁷¹⁻⁷⁶ In spite of the widespread use of chromatography

and capillary electrophoretic methods for the enantioseparation of conventional organic substances, relatively little effort has been made to find suitable separation conditions for racemic transition metal complexes such as tris(diimine)ruthenium(II) complexes.^{77,78}

Tris(diimine)ruthenium(II) complexes were extensively investigated because of their unique photochemical, photophysical, and molecular recognition properties.⁷⁹⁻⁸¹ Diastereoselective interactions are often observed between these chiral transition metal complexes and organized biological media such as nucleic acids or sugars. Tris(diimine)ruthenium(II) complexes are a powerful tool in the elucidation of structural requirements, energetics and dynamics of DNA recognition and also very useful in immunoassays due to their well defined, stereostable three-dimensional structure and their emissive properties.⁸² It is known from several studies that the Δ and Λ enantiomers of tris(diimine)ruthenium(II) complexes bind with different affinities and geometries to DNA.⁸³⁻⁹² Herein the synthesis and the first analytical electrokinetic chromatographic (EKC) separation of racemic tris(diimine)ruthenium(II) complex **11** is described, which contains a hydroxyl-functionalized spacer group, in its enantiomers

by the use of a negatively charged cyclodextrin chiral mobile phase additive.

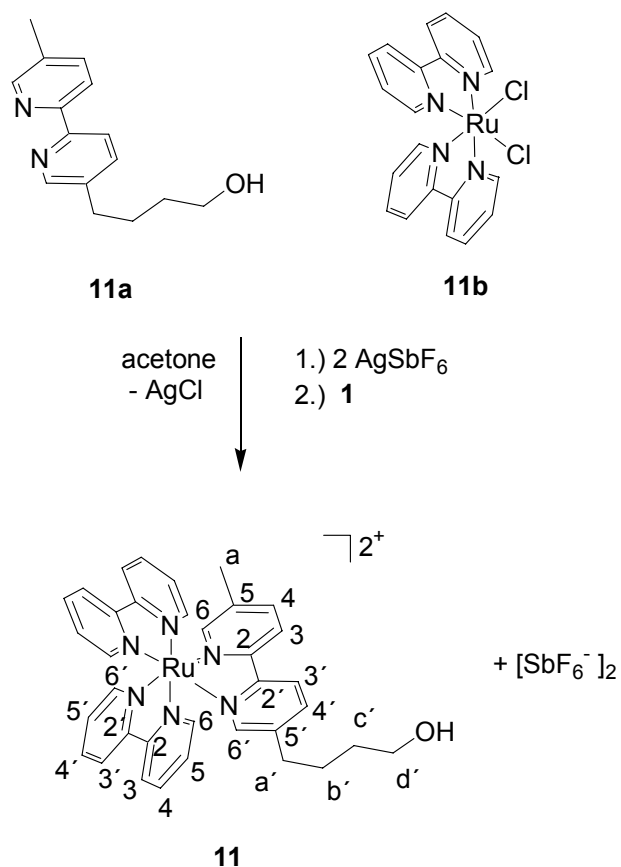
Complexes containing spacer groups, such as **11**, are of interest because they have the propensity to bind to biopolymers. Complex **11** bearing a spacer in *meta*-position offers a wide spectrum of binding reactions, while the favorable substitution position allows unhindered complexation and mobility of the complex itself.

2.2.2 Results and Discussion

2.2.2.1 Synthesis of the Modified Tris(2,2'-bipyridine) ruthenium(II) Complex 11

Silverhexafluoroantimonate was added to a suspension of *cis*-(bpy)₂RuCl₂ · 2 H₂O in acetone to remove both chlorides at ambient temperature. Silverchloride was removed by careful filtration and the modified bipyridine ligand [(5-(4-hydroxybutyl)-5'-methyl-2,2'-bipyridine)] was added at an equivalent ratio, the solution was then refluxed to form the product (Scheme 5). Complex **11** was obtained by precipitation with diethyl ether as an orange fine powder and was additionally purified by column chromatography. It is readily soluble in organic solvents of high polarity. The composition of **11** was verified by its EI mass

spectrum showing the expected molecular peak. Analytical data are summarized in the Experimental Section.



Scheme 5. Synthesis of complex **11**.

The assignments⁹³ of most of the proton and carbon signals in the ¹H and ¹³C{¹H} NMR spectra of **11** were achieved by using two-dimensional techniques (COSY and HMQC). The integration of the aromatic protons show clearly the presence of one 5-(4-hydroxybutyl)-5'-methyl-2,2'-bipyridine and two native 2,2'-bipyridine ligands. By a 2D COSY spectrum the correlation

between the aromatic protons could be easily recognized. The HMQC experiment allows the assignment of the ^{13}C signals with the exception of the quaternary carbon atoms. The NMR data are summarized in the Experimental Section.

2.2.2.2 Electrokinetic Chromatography of Complex 11

EKC trials were carried out using 20, 40, and 60 mM borate buffer solutions at a pH of 9.5 as background electrolytes (bge). Carboxymethyl- β -cyclodextrin dissolved in the respective buffer (7.5 mg/ml) was used as anionic chiral mobile phase additive (CMPA). Resolution R_s , selectivity α and the mean plate numbers N were calculated using the following equations:

$$R_s = \frac{1.177(t_R^B - t_R^A)}{w_h^A + w_h^B} \quad (5)$$

$$\alpha = \frac{t_R^B}{t_R^A} \quad (6)$$

$$N = 5.54 \left(\frac{t_R}{w_h} \right)^2 \quad (7)$$

$$\bar{N} = \frac{1}{2}(N_A + N_B) \quad (8)$$

where t_R^A and t_R^B are the migration time of the first and second eluted enantiomer, w_h^A and w_h^B the respective peak widths

(Figure 7).

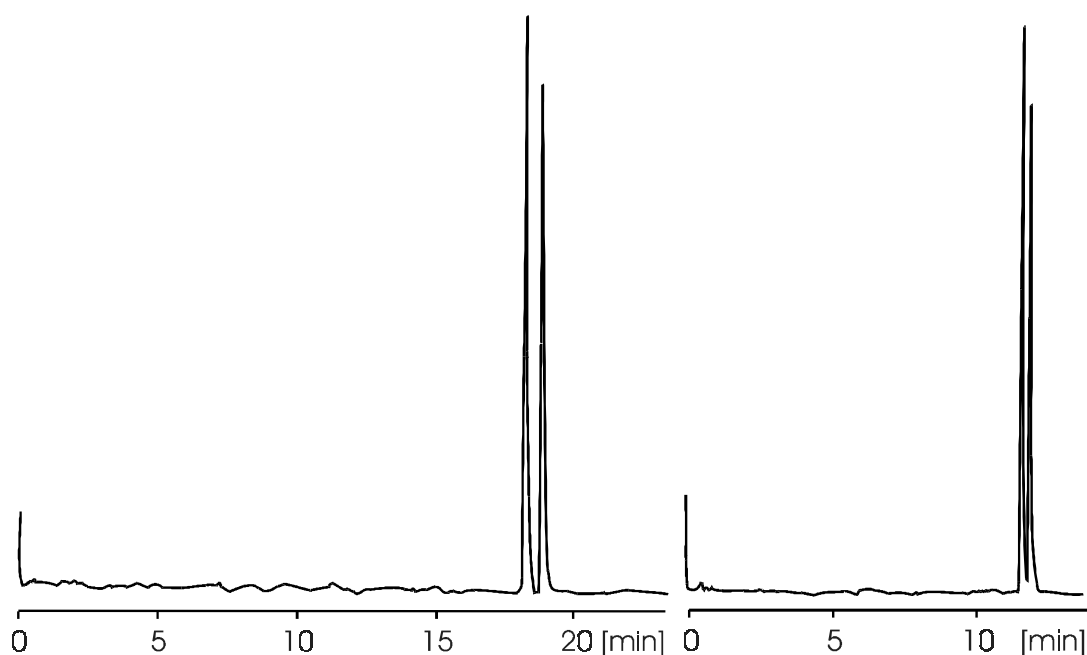


Figure 7. Chromatograms of the enantiomer separation of **3**. Conditions: fused silica capillary, 95 cm effective length (112 cm total length), bge: 20 mM borate buffer pH 9.5, C_{MPA}: 7.5 mg/ml of carboxymethyl- β -cyclodextrin, applied voltage: 30 kV, UV detection: 254 nm; temperature: 20°C (left) and 50°C (right).

As evident from the data given in Table 4, carboxymethyl- β -cyclodextrin is able to separate the two enantiomers of **11**. As the selectivity α is almost independent on temperature T and background electrolyte (bge) concentration C_{bge} , the mean plate number \bar{N} as well as the resolution R_s greatly improves with increasing concentration of the background

electrolyte from 20 to 40 mM. At a bge concentration c_{bge} of 60 mM the separation deteriorates and also strong peak tailing is observed. At lower temperatures a better separation of the two enantiomers is obtained, but also the migration time is significantly increased.

Table 4. Effect of background electrolyte (bge) concentration and temperature on the resolution R_s , selectivity α and mean plate number \bar{N} . Chromatographic conditions c.f. Figure 7.

T [°C]	c_{bge} [mM]	t_R^a [min]	t_R^b [min]	α	R_s	\bar{N}
20	20	17.35	17.96	1.04	1.6	41 000
50	20	11.55	11.83	1.02	2.3	164 000
20	40	18.39	18.89	1.03	2.9	216 000
50	40	11.33	11.52	1.02	1.56	176 000
20	60	24.53	25.23	1.03	2.5	152 000
50	60	11.09	11.27	1.02	1.1	100 000

2.2.3 Conclusion

In recent years there has been an extensive growth in the use of chiral transition metal complexes for asymmetric catalysis, chiral recognition phenomena, and electron transfer studies. Therefore an increasing demand arises for reliable measurements of the enantiomeric purity of these complexes. The described EKC

separation offers the possibility of determining enantiomeric ratios with minute sample consumption. This is important for purity control in stereoselective synthesis of spacers UV-active transition metal complexes which are commonly employed for biopolymer characterization because of the unique binding properties of the enantiomers to biomolecules e.g. DNA. The carbon chain in *meta*-position offers free and unhindered rotational mobility without disturbing interactions of heteroatoms. The OH group is an ideal linkage function for the attachment of the transition metal complex to a biomolecule or any other surface.

2.3 Synthesis, Characterization, and Luminescence Spectroscopic Accessibility Studies of Tris(2,2'-bipyridine)ruthenium(II)-Labeled Inorganic-Organic Hybrid Polymers

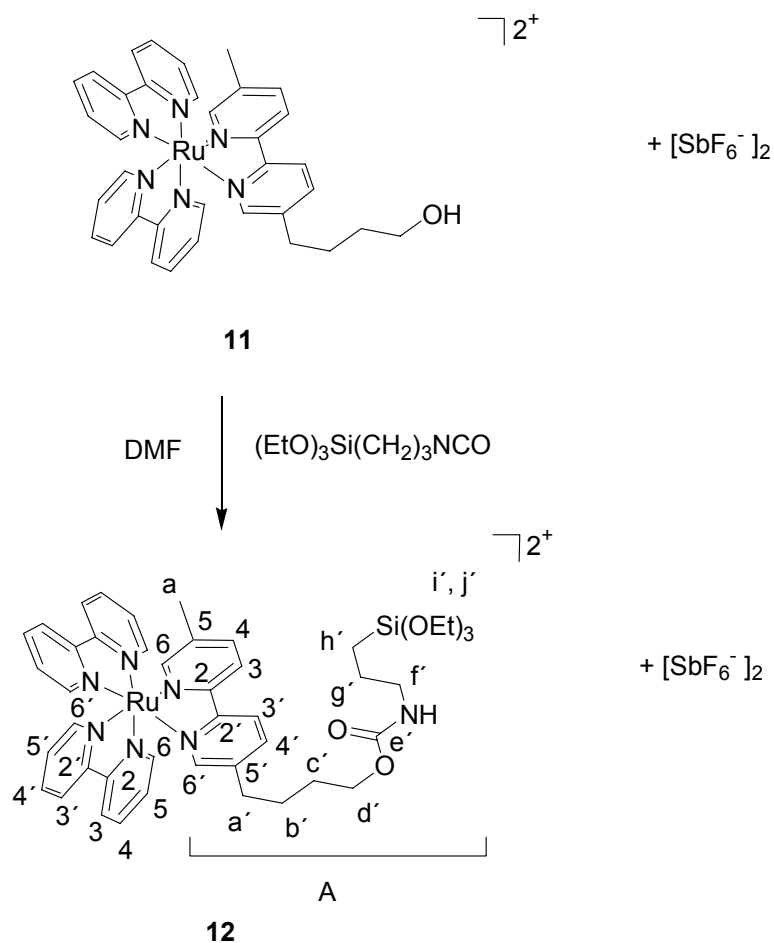
2.3.1 Introduction

Sol-gel processed polysiloxanes are widely investigated as potential supports for reporter molecules in chemical sensors.^{94,95} However, only little use has been made of sol-gel processed polymeric materials as supports for catalytically active transition metal complexes.^{5,14} Upon swelling of the polymer in appropriate

solvents, an interphase is formed, in which solid and liquid phase interpenetrate on a molecular level without forming a homogeneous phase. Ideally, these materials combine the convenient handling of solids with the molecular dispersity of the active sites encountered in homogeneous solutions. Real samples suffer from several problems, among which chemical stability and accessibility of the active centers are the most serious ones. Decomposition of the matrix is reduced by increasing the cross-linking of the polymer, i.e. by using tri- (T) or quater- (Q) functionalized silanes. Leaching of the active centers is impeded by covalently binding them to the matrix via long-chain T-silyl functionalized spacers and by the employment of polyfunctionalized ligands. However, by increasing the cross-linking of the material, the swelling of the polymer in liquids is reduced, which leads to diffusion problems and to markedly reduced accessibilities of the active centers for the reactants dissolved in the mobile phase. A possible approach to solve this dilemma is to use hybrid polymers⁵ instead of pure polysiloxanes. In these hybrid polymers,⁵ the functionalized silanes **12** (Schemes 6 and 7) are subjected to the sol-gel process together with the co-condensation agents **13**, **14**, **15**, **16**, and **17** (Scheme 7). The siloxane groups provide the

desired degree of cross-linking, while the organic substituents of the co-condensation agents are supposed to enhance the swelling ability of the hybrid polymers.

The intention of this study is the optimization of organically modified polysiloxanes as supports for tethered transition metal complexes, which are employed as catalysts in the hydrogenation or hydroformylation of unsaturated organic substrates. In catalytic reactions in heterogeneous systems, turnover rates are determined by the activity of the complex itself, but also by its accessibility for the organic and gaseous reactants.

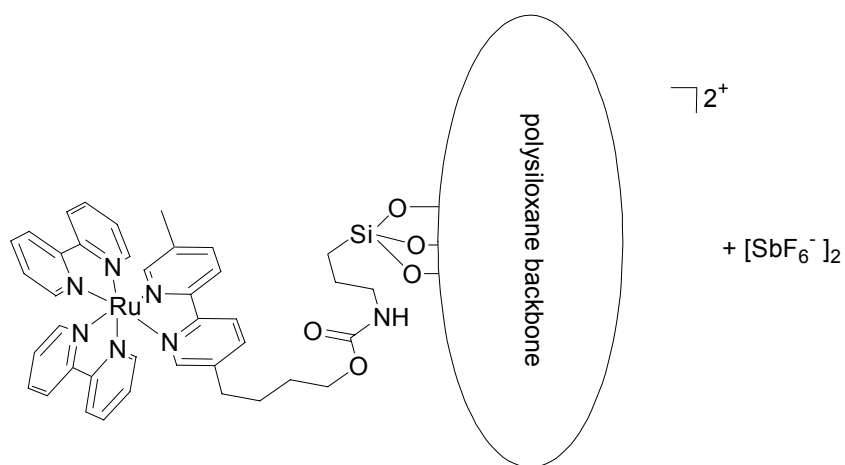
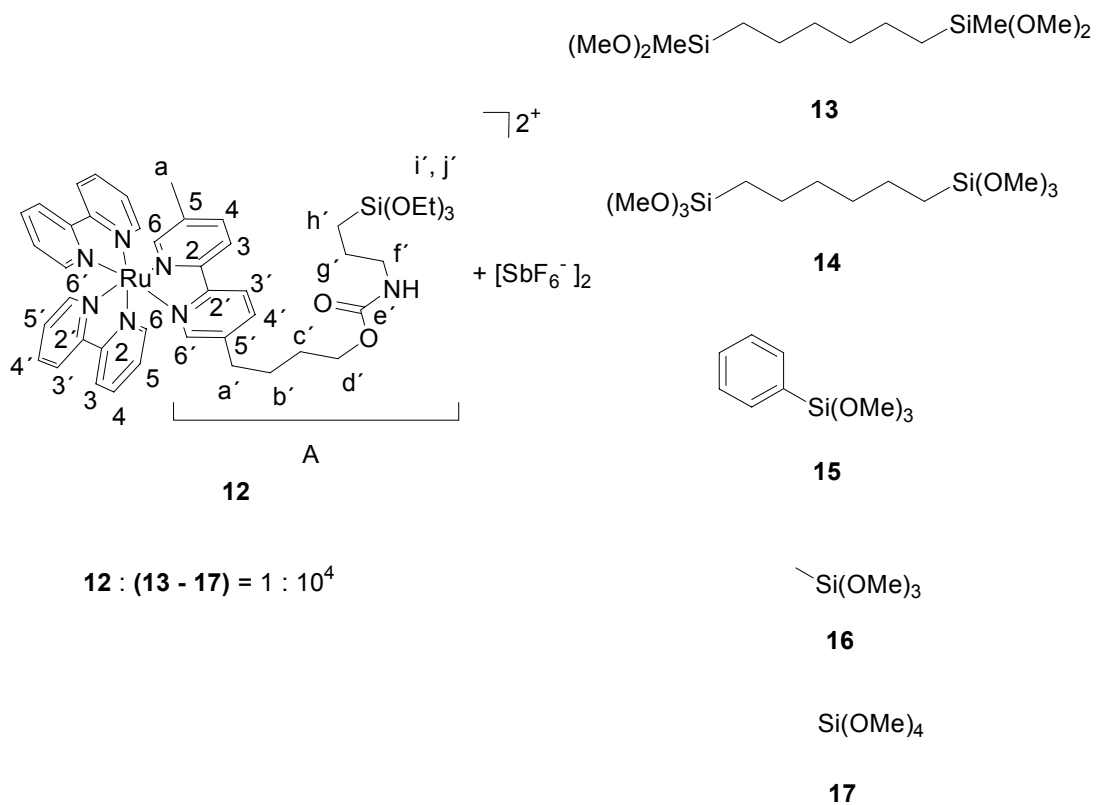


Scheme 6. Synthesis of complex **12**.

A variety of spectroscopic techniques, including NMR and UV/VIS spectroscopy, has been applied to determine the accessibilities and mobilities of reactive centers in polymeric phases. NMR spectroscopy provides mainly information on the polymeric matrix and highly concentrated active centres.^{9,18} For the investigation of species present in the mobile phase at low

concentrations, the highly sensitive UV/VIS luminescence spectroscopy is more appropriate. Ample use has been made of luminescent probes to characterize the microenvironment in sol-gel processed materials.²⁶⁻³⁹ The vast majority of these publications deals with probe molecules sequestered within the matrix, while only few studies employ covalently attached probes.^{40-55,96}

In this work we investigate the bimolecular quenching of the long lived luminescence of the ruthenium(II) complex **12** by energy transfer to dioxygen and anthracene, respectively. The ruthenium complex is either dissolved in solution or covalently bound to the siloxane polymers **18-22** (Scheme 7) which are suspended in different liquids.



polysiloxanes:

$$\mathbf{12 + 13 = 18}$$

$$\mathbf{12 + 14 = 19}$$

$$\mathbf{12 + 15 = 20}$$

$$\mathbf{12 + 16 = 21}$$

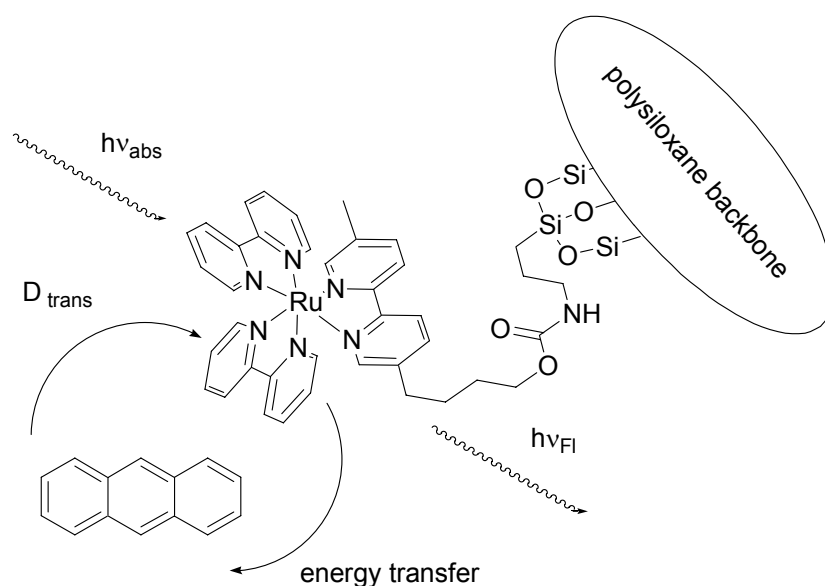
$$\mathbf{12 + 17 = 22}$$

Scheme 7. Co-condensation of complex **12** with the silanes **13–17**.

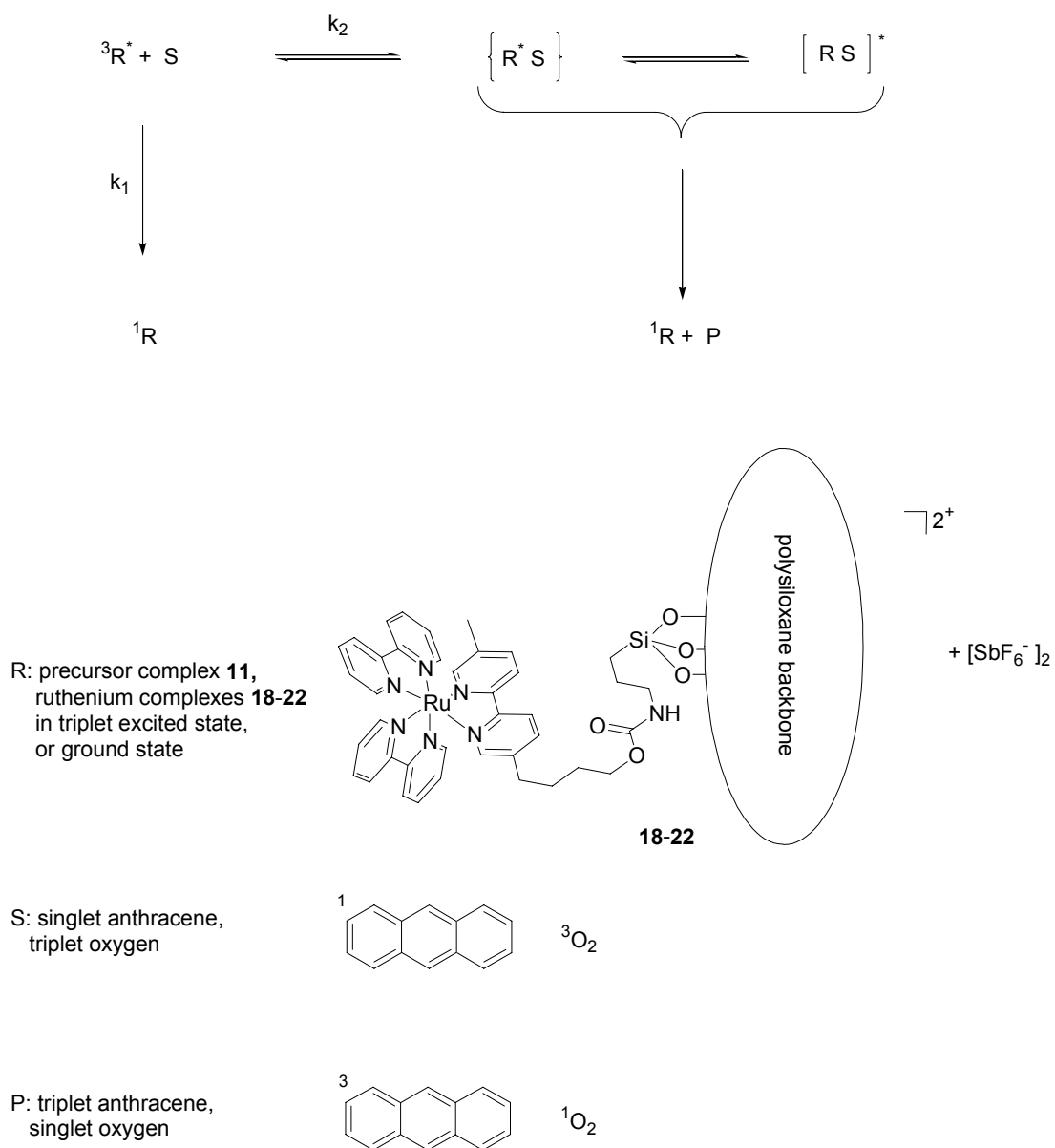
Complexes of the ruthenium(II)–polypyridine family have attracted great attention since they proved to be useful for the design of excitation energy transfer schemes and the storage of excitation energy.⁹⁷⁻⁹⁹ Ruthenium(II)–polypyridine complexes were also interesting in the development of various sensing devices based on luminescence.¹⁰⁰ Light absorption by $[\text{Ru}(\text{bpy})_3]^{2+}$ results in the Franck–Condon singlet metal to ligand charge transfer $^1\text{MLCT}$ excited state which undergoes subpicosecond intersystem crossing to a long lived $^3\text{MLCT}$ excited state $^1\text{R} \xrightarrow{h\nu} ^1\text{R}^* \rightarrow ^3\text{R}^*$.^{101,102} The triplet state decays by nonradiative deactivation and luminescence. Due to their long lifetimes, $^3\text{MLCT}$ excited states are quenched efficiently by electron or energy transfer to appropriate molecules, such as dioxygen and anthracene.¹⁰³⁻¹⁰⁶ Energy transfer takes place by an electron exchange mechanism¹⁰⁷ upon close contact of **12** and the quencher molecules, according to the reactions $^3\text{R}^* + ^3\text{O}_2 \rightarrow ^1\text{R} + ^1\text{O}_2$ and $^3\text{R}^* + ^1\text{A} \rightarrow ^1\text{R} + ^3\text{A}$, respectively (Schemes 8 and 9).

The analysis of the kinetics of luminescence quenching presented in this work will provide a detailed picture of the factors affecting the accessibility of matrix–bound transition metal

catalysts by organic and gaseous reactants dissolved in the liquid phase. The insight thus gained will be useful in the design of new polysiloxane matrices with improved turnover rates in transition metal complex catalyzed hydrogenations and hydroformylations of unsaturated organic compounds.



Scheme 8. Energy transfer Energy transfer takes place by an electron exchange mechanism upon close contact of **12** and the quencher molecules, according to the reactions $^3\text{R}^* + ^3\text{O}_2 \rightarrow ^1\text{R} + ^1\text{O}_2$ and $^3\text{R}^* + ^1\text{A} \rightarrow ^1\text{R} + ^3\text{A}$, respectively.



Scheme 9. Reaction scheme of the quenching reaction between the excited ruthenium complex in the polymers **18-22** and singlet anthracene and triplet atmospheric oxygen.

2.3.2 Results

2.3.2.1 Synthesis of the T-Silyl Functionalized Tris(2,2'-bipyridine)ruthenium(II) Complex **12**

To furnish the starting material **11** with a spacer unit equipped with a terminal T-silyl function, a solution of triethoxysilyl(propyl)-isocyanate in DMF was added in a molar ratio (Scheme 6). An addition reaction takes place, binding the spacer with its isocyanate substituent to the hydroxy group of the 5-(4-hydroxybutyl)-5'-methyl-2,2'-bipyridine moiety of **11**. After column chromatographic purification **12** represents a red solid which is sensitive to moisture and dissolves readily in organic solvents of high polarity due to the ionic character. The composition of **12** was verified by an EI mass spectrum showing the expected molecular peak. Detailed analytical data are summarized in the Experimental Section.

2.3.2.2 Synthesis of the Polymeric Tris(2,2'-bipyridine)-ruthenium(II) Complexes **18-22**

Stationary phases containing tris(2,2'-bipyridine)ruthenium(II) as a reactive center have to be investigated by luminescence spectroscopy in a highly diluted form. Therefore the sol-gel process of **12** was carried out in the presence of high amounts (1:10⁴) of the mono- and bifunctional co-condensation

agents **13**, **14**, **15**, **16**, and **17** (Scheme 7) influencing the properties of the resulting polymeric materials essentially. The properties of sol-gel processed materials strongly depend on the applied reaction conditions such as concentration of the starting materials, amount and type of solvent, temperature, reaction time, drying conditions of the wet gel, and type of catalyst. To ensure the same reaction kinetics for the synthesis of each polymer as a prerequisite for comparable results, the adherence to uniform reaction conditions has to be maintained during the entire hydrolysis and polycondensation procedure.^{5,8} THF/Methanol (1/5 v/v) was added during the sol-gel process to homogenize the reaction mixture. (*n*-Bu)₂Sn(OAc)₂ is an appropriate catalyst, which does not interfere with **12**.¹⁴

¹H and ¹³C{¹H} NMR spectra of **12** reveal the expected resonances. The ²⁹Si solid state and ¹³C CP/MAS NMR spectra of the polymeric materials **18–22** ($\gamma = 10^4$) are dominated by the polymeric parts of **13–17**. Hence no ²⁹Si signals for the polycondensed Tⁿ-functions of **12** are observed. In the case of **18** two very small signals are observed for D⁰- and D¹- silyl species, and an intense resonance occurs for the nearly complete hydrolyzed co-condensation agent. The ²⁹Si CP/MAS NMR

spectrum of **19** reveals resonances for T²- and T³- silyl groups, in which the T²- signal is more intense than that one of T³. This observation is in agreement with former results and points to a medium cross linkage of the polymer. Both spectra are similar to those of the single hybrid polymers **Dⁱ-C₆-Dⁱ** and **T^m-C₆-T^m** which were reported recently.^{14,16} Because of the long distance to the next proton the ²⁹Si CP/MAS NMR spectrum of **20** was not measurable. In the case of the polymer **21** the ²⁹Si CP/MAS NMR spectrum is characterized by two resonances of different intensities which are assigned to T²- (small) and T³- (intensive) silyl species. The ¹³C CP/MAS NMR spectra of the stationary phases **18**, **19**, and **22** show resonances at δ 50.0 which are attributed to the carbon atoms of the silicon bound methoxy groups. Because of steric effects the portion of non-hydrolyzed methoxy residues is higher in the case of the polymer **19**. All polymers **18–22** were aged at 90°C to increase the cross linkage. However, the concentration of residual methoxy groups is rather small, because hydrolysis and condensation of the materials must be fairly complete as is obvious from the similarity of the experimentally determined elemental analyses and the values calculated for fully reacted materials.

2.3.2.3 Scanning Electron Micrographs

The scanning electron micrographs of the polymers **18–22** show irregularly shaped particles with broad size distributions, the diameters ranging from several hundred nanometers to some ten

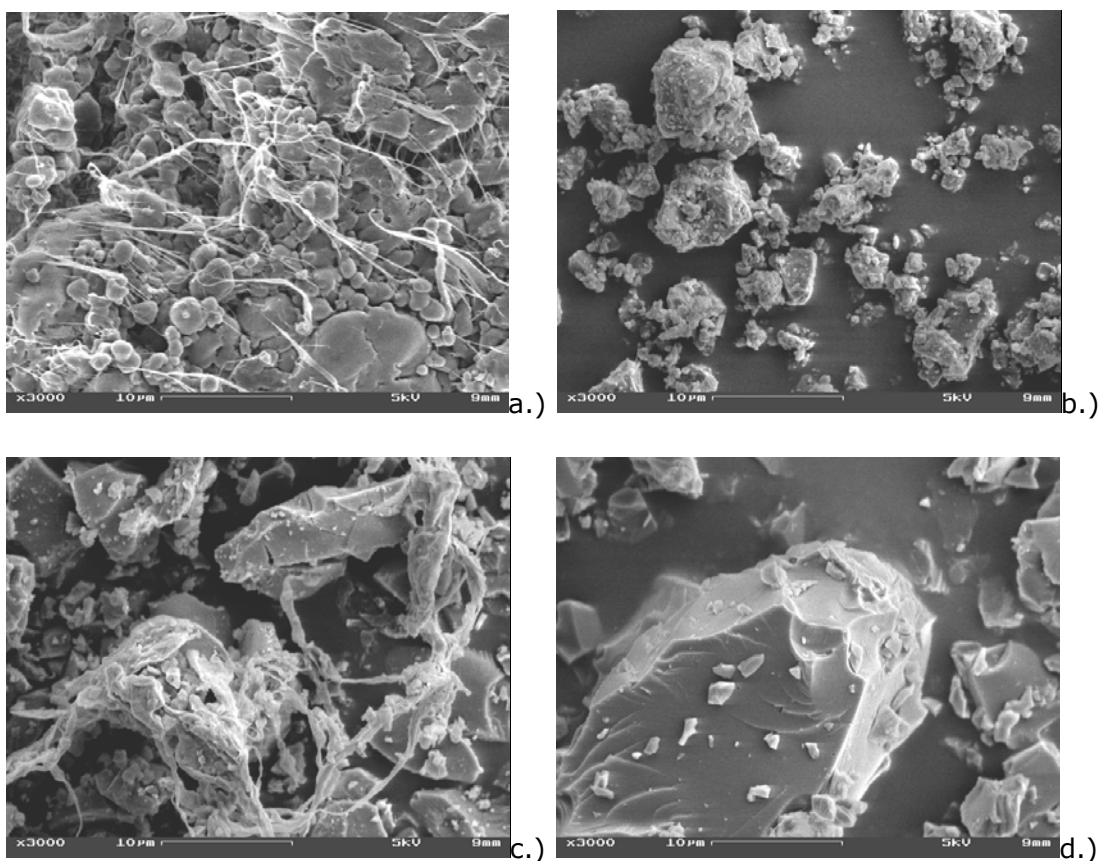


Figure 8. Scanning electron micrographs of polymers **20** (a), **22** (b), **21** (c), and **18** (d). The samples have been ground and sputtered with carbon. Magnification 3000 fold, acceleration voltage $U = 5$ kV.

micrometers. The Q type polymer **22** shows the sharp edges and conchoidal fractures which are typical for brittle, amorphous

materials. The same is true for the hybrid polymers **18**, **19**, and **21** (Figure 8).

In samples of polymer **21**, the irregular particles are accompanied by fibers, whose diameters are between some 100 nm and some 1 μm . In polymer **20**, particles of nearly globular shapes are observed, which are connected by fibers with diameters of some 10 nm to 100 nm. Obviously polymers **18**, **19**, and **22** form three-dimensional networks, whereas in polymers **20** and **21** considerable fractions of low-dimensional structures are found.

2.3.2.4 Luminescence Spectroscopic Investigations

2.3.2.4.1 Luminescence and Luminescence Excitation Spectra of **11**

Figure 9 presents the UV/VIS absorption and luminescence spectra of the ruthenium complex **11** in acetonitrile solution. The maxima of the $^1\text{MLCT}$ absorption and the $^3\text{MLCT}$ luminescence bands of **11** are found at $\tilde{\nu}_{\text{abs}}^{\text{MLCT}} = 22000 \text{ cm}^{-1}$ and $\tilde{\nu}_{\text{em}}^{\text{max}} = 15700 \text{ cm}^{-1}$, respectively. These spectral positions are very similar to those observed for the unsubstituted tris(2,2'-bipyridine)ruthenium(II) complex ($\tilde{\nu}_{\text{abs}}^{\text{MLCT}} = 22000$ and

$\tilde{\nu}_{\text{em}}^{\text{max}} = 16600 \text{ cm}^{-1}$).¹⁰⁸ Whereas the $^1\text{MLCT}$ absorption band does

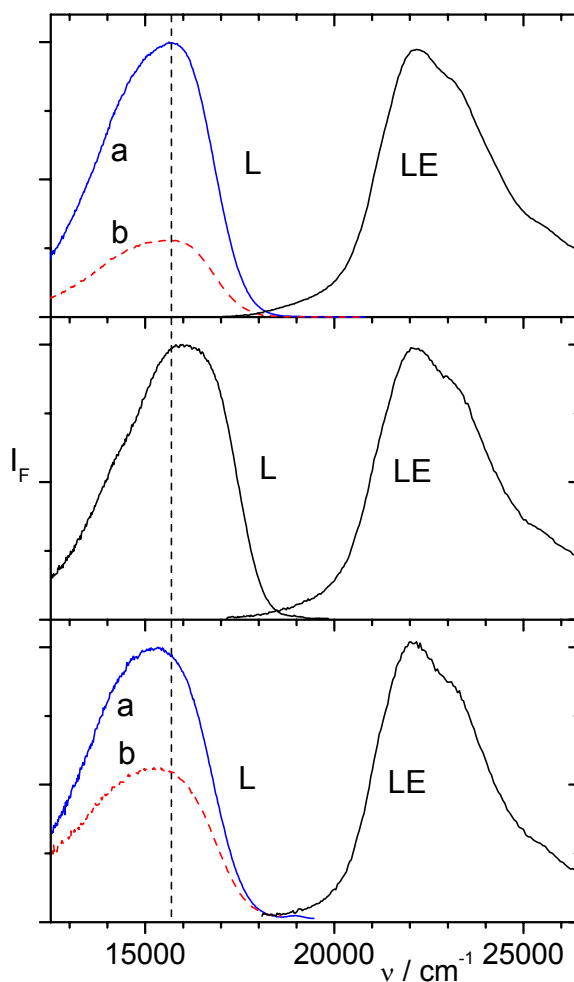


Figure 9. Luminescence (L) and luminescence excitation spectra (LE) of **11** in acetonitrile solution (top panel), of **22** (middle panel) and **18** (bottom panel), both polymers suspended in acetonitrile, (a) under nitrogen atmosphere, (b) quenched by anthracene. Excitation at $\tilde{\nu} = 22000 \text{ cm}^{-1}$, luminescence observed at $\tilde{\nu} = 15700 \text{ cm}^{-1}$.

not show a noticeable solvent dependence, the spectral positions of the luminescence maxima vary significantly, due to the different extents of the stabilization of the $^3\text{MLCT}$ excited state by the various solvents.¹⁰⁹ Whereas in methanol, acetone, and acetonitrile

Table 5. Spectral positions of the luminescence maxima ($\tilde{\nu}$ in cm^{-1})^a of **11** in solutions and of **12** in polymers **18–22**, suspended in a series of liquids.

Sample Solvent	18	19	20	21	22	11
MeOH	15300	15710	15750	15490	16040	15740
MeCN	15300	15650	15330	15410	15970	15695
Acetone	15270	15650	15360	15490	16050	15730
THF	15090	15650	15240	15360	16010	15510
DCM	15380	16050	15480	15500	16020	16330

^a Statistic error is about 5 %.

the luminescence maxima are found at approximately $\tilde{\nu}_{\text{em}}^{\text{max}} = 15700 \text{ cm}^{-1}$, the maximum in THF is red-shifted by $\Delta\tilde{\nu} = 200 \text{ cm}^{-1}$. In DCM where the luminescence spectrum is remarkably structured, the maximum is observed at

$\tilde{\nu}_{\text{em}}^{\text{max}} = 16300 \text{ cm}^{-1}$ (see Table 5). Upon co-polycondensation of the T-silyl functionalized ruthenium complex **12** with the silanes **13–17** and swelling the resulting polymers **18–22** (Scheme 7) in different solvents, the spectral positions of the luminescence maxima undergo slight, but noticeable changes against the values observed for **11** in solution. The spectral shifts correlate with the extent of solvation of the ruthenium complexes by the liquids. In Q type materials, the luminescence maxima are located at $\tilde{\nu} \approx 16000 \text{ cm}^{-1}$ (Figure 9) independent on the solvent (Table 5). This blue-shift, $\Delta\tilde{\nu} = 500 \text{ cm}^{-1}$ in the case of THF, is due to the rigidity of the immediate environment of the luminescence probe, i.e., the absence of significant solvent relaxation during the excited state lifetimes of the ruthenium complex.¹⁰⁹ In the swollen hybrid polymers **18–21**, efficient solvent relaxation is observed, i.e. the luminophores are well solvated by the solvent molecules, whose mobility is comparable to that in bulk liquids.¹¹⁰ In the suspended polymer **19**, the spectral positions are very close to those in homogeneous solutions. In **18**, **20**, and **21** the luminescence maxima are red shifted by $\Delta\tilde{\nu} \approx 100 - 500 \text{ cm}^{-1}$ compared to the spectral positions of **11** in solutions of the respective solvents

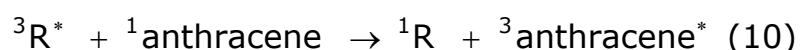
(Figure 9). However, in the case of **20** in methanol, where the polymer is not wetted by the solvent, the luminescence maximum is slightly blue shifted against solution.

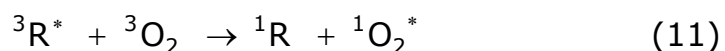
2.3.2.4.2 Kinetic Analysis of Luminescence Decay Curves

An ideal interphase represents a solution-like state. With the simple assumption of such an ideal interphase, the deactivation rate $-d[R^*]/dt$ of photoexcited ruthenium(II) complexes can be described by conventional kinetics for homogeneous systems (Scheme 8 and 9):

$$-\frac{d[R^*]}{dt} = (k_1 + k_q \cdot [S]) \cdot [R^*] \quad (9)$$

Here $[R^*]$ is the concentration of ^3Ru complexes in the materials **11** and **18–22**, and $[S]$ is the concentration of a potential reactant that is dissolved in the mobile liquid compound of the interphase. The rate constant k_1 describes spontaneous deactivation of R^* to the inactive electronic ground state, and k_q the deactivation by interaction with S . The larger k_q the more mobile is S in the interphase. As model reaction we chose intermolecular transfer of excitation energy accompanied by double spin flip, namely





These reactions are possible only by an exchange mechanism after close contact between ${}^3\text{R}^*$ and S or after formation of an exciplex ${}^{1,3}(\text{RS})^*$ (Scheme 9).

In a pulsed laser experiment followed by single photon counting of R^* luminescence, the concentration of $[\text{R}^*]$ is always by orders of magnitude lower than S, $[\text{R}^*] \ll [\text{S}] \approx \text{const.}$, so that equation (9) can be integrated according to

$$[\text{R}^*] = [\text{R}^*]_0 \cdot e^{-(k_1+k_2)t} \quad (12)$$

where $[\text{R}^*]_0$ is the concentration of the excited 3 ruthenium complexes at $t = 0$, and $k_2 = k_q \cdot [\text{S}]$. In a semi-logarithmic plot, equation (12) should give a straight line of 3 ruthenium luminescence intensity versus time. This behavior is observed for **11** in homogeneous solution over 2–3 intensity decades and a large range of anthracene and oxygen concentrations so that k_2 and – if $[\text{S}]$ is known – also k_q can directly be determined from equation (12). However, in interphases formed from **18–22** with a variety of liquids, almost all quenching experiments yield strongly non-exponential decay curves. In order to approximately eliminate

the contribution of fluctuations in k_1 to non-exponentiality (see section 2.3.2.4.3) the decay curves in the presence of S are divided by the decay curves for $[S] = 0$. As long as equation (12) is valid, one obtains for the relative luminescence quenching efficiency at a given time t after the laser flash

$$1 - \frac{[R^*]}{[R_{S=0}^*]} = 1 - e^{-k_2 t} \quad (13)$$

i.e. a straight line in the semi-logarithmic presentation. In real systems the curves bend, and very often a constant plateau at $t \rightarrow \infty$ reveals. This type of curves can be approximated with good accuracy by

$$1 - \frac{[R^*]}{[R_{S=0}^*]} = \alpha \cdot [1 - e^{-k_2 t}] \quad (14)$$

where $0 \leq \alpha \leq 1$ defines an *accessibility factor* α , i.e. the fraction of excited ³ruthenium complexes that are able to convert S into P whereas the fraction $(1-\alpha)$ is non reactive ($k_2 \rightarrow 0$). From the product point of view, the accessibility factor α gives the ratio of actual product yield to the maximum possible product yield at

$$t \rightarrow \infty, [P_{\max}] = [R_0^*] \frac{k_2}{(k_1 + k_2)},$$

$$\alpha = \frac{[P](t \rightarrow \infty)}{[P_{\max}](t \rightarrow \infty)} = \frac{1 - \frac{[R^*]}{[R_{S=0}^*]}}{(1 - e^{-k_2 t})} \quad (15)$$

All time-resolved experiments of this study were evaluated according to equation (15).

2.3.2.4.3 Luminescence Decay Curves of **11 and **18–22** without Quencher**

The luminescence decay curves of **11** dissolved in low viscous solutions are single exponential with decay times of $\tau_F \approx 750 - 950$ ns. For suspensions of the labeled polysiloxanes **18–22** in all investigated solvents, slightly non-exponential decay curves are observed.

This type of decay curves is best described by narrow distributions of decay times, but can also be fitted by sums of two exponential functions without loss of accuracy. In polymer **22**, both components are longer lived than the corresponding lifetime of **11** in solution, due to the rigidity of the matrix which reduces non-radiative deactivation rates.¹⁰⁹ For suspensions of **22** in all liquids, almost identical values of $\tau_1 \approx 1.0$ μ s and $\tau_2 \approx 1.8$ μ s were found for short and long components, respectively. The same values are obtained in the case of **20** in methanol, where the

polymer is not swollen by the solvent. In all other cases the polymers **18–21** exhibit short lifetime components which are close to the decay time of **11** in the corresponding homogeneous solutions, while the long components vary between $\tau_2 \approx 1.1 \mu\text{s} - 1.3 \mu\text{s}$, depending on the polymer and the suspending liquid.

The short lifetime component is ascribed to ruthenium complexes which are solvated by the liquid phase, whereas the long lifetime component is due to complexes whose primary “solvation shell” is formed by the rigid polymer network.¹⁰⁹

2.3.2.4.4 Luminescence Decay Curves of 11 and 18–22 in the Presence of Oxygen

Quenching of ruthenium luminescence by energy transfer to dioxygen¹¹¹ is a bimolecular process, which requires close contact between donor and acceptor.

The efficiency of luminescence quenching thus depends on both the mobility of oxygen in the interphase and the accessibility of the transition metal complex. The steady state luminescence spectra shown in Figure 9 demonstrate that the quenching efficiency in organically modified polysiloxanes is significantly enhanced compared to unmodified Q type materials. Evaluation of

the time-resolved luminescence decay curves according to equation (15) yields values for k_2 and α , which describe the

Table 6. Quenching rate constants^a $k_2 / 10^6 \text{ s}^{-1}$ and accessibility factors, α (in parentheses), for the luminescence quenching by oxygen ($p(\text{O}_2) = 0.21 \text{ bar}$) in solutions of **11** and suspensions of polymers **18–22** in a series of solvents. The values of k_2 and α are obtained by evaluation of the corresponding luminescence decay curves according to eq. (15)

Sample	18	19	20	21	22	11
Solvent						
MeOH	4.1 (0.71)	3.8 (0.71)	2.4 (0.45)	3.4 (0.88)	1 (0.03)	3.9 (1)
MeCN	4.2 (0.73)	4.2 (0.71)	3.0 (0.89)	3.9 (0.91)	1.7 (0.10)	4.7 (1)
Acetone	4.1 (0.77)	3.1 (0.83)	3.9 (0.98)	3.6 (0.90)	3.9 (0.06)	4.3 (1)
THF	2.8 (0.53)	2.8 (0.67)	2.8 (0.95)	3.0 (0.85)	1 (0)	3.4 (1)
DCM	1.6 (0.66)	1.4 (0.67)	1.5 (0.98)	1.6 (0.89)	4.8 (0.08)	1.4 (1)

^a Statistic error is about 5 %.

mobility of oxygen and the fraction of accessible ruthenium complexes, respectively (Figure 10 and Table 6). In homogeneous solutions of **11**, $\alpha \approx 1$, i.e. all ruthenium complexes are equally accessible by oxygen (Figure 11 and Table 6). The rate constants

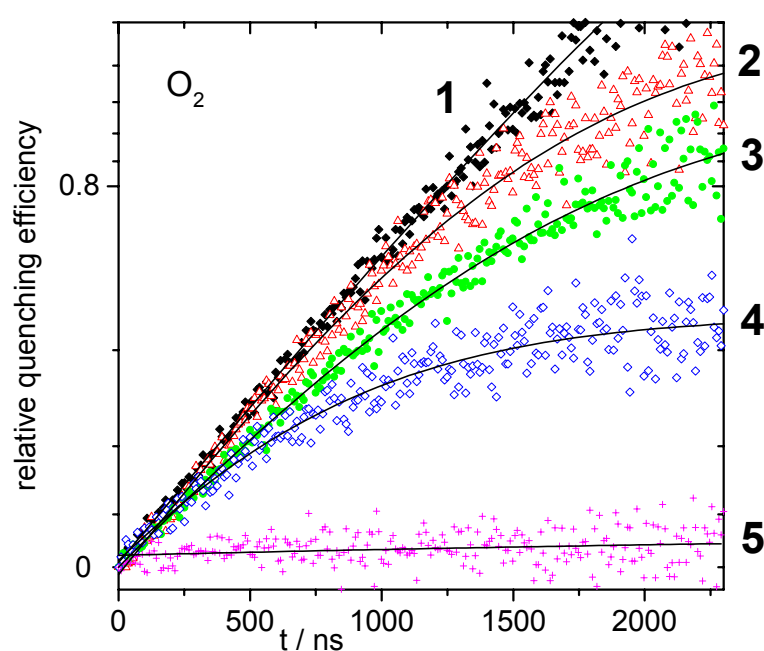


Figure 10. Relative efficiencies, $1 - \frac{[R^*]}{[R^*]_{S=0}}$, for the quenching of ruthenium luminescence by oxygen. The curves are calculated from the corresponding luminescence decay curves according to eq. (15). (1) **11** in dichloromethane solution, (2) **20**, (3) **21**, (4) **18**, and (5) **22**, all polymers suspended in dichloromethane. The concentration of oxygen in the liquid phases is $c(\text{O}_2) \approx 2 \cdot 10^{-3}$ M.

k_2 are far below the diffusion controlled limit for all solvents.¹¹² The ratios between the quenching rate constant k_q , calculated from k_2

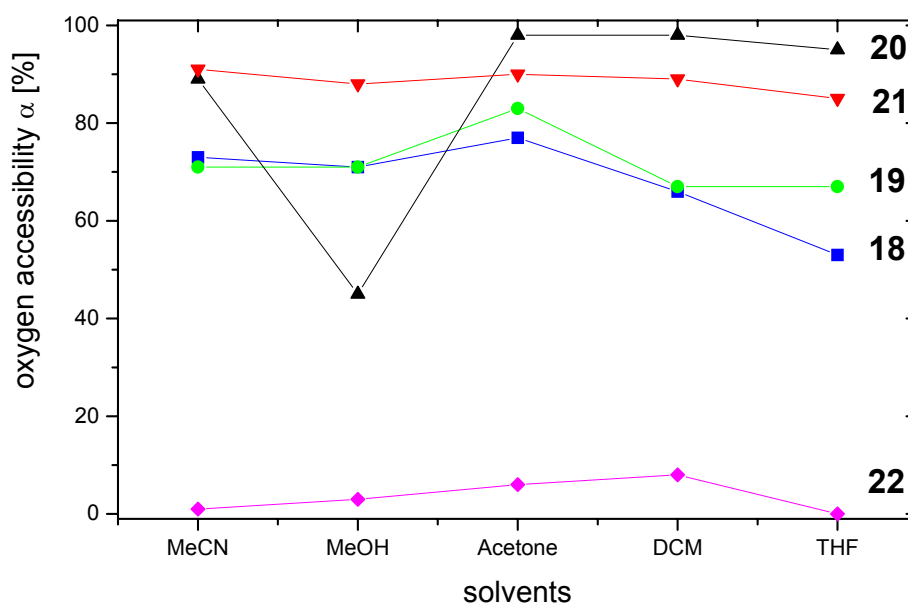


Figure 11. Accessibility factor α for luminescence quenching by oxygen in the polymers **18–22**, suspended in a series of solvents. The values of α are obtained by evaluation of the corresponding luminescence decay curves according to eq. (15).

and the concentration of oxygen by $k_q = k_2 / c[\text{O}_2]$, and the rate

constants of diffusion k_d , are approximately $\frac{k_q}{k_d} \approx 0.05$ for all

solvents, except for dichloromethane for which $\frac{k_q}{k_d} \approx 0.02$ is found.

These values are in close agreement with literature data for $[\text{Ru}(\text{bpy})_3]^{2+}$.¹¹²

In the polymers **18–22**, the fraction of accessible ruthenium complexes α varies considerably with both the type of the polymer and the suspending liquid (Figure 10 and 11). In polymer **22** only a minor fraction of the tethered complexes is accessible to oxygen, due to the high degree of cross linking in this material. The polymers **18** and **19**, which are prepared from bifunctional monomers, behave very similarly with respect to the accessibility by oxygen. The fraction of accessible groups α in these polymers is around 0.5 – 0.8, the lower values being found in liquids of medium and large dielectric constants. In polymer **21**, the fraction of accessible complexes is $\alpha \approx 0.9$, regardless of the suspending liquid. In contrast to all other polymers, material **20** shows a strong dependence of the accessibility on the solvent. Whereas $\alpha \rightarrow 1$ in less polar solvents like THF, DCM or acetone, in acetonitrile and methanol values of $\alpha \approx 0.9$ and $\alpha \approx 0.45$ are found, respectively. Obviously, the replacement of the methyl group by a phenyl substituent in the silane monomers imparts a strongly hydrophobic nature to the polymer, which impedes its penetration by hydroxylic solvents.

For nearly all polymers in most liquids, the quenching rate constants k_2 are close to the values observed for **11** in the corresponding solutions (Table 6). This indicates that those ruthenium complexes whose luminescence is quenched by dioxygen are well solvated by the liquid phase.

In cases where the solvent does not penetrate the polymer (e.g. **20** in methanol), k_2 is significantly lower than for **11** in solution. For all polymers in DCM k_2 is slightly larger than the corresponding solution value. This indicates that the factors which lead to the unusually low value $\frac{k_q}{k_d}$ in dichloromethane solution are not fully effective in the polymers. The ruthenium complexes are either not completely solvated by DCM or the reorientational motions of dichloromethane molecules are impeded by the polymer matrix.¹¹⁰

In summary, two types of ruthenium complexes can be distinguished in organically modified polysiloxanes. The first type is not accessible to oxygen dissolved in the liquid phase. The luminescence of the second type is quenched by oxygen with rate constants which are close to those obtained for ruthenium complexes dissolved in solvents. In liquids of low and medium

polarity, polymer **20** provides solution like accessibilities, whereas in highly polar solvents polymer **21** shows the best results. Acetone represents an all purpose solvent, with α values ≥ 0.7 for all polymers.

2.3.2.4.5 Luminescence Decay Curves of 11 and 18–22 in the Presence of Anthracene as Quenching Substrate

In order to determine the accessibility of tethered ruthenium complexes for organic molecules, anthracene is added to the liquid phase of polymer suspensions. Energy transfer from the $^3\text{MLCT}$ excited state of the ruthenium complex to anthracene leads to the quenching of ruthenium luminescence. In solution, quenching results in the reduction of luminescence lifetimes, the decay curves remaining single exponential (Figure 12). In the polymers, luminescence decay curves reveal two components, each representing a narrow distribution of decay curves with distinctly different mean decay times. The lifetime of the long component is approximately the same as the mean lifetime in the unquenched case. The lifetime of the short component decreases with increasing anthracene concentrations. From the luminescence decay curves the rate constants k_2 and accessibility factors α for the quenching process are calculated according to eq. (15). In

solutions of **11**, $\alpha = 1$ is obtained, i.e., all ruthenium complexes are equally accessible by anthracene (Table 7). From the observed

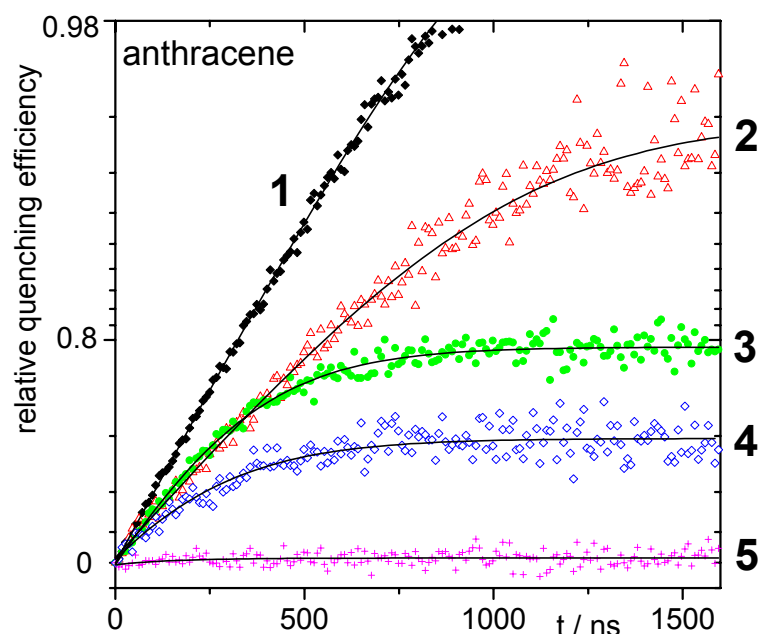


Figure 12. Relative efficiencies, $1 - \frac{[R^*]}{[R^*]_{S=0}}$, for the quenching of ruthenium luminescence by anthracene. The curves are calculated from the corresponding luminescence decay curves according to eq. (15). (1) **11** in dichloromethane solution, (2) **20**, (3) **21**, (4) **18**, and (5) **22**, suspended in dichloromethane. The concentration of anthracene in the liquid phases is $c(\text{anthracene}) \approx 5 \cdot 10^{-4}$ M.

Table 7. Quenching rate constants^a $k_2 / 10^6 \text{ s}^{-1}$ and accessibility factors, α (in parentheses), for the luminescence quenching by anthracene ($c(\text{anthracene}) \approx 5 \cdot 10^{-4} \text{ M}$ in the liquid phases) in solutions of **11** and suspensions of polymers **18–22** in a series of solvents. The values of k_2 and α are obtained by evaluation of the corresponding luminescence decay curves according to eq. (15)

Sample	18	19	20	21	22	11
Solvent						
MeOH	5.6 (0.80)	3.0 (0.62)	8.6 (0.45)	3.9 (0.78)	1 (0.22)	5.1 (1)
MeCN	3.8 (0.69)	7.0 (0.66)	3.4 (0.77)	8.6 (0.81)	– (0)	7.0 (1)
Acetone	4.6 (0.60)	4.4 (0.51)	3.2 (0.96)	5.3 (0.79)	6.3 (0.04)	5.1 (1)
THF	3.1 (0.46)	2.9 (0.50)	1.5 (0.88)	5.1 (0.69)	– (0)	9.4 (1)
DCM	4.6 (0.60)	9.9 (0.57)	3.2 (0.96)	5.1 (0.79)	6.3 (0.04)	5.1 (1)

^a Statistic error is about 5 %.

k_2 values, the quenching constants k_q are obtained by $k_q = k_2 / c_A$, where c_A is the concentration of anthracene ($c_A = 5 \cdot 10^{-4} \text{ M}$). The

quenching rate constants k_q are close to the diffusion rate constants k_d which are calculated by $k_d = 4\pi N_A R D$, where N_A is Avogadro's number, R represents the encounter radius ($R = 0.8$ nm), and D is the diffusion coefficient of anthracene in the respective solvent. The fraction of successful encounters is found to be $k_q/k_d \approx 0.5 - 1$ for the solvents used in this study. In the polymeric materials, the kinetics of quenching by anthracene are in close analogy to the quenching by oxygen. Two kinds of ruthenium complexes can be distinguished. One of these populations is not quenched by anthracene, whereas the other one is quenched with the rate constant k_2 . In the hybrid polymers **18–22** the k_2 values reach approximately 80 – 90% of the values observed for **11** in homogeneous solutions. Remarkably low values are observed for polymers suspended in THF. The accessibility factors α found for anthracene are slightly smaller than those observed for oxygen (Figure 13 and Table 7). However, the dependence of α on polymer and suspending liquid observed for anthracene and oxygen are similar. In the Q type material **22**, the ruthenium complexes are practically not accessible by anthracene. Only in methanol a significant fraction of complexes is reached by the organic quencher. In the polymers **18** and **19**, formed from bifunctional

monomers accessibilities vary between $\alpha \approx 0.4$ for less polar solvents and $\alpha = 0.8$ for highly polar solvents. In polymer **21**, accessibility factors are $\alpha \approx 0.7 - 0.8$, practically independent on the liquid phase. Maximum accessibilities of $\alpha \approx 0.9 - 0.95$ are

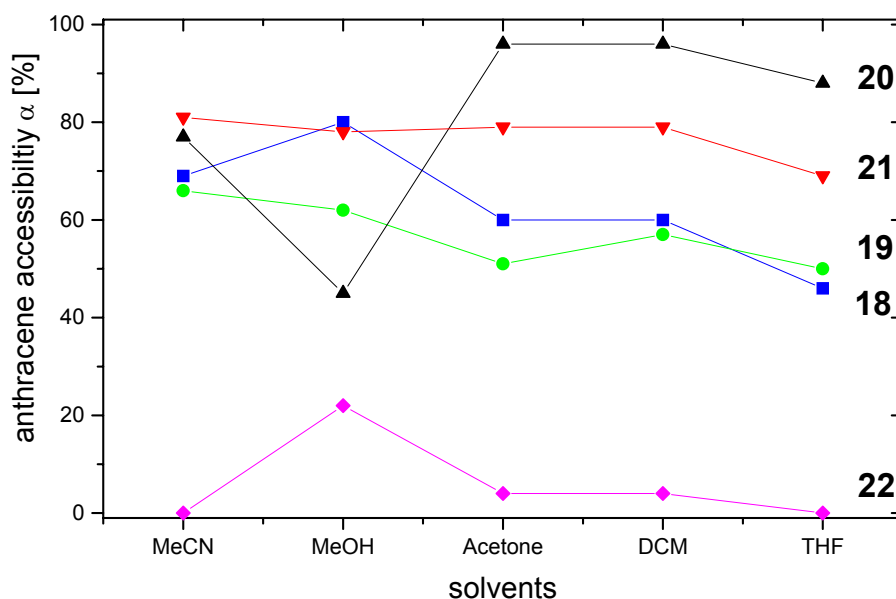


Figure 13. Accessibility factor α for luminescence quenching by anthracene in the polymers **18–22**, suspended in a series of solvents. The values of α are obtained by evaluation of the corresponding luminescence decay curves according to eq. (15).

achieved for polymer **20** in solvents of low and medium polarity, whereas in acetonitrile and methanol only values of $\alpha \approx 0.8$ and $\alpha \approx 0.45$ are obtained, respectively.

2.3.3 Conclusion

The triethoxysilane modified ruthenium(II)–tris(bipyridyl) complex **12** was synthesized and sol–gel–processed with a series of different silane monomers to give the new organically modified polysiloxanes **18–22**, which serve as model systems for inorganic–organic hybrid catalysts employed in hydrogenation and hydroformylation reactions. The materials were characterized by solid–state NMR spectra, BET measurements, elemental analysis, scanning electron microscopy, as well as steady–state and time–resolved luminescence spectroscopy. With the exception of polymer **19**, all materials have small BET surface areas ($A < 5 \text{ m}^2/\text{g}$). This result is supported by the absence of visible pores in SEM pictures. The appearance of polymer particles in the SE micrographs suggest that polymers **18**, **19**, and **22** are brittle particles with highly cross linked three–dimensional structures, whereas **20** is a soft material with low–dimensional cross linking. Polymer **21** shows an intermediate behavior.

Steady-state and time-resolved luminescence spectroscopy provides a detailed picture of the materials on the molecular level. Spectral shifts of the luminescence spectra and long luminescence decay times reveal that ruthenium complexes in the unmodified polysiloxane are solvated by a rigid solvation shell, which is probably formed by the polymer matrix itself. Ruthenium complexes in the organically modified polysiloxanes **18**, **19**, and **21** are preferentially solvated by the liquid phase. In the phenyl-modified polymer, the degree of solvation by the liquid depends strongly on the polarity of the liquid. Liquids of low and medium polarity provide high degrees of solvation, whereas highly polar, hydroxylic solvents like methanol do not even wet the particles. The non-exponential luminescence decay curves observed in all polymers indicate that complexes with distinctly different solvation conditions are existent.

Time-resolved studies of luminescence quenching by oxygen and anthracene reveal that the tethered ruthenium complexes can be divided into two populations. One of these populations is not accessible by the quenchers, while the other one is quenched with rate constants which approach the values observed in homogeneous solutions. The accessibilities established for

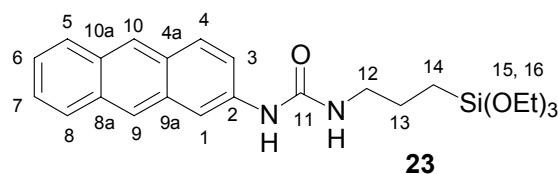
anthracene fall slightly below those obtained for oxygen, which is mainly due to the larger size of the organic molecule. In the unmodified Q type material, the fraction of accessible ruthenium complexes is close to zero, irrespective of the suspending liquid. Solution-like accessibilities are found for the hybrid polymers **20** and **21** in solvents of low and medium polarity. In polar solvents, especially in methanol, the accessibility in the phenyl-containing polymer is poor, due to the reduced penetration of the polymeric networks by these solvents. In polar solvents, polymer **21** and to a lesser extent polymers **18** and **19**, provide good accessibilities for both oxygen and anthracene.

2.4 Novel Mesoporous Stationary Phases Incorporating Anthracene as Interaction Centers and their Application in HPLC

2.4.1 Introduction

The preparation and application of mesoporous materials using surfactants as templates have attracted great attention since the discovery of the M41S family as mesoporous molecular sieves by the Mobil Corporation.^{113,114} So far, most synthetic methods typically yield products in form of fine powders used in catalysis

and in separation technologies. In this communication we combine the advantage of an easy template synthesis for mesoporous materials with the incorporation of an anthracene derivative as an interaction center. Variation of the anthracene concentration in these new materials determines the column properties. Thus, shape selectivity of these stationary phases and conclusively their separation efficiency in HPLC applications can be controlled.



24, silica modified with **23**

25, **23** : Si(OEt)₄ 1: 30

26, **23** : Si(OEt)₄ 1: 40

Scheme 10. *Synthesis of the mesoporous polymers.*

2.4.2 Results

For the access to the ordered mesoporous hybrid materials **25** and **26** (Scheme 10) a template synthesis was necessary.^{115,116} Spaced interaction centers such as N-2-anthracenyl-N'-[3-(triethoxysilyl)propyl]urea¹¹⁷ **23** which are latterly used for liquid chromatography were introduced into the starting materials.¹¹⁸⁻¹²⁴ The modified silica gel **24** was synthesized according to literature methods and afforded a novel reversed

phase separation material.⁵³ The mesoporous materials **25** and **26** were obtained in the presence of *n*-hexadecylamine as template which concomitantly serves as a catalyst. The precursors and the co-condensation agent Si(OEt)₄ (TEOS) were sol-gel processed in different ratios (Scheme 10). A mixture of EtOH and H₂O was employed to improve the solubility of the template. The properties of the polycondensation products strongly depend on boundary conditions, such as concentration of the monomers, type of solvents, temperature, reaction time, and kind of catalyst. To ensure comparable results, uniform reaction conditions throughout hydrolysis and the sol-gel transition must be maintained. After sol-gel processing at ambient temperature the amine was removed from the xerogels by Soxhlet extraction with ethanol. The purity of all materials after removing the template was proved by using CP-MAS (cross polarization-magic angle spinning) solid-state NMR techniques. The ¹³C CP-MAS NMR spectra of the materials **24–26** show the expected peaks for the respective carbon atoms: δ 127 (anthracene), δ 157 (carbonyl), δ 43, 23, and 9 (spacer). The resonances for the carbon atoms of the non-hydrolyzed Si-O-Et groups are found at δ 59 and 15. No relevant ¹³C signals for the template could be found. All ²⁹Si CP-MAS NMR spectra of **24–26**

show resonances for $\text{Si}(\text{OSi})_4$ (Q^4 δ -110), $(\text{HO})\text{Si}(\text{OSi})_3$ (Q^3 δ -101), $\text{RSi}(\text{OSi})_3$ (T^3 δ -66), and $\text{R}(\text{HO})\text{Si}(\text{OSi})_2$ (T^2 δ -56) groups. In the case of the modified silica gel **24** the ^{29}Si CP-MAS NMR spectrum indicates more hydrolyzed T-groups which is in agreement with the ^{13}C CP-MAS NMR spectrum. Further characteristics of the materials **24–26** were gained by elemental analysis, scanning electron microscopy (SEM), and HPLC separation technology. Typical elemental analyses for **24–26** in wt% are: C, 10.40; H, 1.17; N, 1.51 for **24**. C, 14.92; H, 2.81; N, 1.61 for **25**. C, 13.57; H, 1.94; N, 1.10 for **26**. The N values for **25** and **26** demonstrate that the surfactant was successfully removed.

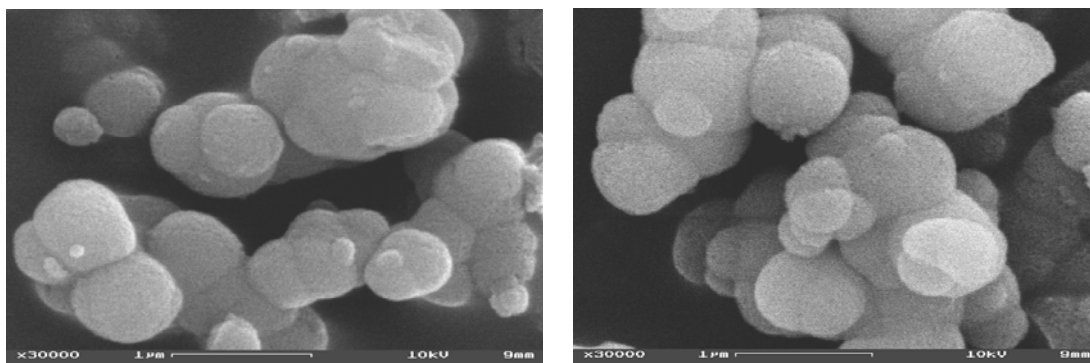


Figure 14. SEM micrographes of **25** and **26**. Magnification 30000 fold, acceleration voltage $U = 10$ kV.

From the SEM micrographs depicted in Figure 14 [recorded on a Zeiss DSM 962 with a tungsten cathode (4.5 nm diameter)] it can be derived that the particle size is around 1 μm for **25** and **26**.

The chromatographic performance of each stationary phase was investigated with SRM 869a,¹²⁵ which is a shape selectivity test mixture consisting of 1,2–3,4–5,6–7,8–tetrabenzonaphthalene (TBN), phenanthro[3,4–c]phenanthrene (PhPh), and benzo[*a*]pyrene (BaP) in acetonitrile. Depending on the elution order of the three components, column selectivity can be predicted for complex polyaromatic hydrocarbon (PAH) mixtures and even helps to characterize the column selectivity for other classes of compounds such as carotene isomers.^{126,127} The mentioned test mixture served to characterize the column selectivity when the new materials **24–26** were employed as stationary phases. Figure 15 depicts HPLC runs with the xerogels **24**, **25**, and **26** leading to an elution order of BaP < TBN. This behavior points to a limited shape selectivity which is in agreement with a reduced recognition towards geometric isomers. With an increasing amount of anthracene (**24** > **25** > **26**) BaP is shifted to longer retention times indicating a higher shape selectivity of these stationary phases. However, the highest selectivity for geometric isomers is observed

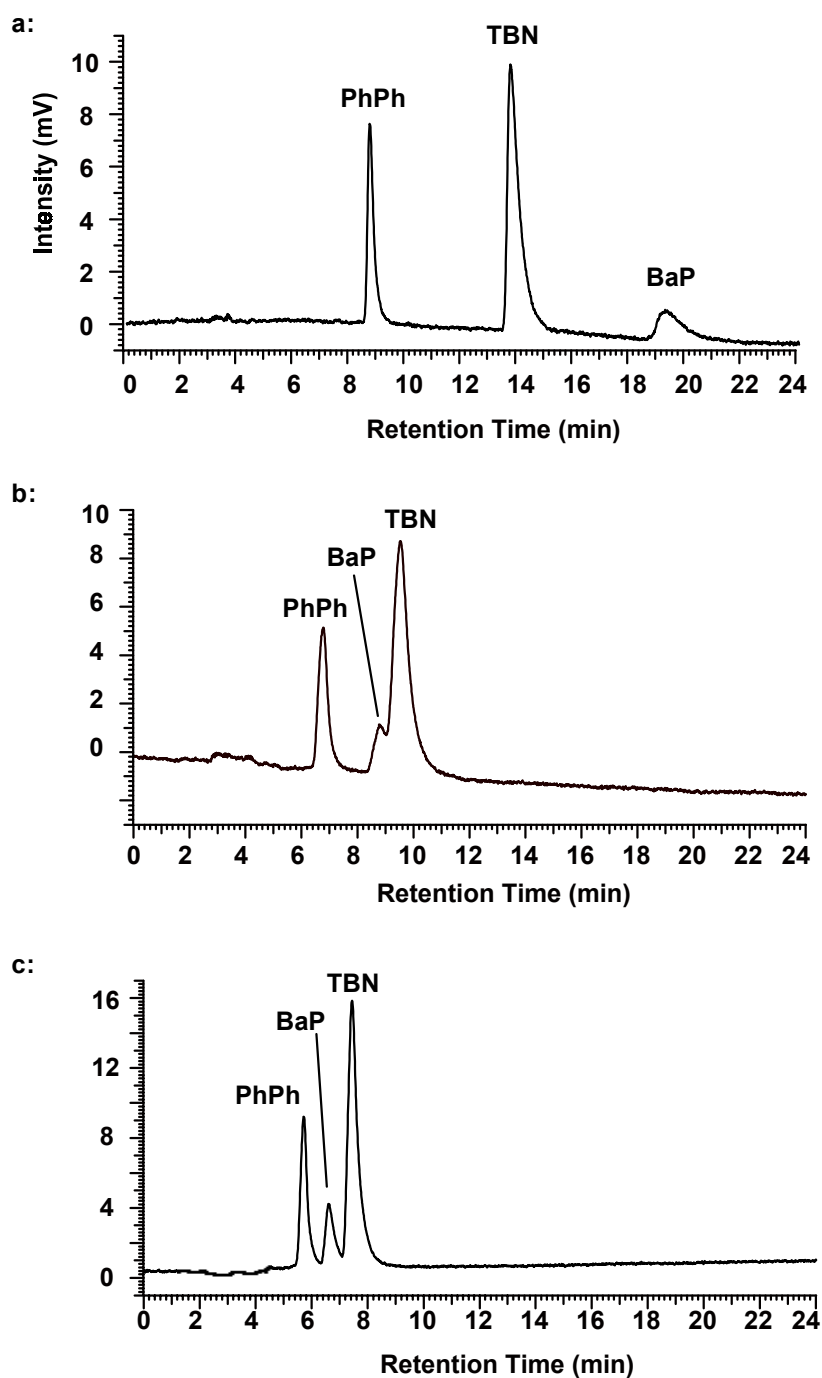


Figure 15. Chromatograms of the materials 24–26.

in the case of the modified silica particles **24**. The retention time of BaP is increased to more than 19 min and results in an elution order of TBN > BaP.

The ordered mesoporous structure of the novel HPLC materials **25** and **26** was investigated by gas adsorption measurements. The Brunauer–Emmett–Teller (BET) surface areas and pore parameters of the template-free samples were determined by nitrogen adsorption–desorption isotherm measurements on a Coulter SA 3100 analyzer. The mesopore size distributions were calculated by Barrett–Joyner–Halenda (BJH) method using the Halsey equation. The BET surface area data and pore parameters are summarized in Table 8. The surface areas of the mesoporous materials **25** and **26** with more than 950 m²/g are significantly higher than that of the modified silica gel **24** with a surface area of 102 m²/g. Nitrogen adsorption/desorption isotherms of the mesoporous polymers exhibit type IV, which is characteristic for mesoporosity.¹²⁸ The isotherms of the modified silica gel **24** reveal no mesoporous characteristics. **25** and **26** show BET total pore volumes of around 0.8 cm³/g like the modified silica gel **24**. This is in agreement with the BJH pore size (Å) shown in Table 8. The BET total pore volume of **24** is not significantly

smaller than that of the materials **25** and **26**. The BJH total pore volume of **25** and **26** is around $0.2 \text{ cm}^3/\text{g}$ which is in agreement with the BJH average pore diameters (nm). The modified silica gel **24** shows a BJH total pore volume of $0.83 \text{ cm}^3/\text{g}$ and an average pore diameter of 30.71 nm. The XRD measurements of polymers **25** and **26** reveal the typical 2θ scattering angles of mesoporous materials. The scattering angles are in both cases 2.16° . The investigated modified silica gel show no reflex in the small angle powder X-ray measurements (Figure 16).

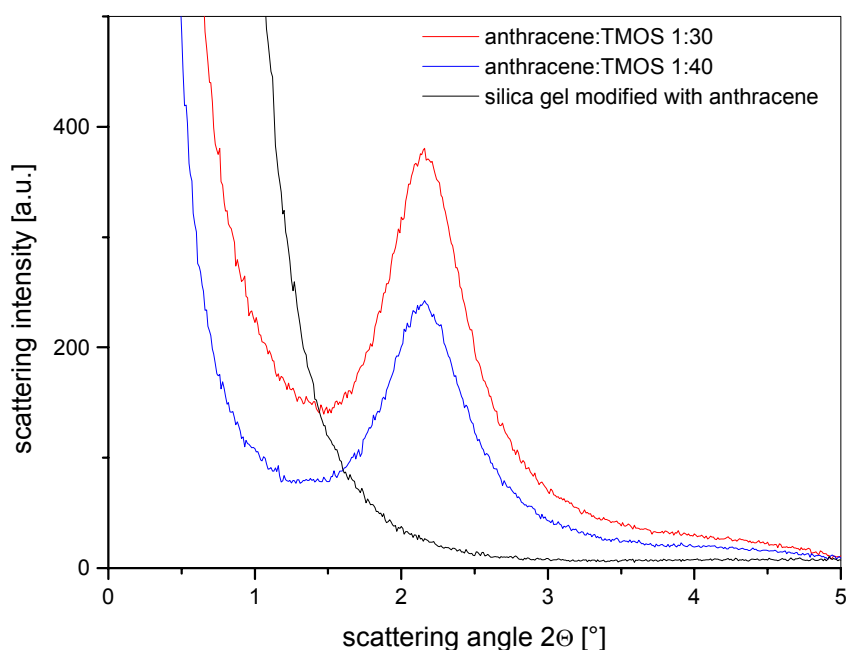


Figure 16. XRD– measurements of the polymers **24–26**.

Table 8. BET and BJH characteristics of the materials **24–26** ($p_s/p_0 = 0.9814$)

Sample	BET surface area/ m ² /g	BET total pore volume/ cm ³ /g	BJH total pore volume/ cm ³ /g	BJH pore size (Å)	Average pore diameter BJH/nm
24	102.1	0.78	0.83	24.7	30.7
25	967.7	0.80	0.23	26.1	3.7
26	954.4	0.82	0.22	26.3	3.7

2.4.3 Conclusion

With the simple synthesis of the new stationary phases **24–26** incorporating aromatic groups as recognition centers in the presence of a surfactant and their first application in HPLC we have pursued a consequent step in the further development of RP materials. For the reproducible access to the novel mesoporous stationary phases **25** and **26** a simple one step process has been established. These new materials can be optimized and further promising investigations are considered.

2.5 Sol–Gel Process on Surfaces for the Application as Chemical Sensors in Liquid Phase

2.5.1 Sol–Gel Layers on Sensors for Liquid Phase

Normally the polymers used for sensing application were synthesized and purified and then brought on the sensor, mainly by air–brush techniques. Another possibility to immobilize the respective polymer on the sensor surface is to synthesize the polymer layer directly on the surface of the sensor. This technique is applied to sensing in liquid phases. The advantage of the synthesis of this type of polymer layers is the easy synthesis without using extreme conditions or purifications. The polymer layers were generated through the sol–gel process. The respective silane monomers were fixed on the sensor surface by cross–linking. The monomers are available in different functional groups and chain length resulting in a broad variety of polymer properties (polarities and functionalities, hydrophilic, hydrophobic rigidity, viscous elastically).

Here the sol–gel process starts with a mixture of alkoxy silane with water in ethanol. If the reaction time is not fast enough $(n\text{-Bu})_2\text{Sn}(\text{OAc})_2$ as catalyst was added. The silanols (sol) were polycondensed and afford the respective polysiloxanes. This

reaction was carried out in the presence of a silane modified gold surface of the sensor. Thus on the sensor surface covalent bound polysiloxanes were formed.

The cross linkage increases during the polycondensation and solvent molecules are encapsulated in the resulting polymer layer. The following drying step allows the shrinkage of the polymer layer by the loss of solvent molecules and unreacted silane molecules. The sensor is coated with a xerogel layer (Figure 17).

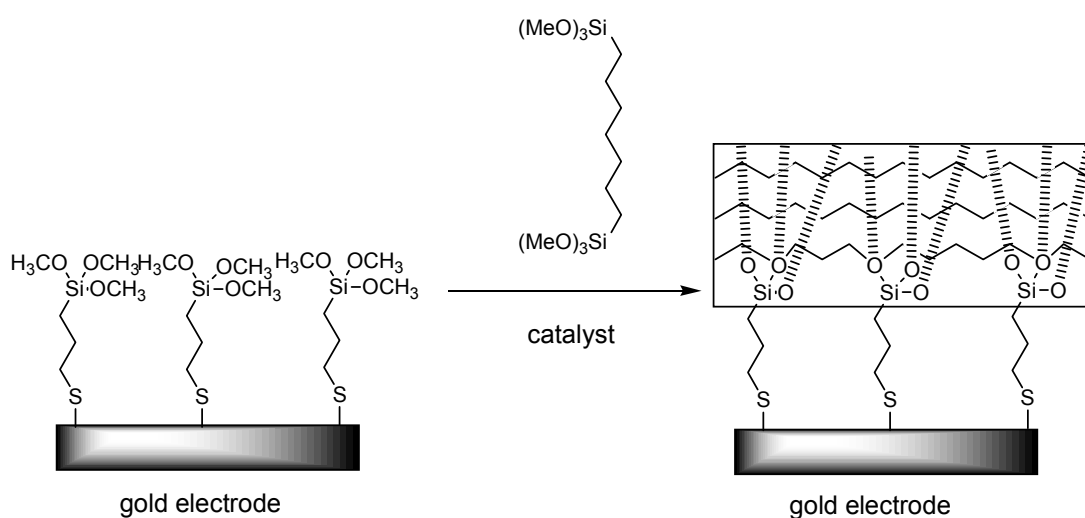


Figure 17. Schematic representation of the sol-gel process on a gold surface.

Such kind of xerogels are used in catalytic processes to bind catalysts if not immobilized on sensor surfaces. For catalytic

reactions like hydrogenation, hydroformylation or other polymer supported catalysis it is necessary to know, how good the solvent molecules diffuse into the carrier polymers. The solvent polymer interactions have an important contribution to the product yield in polymer supported reactions. To get information about the solvent affinity to the respective polymer QCM (Quartz Crystal Microbalance) measurements in liquid phase are helpful.

2.5.2 Preparation of Sol-Gel Layers on Gold and Silicon Surfaces

2.5.2.1 Sol-Gel Layers on Gold Surfaces

To bind the sol-gel polymers on the surface of gold electrodes the gold surface has to be modified by the respective functionalized linkers. First a mono-layer of mercaptopropyl-trimethoxysilane in dried ethanol solution (5 mM) was immobilized via the thiol-function on the gold surface. The reaction time was about 24 hours and the preparation follows directly on the sensors synthesized in the sensor support. Through this step the covalent attachment of the polymerized sol-gel polymer layer is guaranteed. The initially prepared mono-layer provides a source for any sol-gel polymerizable layer.

After several purification steps of the gold surface of the sensor, the whole gold surface was directly brought into the reaction solution. This reaction solution contains 4 ml of ethanol and 30 mg of the respective silane monomer and 10 μ l of the catalyst $(n\text{-Bu})_2\text{Sn}(\text{OAc})_2$. To synthesize the monolayer on the sensor surface 50 μ l of this solution was taken and directly brought onto the sensor surface. To start the sol-gel process some water was added. After the reaction was finished after approximately 16 hours the surface was purified several times with ethanol and water. To ensure a complete cross-linking of the polymer and to get an uniform sensing polymer surface the sensor was tempered for 20 h at 40°–50°C.

2.5.2.2 Sol-Gel Layers on Silicon Surfaces

If the sol-gel polymerization was carried out on silicon surfaces a modification of the surface with linkers is not necessary. It is sufficient to activate the surface with piranha solution and then the sol-gel process with the respective silane monomer can be directly started. The silicon wafers were brought into the above described reaction solution.

2.5.3 Characterization of the Sol-Gel Polymer Modified Surfaces

The respective sol-gel polymers on silicon surfaces were characterized by light microscopy. Figure 18 and 19 show the micrographs of these surfaces.

The influence of the reaction time on the cross linkage and thus the structure of the polymer chains formed out of silane **14** on the silicon surface is depicted in Figure 18. The dark regions are thick polymer chains while the pale parts show regions with not much cross-linked polymer. This can be much better illustrated by light-scattering micrographs. The light parts of the Figure show the cross-linked polymer. The increasing reaction time smoothes the structure of the polymer on the surface. At the beginning of the reaction thread-like polymer chains disappear with the reaction time. Dark and pale regions are uniformly distributed over the whole surface. If the reaction was not allowed to run ten hours no stable polymer layers were formed. The resulting layers can be washed out by a following purification step.

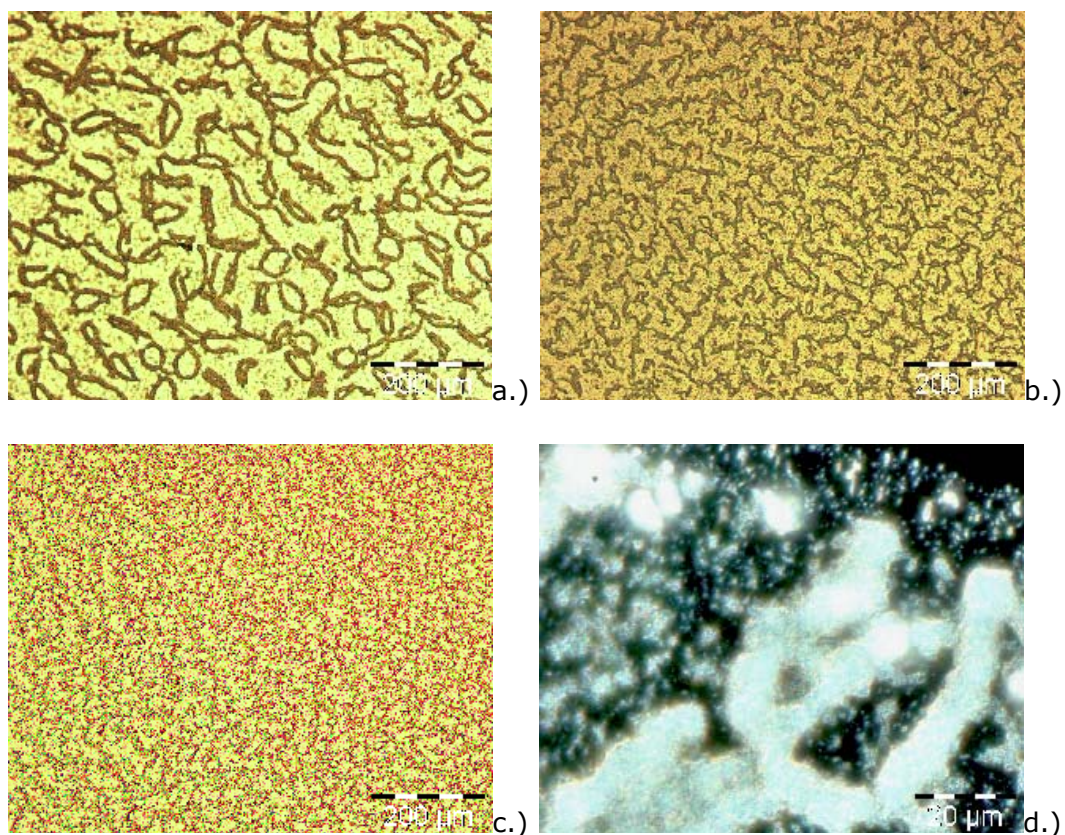


Figure 18. Light microscope pictures. Sol-gel polymers after 13, 14, 16h reaction time magnification 100 fold, light scattering picture after 13 hours reaction time magnification 1000 fold.

A more detailed picture of the different structures of the surface immobilized sol-gel polymers can be depicted by SEM pictures (Figure 19).

These pictures illustrate the influence of the reaction time of the polymer structure on the surface. The difference between 13 and 16 hours reaction time is depicted. The polymer chains

visualized by light microscopy show small polymer globes in the SEM micrographs. The spatial separation of the polymer chains after 13 hours reaction time are transformed into a cross-linked network after 16 hours (part b of Figure 19). If one polymer chain is

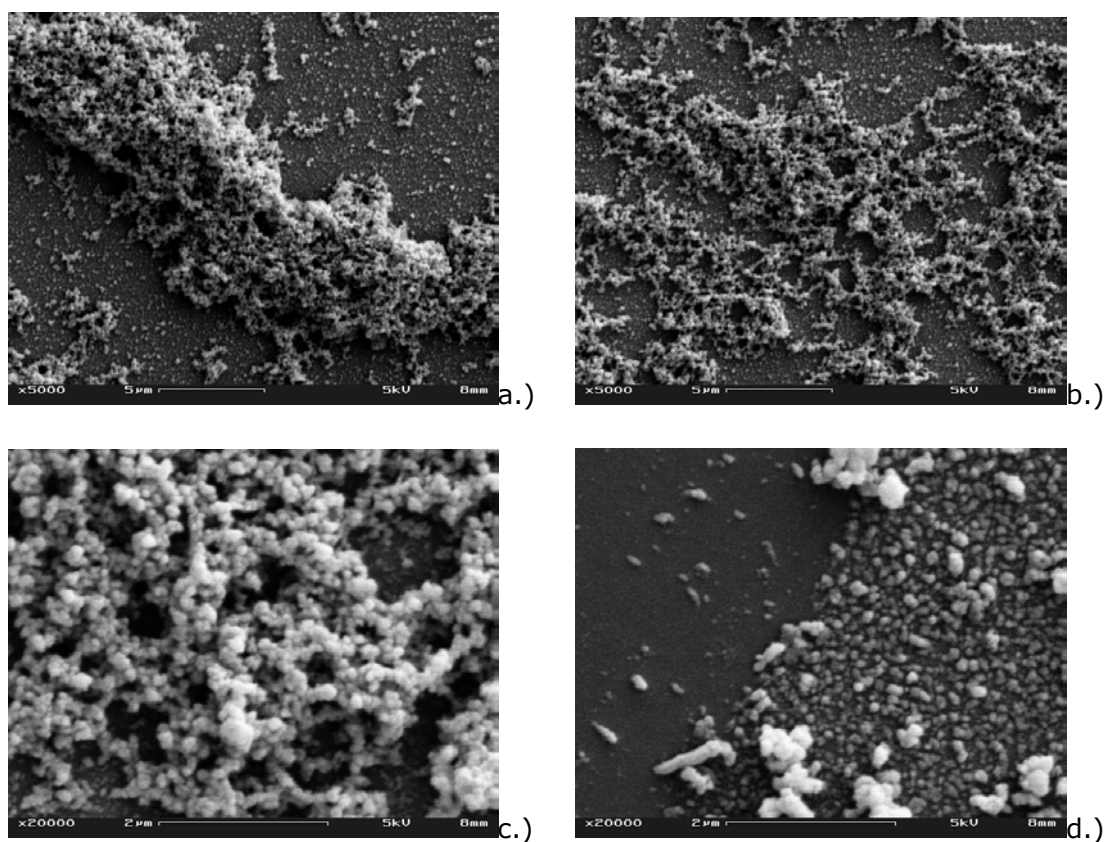


Figure 19. SEM pictures after 13 hours (a, b, and c) and 16 hours reaction time. In part d.) of the figure one part of the polymer layer was removed. Magnification 5000 fold (a and b), magnification 20000 fold (c and d), acceleration voltage $U = 5$ kV.

investigated by a higher resolution it appears that chains of very small polymer globes are formed, leading to a high porosity of the polymer layer. Part c of Figure 19 shows the surface between the polymer chains. In the left side of the micrograph the polymer layer was scratched, demonstrating that the polymer layer is uniformly distributed over the surface. It seems that the "polymer-free" regions are coated with thinner polymer layers. An explanation of this phenomenon can be found in the different development of the polymer chains. On one hand the polymer chains built in solution deposit on the surface and grow their on the existing polymer layer or on the other hand polymer growth starts

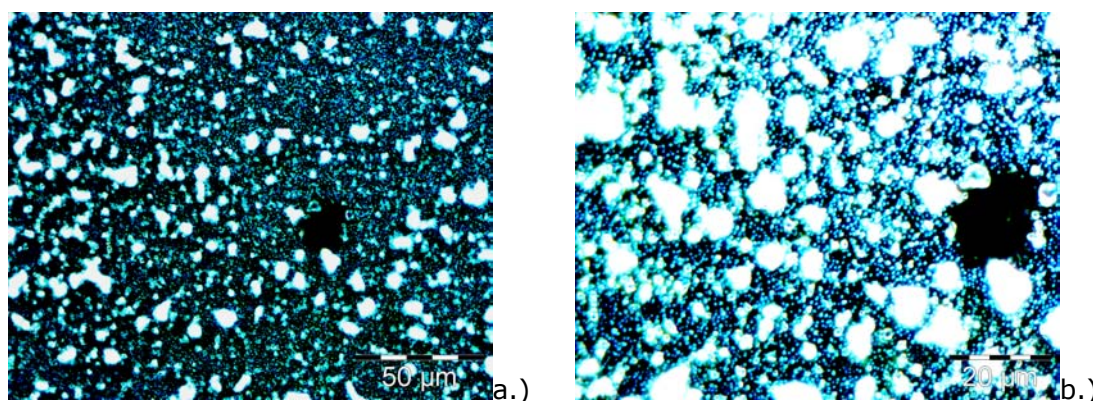


Figure 20. Light microscope pictures of the polymer layers formed out of monomer **15** a.) magnification 500 fold, b.) 1000 fold.

at certain places on the sensor surface. In Figure 20 the light microscope pictures are depicted from sol-gel layers formed out of

silane **15** with a reaction time of 16 hours. Compared to polymer layers out of silane **14** there are many sol-gel polymer clusters with a different size. Between the big polymer clusters are a lot of small polymer globes.

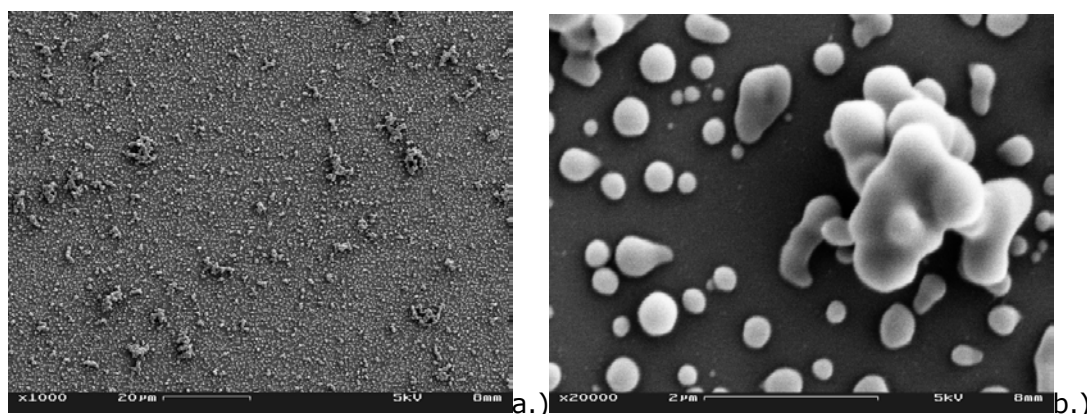


Figure 21. SEM pictures of the polymer layers formed out of monomer **15**. Magnification 1000 fold (a), and 20000 fold (b), acceleration voltage $U = 5 \text{ kV}$.

In Figure 21 SEM micrographs point to the surface structure of sol-gel polymers formed of the silane monomer **15**. The polymer globes are approximately five times bigger than the polymer globes which form the polymer chains of the polymer layers composed of silane **14**. In the case of silane **15** no closed polymer layer is formed. The layer is more like single polymer clusters formed out of some small sol-gel polymer globes.

Both sol-gel polymers generate stable polymer layers after a reaction time of 10 hours. The polymer growth starts with formed

islands and with an increasing reaction time a layer is formed in the case of silane monomer **14**. Closed layers are found in the case of silane monomer **15**. Layers with island like structures are formed. If the AFM graph (Figure 22) of a polymer layer made from monomer **14** is investigated after a reaction time of 20 hours the polymer layer shows a high porosity of approximately 60 nm (rms). This shows clearly an inhomogeneous polymer layer thickness.

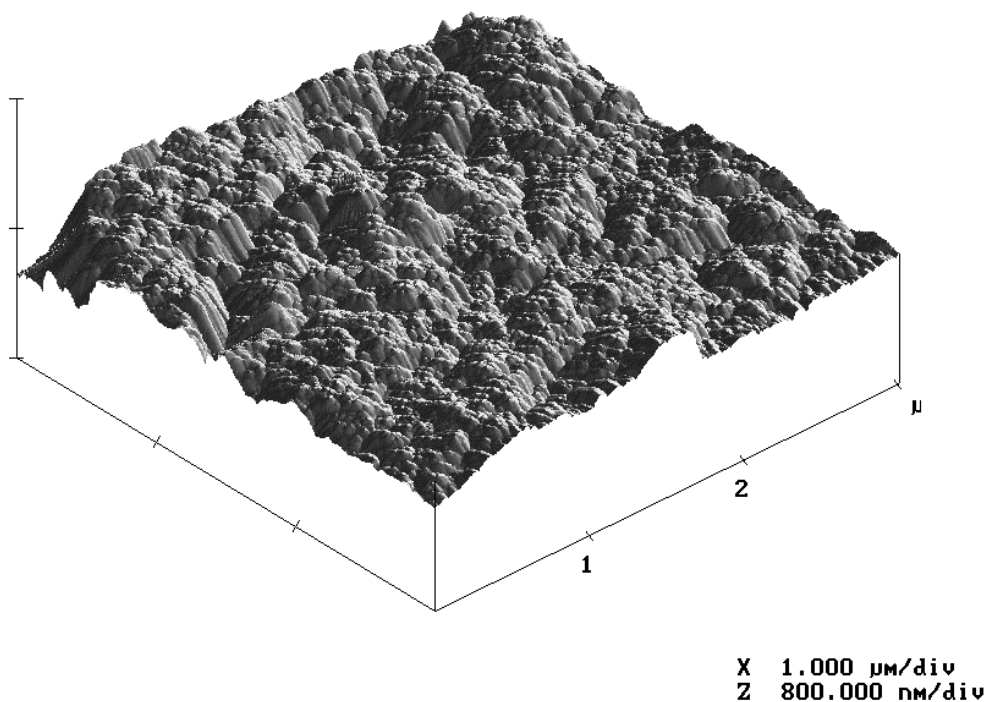


Figure 22. AFM picture of a 2.5 μm thick sol-gel layer after 20 hours reaction time (trapping method).

A classification of these sol–gel polymers was achieved by QCM measurements. This classification is helpful to optimize the reaction conditions of the sol–gel process and allows also a qualitative proposition of the solvent affinity of these polymers. Sol–gel polymers are widely applied for sensing investigations and if a covalent attachment is ensured a further application in the liquid phase can be derived, also with respect to encapsulated reporter molecules. If the respective polymer layers are prepared on a gold electrode of a mass sensitive QCM as described above the solvent affinity behavior results as described in Figure 23. Water was offset with 50 ppm of different organic solvents like toluene, THF, DCM, and chloroform.

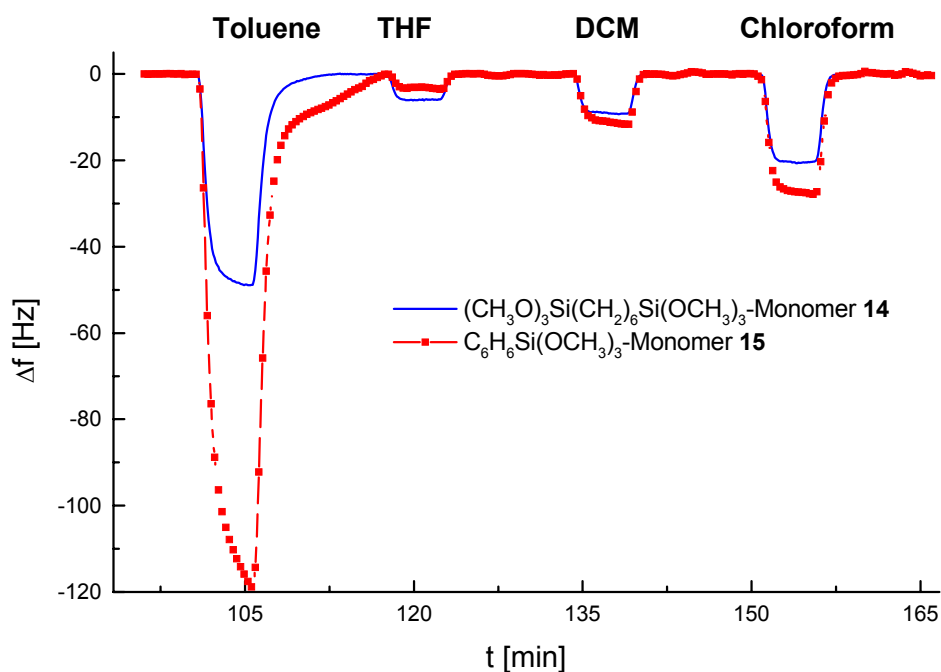


Figure 23. QCM measurements of the compared polymer layers formed of the monomer silanes **14** and **15**.

The frequency shift of the QCM was 8.0 kHz (**14**) and 11.6 kHz (**15**). This shows that the polymer layer in the second case was slightly thicker. The static contact angle measurements wetting the sol-gel polymers covalently bound on the sensor surface with a water drop point out that polymer built with monomer **15** ($115.9^\circ \pm 1.1^\circ$) is more non-polar than the static contact angle for polymers made from **14** ($158.2^\circ \pm 7.5^\circ$), which itself is rather non-polar. Despite of the different layer thickness it is clear recognizable that the sensor coated with the sol-gel

polymer formed of silane monomer **15** shows a remarkably higher sensor response signal. Due to the higher interaction with the polymer a reduced adsorption and desorption kinetics results. This is probably due to the interactions between the phenyl groups in the polymer. The sensor which is coated with the polymer layer made from the silane monomer **14** reveals the half sensor response with a fast kinetics. If more polar solvents like THF were investigated the sensor response is different and smaller signals with an opposite behavior are observed for polymer layers made from **14**. Due to the higher polarity of THF compared to toluene the attempt of THF to diffuse into the very non-polar sol-gel polymer layers is very low. This reveals a much smaller sensor response. Halogen containing solvents like DCM and chloroform behave similar and in the case of chloroform a higher signal was received due to its non-polar character compared to DCM.

Commercial available polysiloxanes are scarcely capable for application in liquid phase, because they are not stable. A stable polymer layer is achieved via covalent linking of the silanes on the gold surface. Through thiol groups a covalent attachment of the silane linker can be derived. By the use of covalent cross-linking co-condensation agents further stability is achieved due to

increased cross-linking avoiding displacement of the polymer layers. The character of the polymer layer is easily tunable by the choice of the silane monomer with a low synthetic effort. By the use of two different monomers the different behavior of the polymers was investigated by a direct synthesis on the sensor surface. These polymer layers show a high chemical stability, because they are much more cross-linked than commercially available polysiloxanes. With the aid of QCM measurements its possible to characterize sol-gel polymers and to develop the reaction conditions for the sol-gel process.

3. Experimental Section

3.1 Fluorescence Measurements

All measurements on the hybrid polymers were obtained by suspending 3 – 4 mg of the powders in 3 ml of solvent and vigorously stirring the samples with a magnetic stirrer to avoid sedimentation. The temperature during the measurements was kept constant at $T = 293$ K. For exciplex experiments, 0.5 – 1.5 ml of freshly distilled triethylamine were added to the liquid phase.

Fluorescence depolarization by light scattering has not been observed at the concentrations of polymeric material in the liquid phase used in the present study. Also, fluorescence depolarization by energy transfer between fluorene moieties did not occur. At the employed molar ratio of 10^{-4} between **3** and co-condensation agents, corresponding to a local concentration of fluorene in the polysiloxane matrix of $c \approx 4 \cdot 10^{-4}$ M, the mean distance between two fluorene molecules of $\bar{R} = 16$ nm is much larger than the critical distance of $R_c = 2.2$ nm calculated for homo transfer between fluorene molecules. This consideration is confirmed by experiment. The observed values of fluorescence anisotropy for local concentrations of fluorene of $c \approx 4 \cdot 10^{-4}$ M and $c \approx 4 \cdot 10^{-5}$ M are identical within experimental error.

Steady-state fluorescence, fluorescence excitation, and fluorescence anisotropy spectra were obtained on a SPEX Fluorolog 222 fluorometer, equipped with Glan-Thompson polarizers.

Fluorescence and fluorescence anisotropy decay curves were acquired by the single-photon counting method. Where nanosecond time-resolution was sufficient, a thyatron-controlled hydrogen/nitrogen flashlamp (Photochemical Research Associates,

Model 510B) was used for excitation and a R928 photomultiplier tube (Hamamatsu) for detection. The signal from the photomultiplier tube was fed into a multichannel analyzer via a picosecond amplifier/discriminator and a time to amplitude converter (EG&G ORTEC). The time resolution of this setup is limited to $\Delta t = 0.5$ ns.

Where picosecond time resolution was required, the instrument for time-domain fluorescence experiments at the "Center for Fluorescence spectroscopy", Baltimore/Md., USA, was used. It comprised a frequency doubled rhodamin dye laser synchronously pumped by a mode-locked argon ion laser. The laser system provided trains of 290 nm light pulses at a repetition frequency of 3.77 MHz and a pulsewidth of about 7 ps FWHM. The collected fluorescence light passed through a polarizer, low-pass filter, and monochromator and was detected by a MCP photomultiplier (Hamamatsu). The time-correlated single photon counting detection system was based on standard NIM modules purchased from EG&G Ortec or Tennelec, and Norland 5700 MCA. The impulse response function of the instrument had a width of 70ps FWHM. The time resolution was comparable with the width of

the response function for experiments analyzed by a direct fitting of the experimental data without deconvolution.

The experimental non-polarized fluorescence decay curves, $I(t)$, were fitted to sums of n exponentials ($n = 1 - 3$), $I(t) = \sum_{i=1}^n A_i \cdot e^{-t/\tau_i}$. The quality of the fit was assessed by the values of χ^2 and the Durbin-Watson parameter, as well as from the plots of residuals and autocorrelation functions. Fits obtained with $n+1$ exponentials were preferred to those with n exponentials only if χ^2 was reduced significantly. The mean fluorescence decay times were calculated by

$$\langle \tau_F \rangle = \frac{\sum_{i=1}^n A_i \tau_i^2}{\sum_{i=1}^n A_i \tau_i} \quad (16)$$

Anisotropy decay curves, $r(t)$, were obtained from polarized fluorescence decay curves $I_{vv}(t)$ and $I_{vh}(t)$

$$r(t) = \frac{I_{vv}(t) - g \cdot I_{vh}(t)}{I_{vv}(t) + 2g \cdot I_{vh}(t)}, \quad (17)$$

where $g = I_{hv}/I_{hh}$ accounts for the polarization dependent sensitivity of the detection system. All polarized decay curves were recorded with picosecond time resolution. The $r(t)$ curves were also fitted to sums of exponentials, allowing for constant offsets. Steady

state anisotropies, r_{ss} , were obtained with the corresponding steady state fluorescence intensities.

3.2 Electrokinetic Chromatography

The separation of the enantiomers of **11** was carried out with a Prince Unicam Crystal 300/31 capillary electrophoresis system equipped with an on-column UV-detector (Bischoff Lambda 1000, Leonberg, Germany) and a thermostated laboratory-built¹²⁹ water cooling system with integrated temperature control (Haake D8-GH, Haake, Karlsruhe, Germany). The effective length of the fused silica capillary (Microquartz, Munich, Germany) was 95 cm (total length 112 cm), the temperature regulated length was 76 cm, and the inner diameter was 50 μm . Sample solutions (1 mg/ml in methanol) were stored at room temperature. Prior to use, sample and buffer solutions were passed through a 0.45 μm disposable filter cartridge (Chromafil, Macherey & Nagel, Düren, Germany). UV On-column detection was performed at 254 nm. Peak integration was carried out with a Chromatopak C-R6A integrator (Shimadzu, Kyoto, Japan).

The borate ($\text{Na}_2\text{B}_4\text{O}_7 \cdot 10 \text{ H}_2\text{O}$ 99.5 %) buffer salt was purchased from Fluka (Deisenhofen, Germany). Carboxymethyl- β -cyclodextrin was received from Wacker Chemie (Burghausen, Germany). Methanol was purchased from Merck (Darmstadt, Germany) and was of HPLC quality. 18.2 M Ω high purity water obtained from a Millipore-Q System (Millipore, Marlborough, Massachusetts, USA) was used to prepare the borate buffer solution.

Untreated fused silica capillaries were conditioned for 30 min with 0.1 M sodium hydroxide solution. Afterwards the capillary was purged with the respective buffer solution for 20 min. Between injections, the capillary was rinsed with 0.1 M sodium hydroxide solution for two min, followed by water for five min and finally buffer solution for 20 min, all at 1 bar. Injections were performed hydrodynamically at the anodic side by applying a pressure of 100 mbar for three seconds. A voltage of 30 kV was used.

3.3 Luminescence Measurements

All measurements on the hybrid polymers were obtained by suspending 3–4 mg of the powders in 3 ml of the respective liquid and vigorously stirring the samples with a magnetic stirrer to avoid

sedimentation. The temperature during the measurements was kept constant at $T = 293$ K. For quenching experiments, anthracene in concentrations of $c = 5 \cdot 10^{-4} - 5 \cdot 10^{-3}$ M was dissolved in the liquid phase. Air saturated liquids contain about $c \approx 3 \cdot 10^{-3}$ M of dioxygen. The employed molar ratio of 10^{-4} between **12** and the co-condensation agents corresponds to a local concentration of **12** in the polysiloxane matrix of $c \approx 4 \cdot 10^{-4}$ M.

Steady-state luminescence, luminescence excitation spectra, were obtained on a SPEX Fluorolog 222 fluorometer, equipped with Glan-Thompson polarizers.

Luminescence decay curves were acquired by the single-photon counting method. A picosecond diode laser (PICO QUANT GmbH, Berlin, Model LDH 400) was used for excitation (wavelength 392 nm) and a R928 photomultiplier tube (Hamamatsu) for detection. The signal from the photomultiplier tube was fed into a multichannel analyzer via a picosecond amplifier/discriminator and a time to amplitude converter (EG&G ORTEC). The time resolution of this set up is limited to decay times of $\tau \geq 0.5$ ns.

3.4 Syntheses

Elemental analyses were carried out on a Vario EL analyzer (Fa. Elementar Analytische Systeme, Hanau). Solution and suspension nuclear magnetic resonance spectra (NMR) were recorded on a Bruker DRX 250 spectrometer at 298 K. Frequencies and standards were as follows: ^1H NMR, 250.13 MHz; $^{13}\text{C}\{^1\text{H}\}$ NMR, 62.90 MHz. All NMR spectra were calibrated relative to partially deuterated solvent peaks which are reported relative to tetramethylsilane (TMS). EI mass spectra were acquired on a Finnigan TSQ 70 instrument and are reported as mass/charge (m/z). IR data were obtained on a Bruker IFS 48 FT-IR spectrometer. BET surfaces and pore volumes were obtained with a Coulter SA3100 (Beckman Coulter GmbH), measuring the adsorption and desorption isotherms after drying the samples for 12 h at $T = 50\text{ }^\circ\text{C}$ under vacuo. Measurements of fluorescence anisotropy before and after the BET experiments yield the same results and thus exclude major changes of the pore structure by the drying procedure. SEM micrographes were recorded on a Zeiss DSM 962 with a tungsten cathode (4.5 nm diameter). CP/MAS solid state NMR spectra were recorded on Bruker DSX 200 (4.7 T) (^{29}Si) and ASX 300 (7.05 T) (^{13}C) multinuclear spectrometers equipped

with wide-bore magnets. Magic angle spinning was applied at 3.5 kHz (^{29}Si) and 10 kHz (^{13}C), respectively. All samples were packed under exclusion of molecular oxygen. Frequencies and standards: ^{29}Si , 39.75 MHz (Q_8M_8); ^{13}C , 75.47 MHz [TMS, carbonyl resonance of glycine (δ 170.09) as the second standard]. No relative intensities are given for ^{29}Si NMR spectra, due to the different efficiencies of magnetization transfer to inequivalent ^{29}Si nuclei.

All manipulations were performed under an atmosphere of dry argon by employing usual Schlenk techniques. The solvents were dried according to common methods, distilled, and stored under argon. 9-(5'-Hexenyl-9H-fluorene (**1**)⁵³ and the co-condensation agents **5**,¹³⁰ and **6**⁸ were synthesized according to literature methods. **4** was purchased from Fluka.

3-Iodopropanol, 1-iodo-3-(tetrahydropyryloxy)propane, 5-(4-hydroxybutyl)-5'-methyl-2,2'-bipyridine (**11a**),¹³¹ *cis*-(bpy)₂RuCl₂ · 2 H₂O (**11b**),¹³² and the modified tris(2,2'-bipyridine)ruthenium(II) complex (**11**)¹³³ were synthesized according to literature methods. 5,5'-Dimethylbipyridine was purchased from Aldrich. 3-Chloropropanol, 3,4-dihydro-2H-pyran, *n*-butyllithium, TMEDA, triethylamine, and diisopropylamine were purchased from Merck.

Complex **11**¹³⁴ and the co-condensation agents **13**⁸ and **14**,¹³⁰ were synthesized according to literature methods. Compounds **15**, **16**, and **17** were purchased from Fluka.

3.5 Preparation of the Compounds

3.5.1 6-(9H-Fluorenyl)hexyltrimethoxysilane **3**

9-(5'-hexenyl)-9H-fluorene (**1**) (8.00 g, 32.0 mmol) was treated with trichlorosilane (4.0 ml, 40.00 mmol) and a suspension of hexachloroplatinic acid (15.0 mg, $2.9 \cdot 10^{-2}$ mmol) in 25 ml of THF. The mixture was stirred for 48 h at 20°C and a dark brown solution was formed. This solution was added dropwise to trimethyl orthoformate (11.5 ml, 105.00 mmol) and the mixture was stirred overnight at room temperature. The volatile components of the solution were removed in vacuo and the residual oil was purified on a silica gel column (length 15 cm, diameter 4 cm, solvents: *n*-hexane, toluene, and THF). Yield 8.52 g (71.8 %); ¹³C{¹H} NMR (CDCl₃, for labeling and assignment see Scheme 3 and ref.⁵³) δ = 148.5 (s, C9a, C8a), 142.0 (s, C5a, C4a), 127.8 (s, C3, C6), 127.7 (s, C2, C7), 125.2 (2, C1, C8), 120.7 (s, C4, C5), 51.4 (s, C16), 48.4 (s, C9), 34.0 (s, C10), 33.7 (s, C13), 30.4 (s, C12), 26.4 (s,

C11), 23.4 (s, C14), 9.9 (s, C15); ^1H NMR (CDCl_3 , for labeling and assignment see Scheme 3 and ref.⁵³) δ = 7.74 (d, $^2J_{\text{CH}}$ = 6.6 Hz, 2H, C1H, C8H), 7.50 (d, $^2J_{\text{CH}}$ = 6.9 Hz, 2H, C4H, C5H), 7.34 – 7.10 (m, 4H, C2H, C3H, C6H, C7H), 3.95 – 3.92 (m, 1H, C9H), 3.41 (s, 9H, C16H), 1.99 – 1.95 (m, 2H, C10H), 1.60 (m, 2H, C11H), 1.32 – 1.17 (m, 6H, C12H, C13H, C14H), 0.60 – 0.54 (m, 2H, C15H); EI-MS m/z 370.2 [M^+]. Anal. Calcd for $\text{C}_{22}\text{H}_{30}\text{O}_3\text{Si}$: C, 71.31; H, 8.16. Found: C, 71.29; H, 6.72%.

3.5.2 Sol-Gel Processing of **3** with Different Co-condensation Agents – General Procedure

The silane **3** was polycondensed by itself and with the co-condensation agents **4**, **5**, and **6** (Scheme 4) in a molar ratio of 1 : 10^4 . An appropriate mixture of the respective T^0 and D^0 functionalized monomeric silanes with water, methanol and a catalyst was stirred for 12 h at 30°C until the gels precipitated. Subsequently the solvent was removed under reduced pressure and the resulting gels were dried for 4 h in vacuo. Solvent processing was performed by vigorously stirring the large gel particles in 10 ml of *n*-hexane overnight. The wet gels were triturated and washed twice with 20 ml of *n*-hexane, methanol,

and dichloromethane and dried in vacuo for 4 h. Before starting the fluorescence measurements on these samples, they were allowed to sit for two weeks at room temperature.

3.5.2.1 Preparation of the Polysiloxane 7

A mixture of **3** (560 mg, 1.51 mmol), methanol (2.5 ml), water (250 μ l), and ammonia (250 μ l of a 0.1 m solution) as catalyst was sol-gel processed. Yield 400 mg (71.4 %); $^{13}\text{C}\{^1\text{H}\}$ NMR (suspension in CDCl_3 , for labeling and assignment see Scheme 3 and ref.⁵³) δ = 146.5 (s, C9a, C8a), 140.0 (s, C5a, C4a), 125.8 (s, C3, C6), 125.7 (s, C2, C7), 123.3 (s, C1, C8), 118.7 (s, C4, C5), 46.4 (s, C16), 43.8 (s, C9), 32.2 (s, C10), 32.1 (s, C13), 28.6 (s, C12), 23.9 (s, C11), 22.1 (s, C14), 10.6 (s, C15); ^1H NMR (suspension in CDCl_3 , for labeling and assignment see Scheme 3 and ref.⁵³) δ = 7.56 (m, 2H, C1H, C8H), 7.30 (m, 2H, C4H, C5H), 7.14 (m, 4H, C2H, C3H, C6H, C7H), 3.92 (m, 1H C9H), 3.32 (m, H, C16H), 1.80 (m, 2H, C10H), 1.53 (m, 2H, C11H), 1.05 (m, 6H, C12H, C13H, C14H), 0.58 (m, 2H, C15H); IR (KBr, cm^{-1}) 3445 m [$\nu(\text{OH})$], 3064 w, 3039 w [$\nu(\text{C-H})_{\text{aromat.}}$], 2931 sst [$\nu(\text{CH}_2)$], 2858 st [$\nu(\text{OCH}_3)$], 1739 w, 1611 w [$\nu(\text{C=C})_{\text{aromat.}}$], 1477 m, 1449 s

$[\delta(\text{CH}_2)]$, 1262 m, 1193 m $[\nu(\text{SiCH}_2)]$, 1111 sst $[\nu(\text{Si}_2\text{O})]$, 917 w $[\nu(\text{SiOCH}_3)]$.

3.5.2.2 Preparation of the Polysiloxane 8

A mixture of **3** (0.4 mg, $1.08 \cdot 10^{-3}$ mmol), **4** (1.36 g, 10.02 mmol), 5 ml of methanol, 500 μl of water, and 500 μl (0.1 mol) of ammonia was sol-gel processed. Yield 1.20 g (88.2 %); ^{13}C CP/MAS NMR $\delta = 49.5$ (SiOCH₃), -0.4 (SiCH₃); ^{29}Si CP/MAS NMR (silicon substructure) $\delta = -56.2$ (T²), -65.6 (T³). Anal. Calcd for C₁₉H₂₁O_{1.5}Si(CH₃O_{1.5}Si)₁₀₀₀₀: C, 17.93; H, 4.51. Found: C, 13.84; H, 4.60 %. BET surface A_{BET} = 0.56 m²/g.

3.5.2.3 Preparation of the Polysiloxane 9

A mixture of **3** (0.8 mg, $2.16 \cdot 10^{-3}$ mmol), **5** (3.37 g, 10.30 mmol), 5 ml of methanol, 500 μl of water, and 500 μl (0.1 mol) of ammonia was sol-gel processed. Yield 3.25 g (96.4 %); ^{13}C CP/MAS NMR $\delta = 49.8$ (SiOCH₃), 33.1 (Si(CH₂)₂CH₂CH₂(CH₂)₂Si), 23.0 (SiCH₂CH₂(CH₂)₂CH₂CH₂Si), 11.4 (SiCH₂(CH₂)₄CH₂Si); ^{29}Si CP/MAS NMR (silicon substructure) $\delta = -41.7$ (T⁰), -49.9 (T¹), -58.7 (T²), -67.4 (T³). Anal. Calcd for C₁₉H₂₁O_{1.5}Si(C₆H₁₂O₃Si)₁₀₀₀₀:

C, 41.82; H 7.02 Found: C, 40.46; H, 6.85%. BET surface $A_{\text{BET}} = 63.0 \text{ m}^2/\text{g}$.

3.5.2.4 Preparation of the Polysiloxane 10

A mixture of **3** (0.75 mg, $2.02 \cdot 10^{-3}$ mmol), **6** (2.95 g, 10.20 mmol), 5 ml of methanol, 500 μl of water, and 500 μl (0.1 M) of hydrochloric acid was sol-gel processed. Yield 2.65 g (89.8 %); ^{13}C CP/MAS NMR $\delta = 49.6$ (SiOCH₃), 33.4 (Si(CH₂)₂CH₂CH₂(CH₂)₂Si), 23.2 (SiCH₂CH₂(CH₂)₂CH₂CH₂Si), 17.7 (SiCH₂(CH₂)₄CH₂Si), -0.1 (SiCH₃); ^{29}Si CP/MAS NMR (silicon substructure) $\delta = -9.7$, -13.3 (D¹), -22.2 (D²). Anal. Calcd for C₁₉H₂₁O_{1.5}Si(C₈H₁₈O₂Si₂)₁₀₀₀₀: C, 47.48; H, 8.96, Found: C, 47.19; H, 8.82 %. BET surface $A_{\text{BET}} = 3.68 \text{ m}^2/\text{g}$.

3.5.3 5-(4-Hydroxybutyl)-5'-methyl-2,2'-bipyridine (11a)

A solution of diisopropylamine (2 ml, 14.25 mmol) in THF (25 ml) was cooled to -18°C and was treated slowly with a solution of *n*-butyllithium in *n*-hexane (1.6 M, 8.5 ml, 13.6 mmol). This solution was added dropwise to a cold (0°C) solution of 5,5'-dimethylbipyridine (2.5 g, 13.6 mmol) and TMEDA (4.5 ml, 30.2 mmol) in THF (75 ml). After stirring the resulting green-black

solution at this temperature for 1 h, freshly distilled 1-iodo-3-(tetrahydroxypyranoyloxy)propane (3.7 g, 13.7 mmol) was added drop wise. After warming to ambient temperature, the mixture was stirred for 24 h. The almost colorless mixture was cooled (0°C), subsequently 10 ml of distilled water and 50 ml of an aqueous hydrogen chloride solution (18%) were added. THF was removed under reduced pressure and the resulting aqueous solution was extracted two times with CH₂Cl₂ (20 ml). The extract was neutralized to pH 7 with NaHCO₃ and an orange solid precipitated. The remaining aqueous solution was extracted five times with ethyl acetate (20 ml). The solid and the combined organic layers were dried over Na₂SO₄ and filtered. The solvent was removed under reduced pressure to give a crude product which was purified by column chromatography (ethyl acetate MeOH 6:1, silica gel column, length: 50 cm, diameter: 7 cm). Yield 1.49 g (45.3 %); mp 69.9–72.2°C; ¹³C{¹H} NMR (CD₃CN, for labeling and assignment see Scheme 5): δ = 17.0 (Ca), 26.9 (Cb'), 31.5 (Cc'), 31.6 (Ca'), 60.9 (Cd'), 119.4 (C3'), 119.5 (C3), 133.1 (C5'), 136.3 (C4'), 136.9 (C4), 137.7 (C5), 148.8 (C6'), 149.1(C6), 153.0 (C2'), 153.3 (C2); ¹H NMR (CD₃CN, for labeling and assignment see Scheme 5): δ = 1.51 – 1.73 (m, 4H, c', b'), 1.96

(OH), 2.33 (s, 3H, a), 2.65 (t, $^3J(\text{HH}) = 7.4$ Hz, 2H, a'), 3.66 (dt, $^3J(\text{HH}) = 6.6$ Hz, $^3J(\text{HH}) = 4.7$ Hz, 2H, d'), 7.70 (m, 2H, 4,4'), 8.27 (m, 2H, 3,3'), 8.48 (m, 2H, 6,6'); IR (KBr): 3351, 3173 (OH), 3029, 2923, 2858 (CH), 1598, 1555 (C=C and C=N); MS (EI) m/z : 241.9 [M^+]. Anal. Calcd for $\text{C}_{15}\text{H}_{18}\text{N}_2\text{O}$: C, 74.35; H, 7.49; N, 11.56. Found: C, 73.68; H, 7.59; N 11.03%.

3.5.4 *cis*-(bpy)₂RuCl₂ · 2 H₂O (11b)

This complex was prepared by a published method with a little modified procedure. A suspension of $\text{RuCl}_3 \cdot n \text{H}_2\text{O}$ (16 mmol, 3.31 g), 2,2'-bipyridine (32.01 mmol, 5.0 g) and LiCl (106.7 mmol, 4.52 g) in DMF (30 ml) was refluxed for 12 h. The reaction mixture was allowed to cool to 20°C and 125 ml of acetone was added. Finally the mixture was stored in the refrigerator overnight to yield crude black-green crystals. After filtering and washing with water until the filtrate was colorless and repeated washing with diethyl ether (20 ml) the complex was obtained in form of pure black-green crystals. The crystals were well dried under removing solvent molecules under reduced pressure. All experimental data are as expected.

3.5.5 Spacered Ruthenium(II) Complex 11

A suspension of *cis*-(bpy)₂RuCl₂ · 2 H₂O (**11b**) (0.83 mmol, 0.4 g) and AgSbF₆ (1.65 mmol, 0.57 g) in acetone was stirred for 48 h, followed by filtration of AgCl. 5-(4-Hydroxybutyl)-5'-methyl-2,2'-bipyridine (0.83 mmol, 0.2 g) was added to the filtrate and the mixture was refluxed for 24 h. The solvent was removed under reduced pressure. The crude product was dissolved in CH₂Cl₂ (5 ml) and precipitated with diethyl ether. The precipitate was stirred overnight and then filtered. To remove some silver impurities the complex was again purified by column chromatography (acetone, neutral aluminiumoxide column, length: 4 cm, diameter: 2 cm). The solvent was removed under reduced pressure and the resulting orange powder was washed with *n*-hexane. Yield 0.71 g (75.9 %); ¹³C{¹H} NMR (CD₃CN, for labeling and assignment see Scheme 5): δ = 17.2 (Ca), 26.0 (Cb'), 31.1 (Cc'), 31.3 (Ca'), 60.7 (Cd'), 122.9, 123.1 (C3,3'), 123.9 (bpy-C3,3'), 127.1, 127.2 (bpy-C5,5'), 137.3 (bpy-C4,4'), 138.0 (C4,4'), 142.1, 149.2 (C5,5'), 150.4, 151.1 (C6,6'), 151.3 (bpy-C6,6'), 154.0, 154.4 (C2,2'), 156.7, 156.8 (bpy-C2,2'); ¹H NMR (CD₃CN, for labeling and assignment see Scheme 5): δ = 1.26 – 1.49 (m, 4H, c', b'), 1.99 (OH), 2.23 (s, 3H, a), 2.59 – 2.92 (m,

2H, a'), 3.39 – 3.44 (m, 2H, d'), 7.41 – 7.46 (m, 4H, bpy-5,5'), 7.53 (s, 1H, 6'), 7.73 (s, 1H, 6) 7.75 – 7.87 (m, 4H, bpy-6,6') 7.87 – 7.92 (m, 2H, 4,4'), 8.04 – 8.13 (m, 4H, bpy-4,4'), 8.36 – 8.51 (m, 2H, 3,3'), 8.52 – 8.56 (m, 4H, bpy-3,3'); IR (KBr, cm⁻¹): 3097, 2931, 2863, 1605, 1475, 1476, 1425, 763, 657; MS (EI) *m/z*: 1125.8 [M⁺]. Anal. Calcd for C₃₅H₃₄N₆ORuSb₂F₁₂: C, 37.29; H, 3.04; N, 7.46. Found: C, 37.46; H, 2.96; N, 7.01%.

3.5.6 Preparation of Complex 12

The orange [bis(2,2-bipyridyl)(5-(4-hydroxybutyl)-5'-methyl-2,2'-bipyridyl)-ruthenium(II)]-bis(hexafluoroantimonate) (**11**) (0.71 g, 0.629 mmol) was dissolved in 25 ml of DMF. A solution of triethoxysilyl(propyl)isocyanate (155 µl, 0.629 mmol) in 5 ml of DMF was added dropwise. The mixture was stirred for 48 h at 130°C until a red solution was formed. The volatile components of the solution were removed in vacuum and the residual red solid complex was purified by column chromatography (acetone, neutral and water-free aluminium oxide column, length: 4 cm, diameter: 2 cm). The solvent was removed under reduced pressure and the resulting red solid was washed with 10 ml of *n*-hexane. Yield 0.78 g (90.1 %); ¹³C{¹H} NMR (CD₂Cl₂, for labeling and assignment see

Scheme 6): δ = 6.8 (Ch'), 14.9 (Cg'), 18.5 (Cj'), 18.8 (Ca), 19.5 (Cb'), 34.6 (Cc'), 36.3 (Ca'), 45.5 (Cf'), 58.8 (Ci'), 60.2 (Cd'), 124.4 (C3,3'), 124.6 (bpy-C3,3'), 128.4 (bpy-C5,5'), 138.4 (bpy-C4,4'), 139.9 (C4A, 4'A), 145.5 (C5A, 5'A), 150.9, 151.0 (C6A, 6'A), 151.7 (bpy-C6,6'), 155.5, 155.6 (C2A, 2'A), 157.2 (bpy-C2,2'); ^{13}C NMR (CD_2Cl_2 , for labeling and assignment see Scheme 6): δ = 0.55 (m, 2H, h'), 1.13 (m, 2H, j'), 1.31 – 1.47 (m, 4H, c', b'), 2.18 (s, 3H, a), 2.46 (m, 2H, g'), 2.75 – 2.84 (m, 2H, a'), 3.03 (m, 2H, f'), 3.72 (m 6 H, i'), 3.97 (m, 2H, d'), 7.31 – 7.36 (m, 5H, bpy-5,5', 6'A), 7.79 (m, 5H, bpy-6,6', 6A) 7.87 – 7.92 (m, 2H, 4A, 4'A), 7.96 (s, NH), 8.02 – 8.19 (m, 4H, bpy-4,4'), 8.19 – 8.22 (m, 2H, 3A, 3'A), 8.36 – 8.39 (m, 4H, bpy-3,3'); FD-MS m/z 451.5 [M^{2+}], 1140.75 [M^+]. Anal. Calcd for $\text{C}_{45}\text{H}_{55}\text{N}_7\text{O}_5\text{SiRuSb}_2\text{F}_{12}$: C, 39.32; N, 7.13; H, 4.03. Found: C, 39.31; N, 7.77; H, 4.57%.

3.5.7 Sol-Gel Processing of **12** with Different Co-condensation Agents – General Procedure

The T-silane **12** was polycondensed with the co-condensation agents **13**, **14**, **15**, **16**, and **17** (Scheme 7) in a molar ratio of 1 : 10^4 . An appropriate mixture of the respective T^0 - and D^0 -

functionalized monomeric silanes with water, methanol / THF (1/5, v/v), and $(n\text{-Bu})_2\text{Sn}(\text{OAc})_2$ as catalyst was stirred for 12 h at 30°C until the gels precipitated. Subsequently the solvent was removed under reduced pressure and the resulting gels were dried for 4 h in vacuo. Solvent processing was performed by vigorously stirring of the large gel particles in 10 ml of *n*-hexane overnight. The wet gels were triturated and washed twice with 20 ml of *n*-hexane and dichloromethane and dried in vacuo for 4 h. Prior to luminescence measurements the samples were aged artificially for one week at 90°C to ensure complete cross-linking.

3.5.7.1 Preparation of the Polysiloxane 18

A mixture of **12** (0.6 mg, $4.36 \cdot 10^{-4}$ mmol), **13** (1.45 g, 4.99 mmol), 1 ml of methanol, 5 ml of THF, 500 μl of water, and $(n\text{-Bu})_2\text{Sn}(\text{OAc})_2$ (25 mg, 0.073 mmol) was sol-gel processed. Yield 0.86 g (59.3 %); ^{13}C CP/MAS NMR δ = 50.2 (SiOCH₃), 33.6 (Si(CH₂)₂CH₂CH₂(CH₂)₂Si), 23.5 (SiCH₂CH₂(CH₂)₂CH₂CH₂Si), 18.1 (SiCH₂(CH₂)₄CH₂Si), -0.1 (SiCH₃); ^{29}Si CP/MAS NMR (silicon substructure) δ = -11.7 (D¹), -22.4 (D²). Anal. Calcd for C₄₅H₅₅N₇O₅SiRuSb₂F₁₂(C₈H₁₈O₂Si₂)₁₀₀₀₀: C, 47.40; H, 8.93, Found: C, 47.30; H, 8.86%. BET surface A_{BET} = 1.25 m²/g.

3.5.7.2 Preparation of the Polysiloxane 19

A mixture of **12** (0.90 mg, $6.54 \cdot 10^{-4}$ mmol), **14** (1.63 g, 4.99 mmol), 1 ml of methanol, 5 ml of THF, 500 μ l of water, and (*n*-Bu)₂Sn(OAc)₂ (25 mg, 0.073 mmol) was sol-gel processed. Yield 0.91 g (55.83 %); ¹³C CP/MAS NMR δ = 50.4 (SiOCH₃), 33.3 (Si(CH₂)₂CH₂CH₂(CH₂)₂Si), 23.2 (SiCH₂CH₂(CH₂)₂CH₂CH₂Si), 13.0 (SiCH₂(CH₂)₄CH₂Si); ²⁹Si CP/MAS NMR (silicon substructure) δ = -58.5 (T²), -67.5 (T³). Anal. Calcd for C₄₅H₅₅N₇O₅SiRuSb₂F₁₂(C₆H₁₂O₃Si₂)₁₀₀₀₀: C, 38.25; H 6.40 Found: C, 37.10; H, 6.85%. BET surface A_{BET} = 21.18 m²/g.

3.5.7.3 Preparation of the Polysiloxane 20

A mixture of **12** (1.8 mg, $1.31 \cdot 10^{-3}$ mmol), **15** (2.01 g, 10.13 mmol), 1 ml of methanol, 5 ml of THF, 500 μ l of water, and (*n*-Bu)₂Sn(OAc)₂ (25 mg, 0.073 mmol) was sol-gel processed. Yield 0.96 g (47.76 %); ¹³C CP/MAS NMR δ = 134.5, 130.7, 127.9 (aromatic ring); ²⁹Si CP/MAS NMR (silicon substructure) not measurable. Anal. Calcd for C₄₅H₅₅N₇O₅SiRuSb₂F₁₂(CH₃O_{1.5}Si)₁₀₀₀₀: C, 55.59; H, 3.89. Found: C, 50.06; H, 3.18%. BET surface A_{BET} = 2.08 m²/g.

3.5.7.4 Preparation of the Polysiloxane 21

A mixture of **12** (1.7 mg, $1.23 \cdot 10^{-3}$ mmol), **16** (1.36 g, 9.98 mmol), 1 ml of methanol, 5 ml of THF, 500 μ l of water, and $(n\text{-Bu})_2\text{Sn}(\text{OAc})_2$ (25 mg, 0.073 mmol) was sol-gel processed. Yield 0.49 g (36.02 %); ^{13}C CP/MAS NMR $\delta = 49.8$ (SiOCH₃), -3.1 (SiCH₃); ^{29}Si CP/MAS NMR (silicon substructure) $\delta = -56.8$ (T²), -65.3 (T³). Anal. Calcd for C₄₅H₅₅N₇O₅SiRuSb₂F₁₂(C₆H₅O_{1.5}Si)₁₀₀₀₀: C, 18.24; H 4.48 Found: C, 17.01; H, 4.86%. BET surface A_{BET} = 3.51 m²/g.

3.5.7.5 Preparation of the Polysiloxane 22

A mixture of **12** (1.30 mg, $9.45 \cdot 10^{-4}$ mmol), **7** (1.56 g, 10.24 mmol), 1 ml of methanol, 5 ml of THF, 500 μ l of water, and $(n\text{-Bu})_2\text{Sn}(\text{OAc})_2$ (25 mg, 0.073 mmol) was sol-gel processed. Yield 0.99 g (63.46 %); ^{29}Si CP/MAS NMR (silicon substructure) $\delta = -110$ (Q⁴), -101 (Q³). Anal. Calcd for C₄₅H₅₅N₇O₅SiRuSb₂F₁₂(O₄Si)₁₀₀₀₀: C, 0.76; H 0.07 Found: C, 9.47; H, 2.13%. BET surface A_{BET} = 4.89 m²/g.

3.5.8 N-2-anthracenyl-N'-[3-(triethoxysilyl)propyl]urea 23

2-Aminoanthracene (193.3 mg, 1 mmol) was dissolved in 10 ml of methylene chloride. 3-(Triethoxysilane)propylisocyanate (494.7 mg, 2 mmol) was added dropwise and the reaction mixture was refluxed for 24 h. The solvent of the brown solution was removed under reduced pressure and the residue was again dissolved in 5 ml of methylene chloride. To obtain crystals of the brown product *n*-hexane was added. For a complete crystallization the mixture was cooled to 0°C over night. The brown crystals were filtered and washed with 20 ml of cold *n*-hexane. The brown crystals were dried under vacuo. Yield 330 mg (74.0 %); $^{13}\text{C}\{^1\text{H}\}$ NMR (CD_2Cl_2 , for labeling and assignment see Scheme 10) $\delta =$ 158.4 (s, C11), 143.7 (s, C2), 129.6 (m, C8a, C9a), 128.1 (m, C4, C10a, C5, C8,), 124.5 (m, C4a, C10, C6, C7, C9), 119.4 (m, C3, C1), 55.4 (s, C12), 50.3 (s, C15), 43.5 (m, C13, C16), 15.9 (m, C14); ^1H NMR (CD_2Cl_2 , for labeling and assignment see Scheme 10) $\delta =$ 8.04 (m, 5H, C4H, C10H C5H, C8H, C9H), 7.48 (m, C6H, C7H), 7.10 (m, 2H, C1H, C3H), 5.92 (m, 2H, NH), 3.90 (m, 6H, C15H), 3.41 (m, 2H, C12H), 1.85 – 1.78 (m, 2H, C13H), 1.60 (m, 9H, C16H), 0.60 (m, 2H, C14H); EI-MS m/z 440.1 [M^+]. Anal.

Calcd for $C_{24}H_{32}N_2O_4Si$: C, 65.42; N, 6.36; H, 7.32. Found: C, 64.43; N, 6.47; H, 7.41%.

3.5.8.1 Modified Silica Gel 24

A mixture of 881.2 mg (2.0 mmol) of N-2-anthracenyl-N'-[3-(triethoxysilyl)propyl]urea (**23**) and 3.50 g of silica gel in 20 ml of toluene was allowed to react for 3d. The modified silica gel was washed with *n*-hexane and dried under vacuo. Yield 2.95 g (84 %); ^{13}C CP/MAS NMR: $\delta = 9.4$ (SiCH₂), 23.4 (CH₂), 42.3 (CH₂), 59.4 (OCH₂CH₃), 127.4 (m, CH) 157.4 (OCNH); ^{29}Si CP/MAS NMR: $\delta = -56.6$ (T²), -66.1 (T³), -102.2 (Q³), -110.7 (Q⁴). Anal. Found for silica gel modified with $C_{24}H_{32}N_2O_4Si$: C, 10.40; N, 1.52; H, 1.17%. BET surface $A_{BET} = 102$ m²/g.

3.5.9 Sol-Gel Processing of 23 with Different Concentrations of Co-condensation Agent – General Procedure

To a 0.27 M solution of *n*-hexadecylamine in a 55:45 EtOH(95 %)/H₂O mixture the monomeric precursors were added. This mixture was stirred for 24 h at room temperature until a gel was formed. Then the solvent was removed under reduced

pressure. For the removal of *n*-hexadecylamine the crude xerogels were placed in a Soxhlet extractor containing 300 ml of ethanol and the mixture was refluxed for 3 d. Subsequently the gels were washed three times with *n*-hexane (10 ml) and dried under vacuum for 12 h.

3.5.9.1 Mesoporous Polysiloxane 25

A mixture of of N-2-anthracenyl-N'-[3-(triethoxysilyl) propyl]urea (**23**) (881.2 mg, 2.0 mmol) and TEOS (12.50 g, 60.0 mmol) in 32 ml of a 0.27 M solution of *n*-hexadecylamine in an ethanol/water mixture was sol-gel processed to yield a colorless swollen gel. After purification and drying of a colorless powder was formed. Yield 11.0 g (88 %); ¹³C CP/MAS NMR: $\delta = 15.6$ (SiCH₂), 23.2 (CH₂), 43.2 (CH₂), 59.3 (OCH₂CH₃), 127.9 (m, CH) 157.9 (OCNH); ²⁹Si CP/MAS NMR: $\delta = -57.6$ (T²), -64.3 (T³), -101.5 (Q³), -109.9 (Q⁴). Anal. Found for silica gel modified with C₂₄H₃₂N₂O₄Si: C, 14.92; N, 1.61; H, 2.81%. BET surface A_{BET} = 968 m²/g.

3.5.9.2 Mesoporous Polysiloxane 26

A mixture of of N-2-anthracenyl-N'-[3-(triethoxysilyl) propyl]urea (**23**) (881.2 mg, 2.0 mmol) and TEOS (16.67 g, 80.0

mmol) in 40 ml of a 0.27 M solution of *n*-hexadecylamine in an ethanol/water mixture was sol-gel processed to yield a colorless swollen gel. After purification and drying of a colorless powder was formed. Yield 14.2 g (85 %); ^{13}C CP/MAS NMR: $\delta = 8.3$ (SiCH₂), 23.2 (CH₂), 41.9 (CH₂), 59.3 (OCH₂CH₃), 125.2 (m, CH) 156.2 (OCNH); ^{29}Si CP/MAS NMR: $\delta = -56.6$ (T²), -65.9 (T³), -101.2 (Q³), -109.5 (Q⁴). Anal. Found for silica gel modified with C₂₄H₃₂N₂O₄Si: C, 13.57; N, 1.10; H, 1.94%. BET surface A_{BET} = 954 m²/g.

4. References

1. A. D. Pomogailo *Russ. Chem. Rev.* 1992, **61**, 133.
2. J. A. Marqusee, J. Dill *J. Chem. Phys.* 1986, **85**, 434.
3. L. C. Sander, S. A. Wise, In *Retention and Selectivity Studies in HPLC*; Smith, R. M., Ed.; Elsevier: Amsterdam, 1994, 337.
4. J. G. Dorsey, K. A. Dill *Chem. Rev.* 1989, **89**, 331.
5. E. Lindner, T. Schneller, F. Auer, H. A. Mayer *Angew. Chem.* 1999, **111**, 2288; *Angew. Chem. Int. Ed.* 1999, **38**, 2154.
6. C. J. Brinker, G. W. Scherer, *Sol-Gel Science*; Academic Press: London, 1990.
7. E. Lindner, M. Kemmler, H. A. Mayer, P. Wegner *J. Am. Chem. Soc.* 1994, **116**, 348.
8. L. L. Hench, J. K. West *Chem. Rev.* 1990, **90**, 33.
9. E. Lindner, R. Schreiber, M. Kemmler, T. Schneller, H. A. Mayer *Chem Mater.* 1995, **7**, 951.
10. U. Schubert, *New J. Chem.* 1994, **18**, 1049.
11. R. P. J. Corriu, D. Leclercq, *Angew. Chem.* 1996, **108**, 1524; *Angew. Chem. Int. Ed. Engl.* 1996, **35**, 1420.
12. F. R. Hartley, P. N. Vezey, *Adv. Organomet. Chem.* 1977, **15**, 189.

13. W. Dumont, J.-C. Poulin, T.-P. Dang, H. B. Kagan, *J. Am. Chem. Soc.* 1973, **95**, 8295.
14. E. Lindner, R. Schreiber, T. Schneller, P. Wegner, H. A. Mayer, W. Göpel, C. Ziegler, *Inorg. Chem.* 1996, **35**, 514.
15. E. Lindner, A. Jäger, T. Schneller, H. A. Mayer, *Chem. Mater.* 1997, **9**, 81.
16. E. Lindner, A. Jäger, F. Auer, P. Wegner, H. A. Mayer, A. Benez, D. Adam, E. Plies, *Chem. Mater.* 1998, **10**, 217.
17. E. Lippmaa, M. Mägi, A. Samson, G. Engelhardt, A.-R. Grimmer *J. Am. Chem. Soc.* 1980, **102**, 4889. Q: quadrifunctional silicon; T: trifunctional silicon; D: difunctional silicon.
18. E. Lindner, T. Schneller, H. A. Mayer, H. Bertagnolli, T. S. Ertel, W. Hörner, *Chem. Mater.* 1997, **9**, 1524.
19. E. Lindner, T. Schneller, F. Auer, P. Wegner, H. A. Mayer, *Chem. Eur. J.* 1997, **3**, 1833.
20. T. Schneller, Ph. D. Thesis, Univ. Tübingen 1997.
21. E. Lindner, A. Baumann, P. Wegner, H. A. Mayer, U. Reinöhl, A. Weber, T. S. Ertel, H. Bertagnolli, *J. Mater. Chem.* 2000, **10**, 1655.

22. E. Lindner, W. Wielandt, A. Baumann, H. A. Mayer, U. Reinöhl, A. Weber, T. S. Ertel, H. Bertagnolli *Chem. Mater.* 1999, **11**, 1833.
23. M. T. Murtagh, M. R. Shariari, M. Krihak, *Chem. Mater.*, 1998, **10**, 3862.
24. M. A. Chan, J. L. Lawless, S. K. Lam, D. Lo, *Anal. Chim. Acta*, 2000, **408**, 33.
25. J. H. Clark, D. J. Mcquarrie, *Chem. Soc. Rev.*, 1996, **96**, 303.
26. B. Dunn, J. I. Zink, *Chem. Mater.*, 1997, **9**, 2281.
27. M. A. Meneses-Nava, O. Barbosa-Garcia, L. A. Diaz-Torres, S. Chavez-Cerda, T. A. King, *Opt. Mat.*, 1999, **13**, 327
28. K. Maruszewski, M. Jasiorski, M. Salamon, W. Strek, *Chem. Phys. Lett.*, 1999, **314**, 83.
29. P. Innocenzi, H. Kozuka, T. Yoko, *J. Phys. Chem. B*, 1997, **101**, 2285.
30. G. Hungerford, K. Suhling, J.A. Ferreira, *J. Photochem. Photobiol. A*, 1999, **129**, 71.
31. I. M. Ilharco, J. M. G. Martinho, *Langmuir*, 1999, **15**, 7490.
32. K. K. Flora, M. A. Dabrowski, S. P. Musson, J. D. Brennan, *Canad. J. Chem. Rev. Canad. Chim.*, 1999, **77**, 1617.

33. C. D. Geddes, Chevers, D. J. S. Birch, *J. Fluorescence* 1999, **9**, 73.
34. A. C. Franville, D. Zambon, R. Mahiou, Y. Troin, *Chem. Mater.*, 2000, **12**, 428.
35. Y. W. Hou, A. M. Bardo, C. Martinez, D. A. Higgins, *J. Phys. Chem. B*, 2000, **104**, 212.
36. M. H. Huang, H. M. Soyeyz, B. S. Dunn, J. I. Zink, *Chem. Mater.*, 2000, **12**, 231.
37. S. M. Arabei, T. A. Pavich, J. P. Galaup, P. Jardon, *Chem. Phys. Lett.*, 1999, **306**, 303.
38. D. S. Gottfried, A. Kagan, B. M. Hoffman, J. M. Friedman, *J. Phys. Chem. B*, 1999, **103**, 2803.
39. J. L. H. Jiwan, E. Robert, J. P. Soumillion, *J. Photochem. Photobiol. A*, 1999, **122**, 61.
40. U. Narang, R. A. Dunbar, F. V. Bright, P. N. Prasad, *Appl. Spectrosc.* 1993, **47**, 1700.
41. R. C. Chambers, Y. Haruvy, M. A. Fox, *Chem. Mater.*, 1994, **6**, 1351.
42. P. B. Leezenberg, M. D. Fayer, C. W. Frank, *Pure Appl. Chem.*, 1996, **68**, 1381.

43. T. Suratwala, Z. Gardlund, K. Davidson, D. R. Uhlmann, *Chem. Mater.*, 1998, **10**, 190.
44. J.-L. Habib Jiwan, E. Robert, J.-Ph. Soumillion, *J. Photochem. Photobiol. A*, 1996, **122**, 61.
45. N. Leventis, I. A. Elder, *Chem. Mater.*, 1999, **11**, 2837.
46. Ch. Malins, S. Fanni, H. G. Glever, J. G. Vos, B. D. MacCraith, *Anal. Commun.*, 1999, **36**, 3.
47. A. H. O. Karkkainen, O. E. O. Hormi, J. T. Rantala, *Proc. SPIE-Int. Soc. Opt. Eng.*, 2000, **3943**, 194.
48. J. C. Biazzotto, H. C. Sacco, K. J. Ciuffi, C. R. Neri, A. G. Ferreira, Y. Iamamoto, O. A. Serra, *J. Non-Cryst. Solids*, 1999, **247**, 134.
49. A. Lobnik, I. Oehme, I. Murkovic, O. S. Wolfbeis, *Anal. Chim. Acta*, 1998, **367**, 159.
50. T. Ishikawa, H. Inoue, A. Makishima, *J. Non-Cryst. Solids*, 1996, **203**, 43.
51. R. J. P. Corriu, P. Hesemann, G. F. Lanneau, *Chem. Commun.*, 1996, 1845.
52. M. Plaschke, R. Czolk, J. Reichert, H. J. Ache, *Thin Solid Films* 1996, **279**, 233.

53. W. Wielandt, A. Ellwanger, K. Albert, E. Lindner, *J. Chromatogr. A*, 1998, **805**, 71.
54. I. B. Berlman, *J. Chem. Phys.*, 1970, **52**, 5616.
55. B. Lehr, H.-J. Egelhaaf, H. Fritz, W. Rapp, E. Bayer, D. Oelkrug, *Macromolecules*, 1996, **29**, 7931.
56. B. Lehr, H.-J. Egelhaaf, W. Rapp, E. Bayer, D. Oelkrug, *J. Fluorescence*, 1998, **8**, 171.
57. J. Michl, E. W. Thulstrup, *Spectroscopy with Polarised Light*; Wiley-VCH, Weinheim, Germany, 1995.
58. G. G. Aloisi, F. Masetti, U. Mazzucato, *Chem. Phys. Lett.*, 1974, **29**, 502.
59. G. G. Belford, R. L. Belford, G. Weber, *Proc. Nat. Acad. Sci. USA*, 1972, **69**, 1392.
60. R. K. Harris, R. H. Newman, *Mol. Phys.*, 1979, **38**, 1315.
61. D. R. Bauer, J. I. Brauman, R. J. Pecora, *J. Am. Chem. Soc.*, 1974, **96**, 6840.
62. D. R. Lide, Ed.; *CRC Handbook of Chemistry and Physics* 1999-2000, **80th ed.**, CRC Press LLC: 1999.
63. A. Szabo, *J. Chem. Phys.*, 1984, **81**, 150.
64. P. Wahl, *Chem. Phys.*, 1975, **7**, 210.

65. W. A. Wegener, R. M. Dowben, V. J. Koester, *J. Chem. Phys.*, 1980, **73**, 4086.
66. G. Cerveau, R. J. P. Corriu, *Coord. Chem. Rev.*, 1998, **180**, 1051.
67. A. Katz, M. E. Davis, *Nature*, 2000, **403**, 286.
68. T. J. Ward, *Anal. Chem.* 2000, **72**, 4521.
69. N. M. Maier, P. Franco, W. Lindner, *J. Chromatogr. A* 2001, **906**, 3.
70. V. Schurig, *J. Chromatogr. A* 2001, **906**, 275.
71. R. K. Gilpin, L. A. Pachla, *Anal. Chem.* 2001, **73**, 2805.
72. D. Wistuba, V. Schurig, *Electrophoresis* 2000, **21**, 4136.
73. G. Blaschke, B. Chankvetadze, *J. Chromatogr. A* 2000, **875**, 3.
74. K. Otsuka, S. Terabe, *J. Chromatogr. A* 2000, **875**, 163.
75. S. Fanali, *J. Chromatogr. A* 2000, **875**, 89.
76. H. Nishi, *Electrophoresis* 1999, **20**, 3237.
77. F. Gasparrini, I. D'Acquarica, J. G. Vos, C. M. O'Connor, C. Villani, M. *Tetrahedron: Asymmetry*, 2000, **11**, 3535.
78. J. E. Harris, N. Desai, K. E. Seaver, R. T. Watson, N. A. P. Kane-Maguire, *J. Chromatogr. A*, 2001, **919**, 427.

79. V. Balzani, A. Juris, M. Venturi, S. Campagna, S. Serroni, *Chem. Rev.* 1996, **96**, 759.
80. P. Belser, S. Bernhard, E. Jandracis, A. von Zelewsky, L. De Cola, V. Balzani, *Coord. Chem. Rev.* 1997, **159**, 1.
81. K. Shreder, A. Harriman, B. L. Inverson, *J. Am. Chem. Soc.* 1996, **118**, 3192.
82. H. Szmecinski, E. Terpetschnig, J. R. Lakowicz, *Biophys. Chem.* 1996, **62**, 109.
83. P. Lincoln, B. J. Nordén, *J. Phys. Chem. B* 1998, **102**, 9583.
84. J. E. Coury, J. R. Anderson, L. McFail-Isom, L. D. Williams, L. A. Bottomley, *J. Am. Chem. Soc.* 1997, **119**, 3792.
85. P. Lincoln, A. Broo, B. Nordén, *J. Am. Chem. Soc.* 1996, **118**, 2644.
86. R. M. Hartshorn, J. K. Barton, *J. Am. Chem. Soc.* 1992, **114**, 5919.
87. S. Satyanarayana, J. C. Dabrowiak, J. B. Chaires, *Biochemistry* 1993, **32**, 2573.
88. C. Hiort, B. Nordén, A. Rodger, *J. Am. Chem. Soc.* 1990, **112**, 1971.
89. K. J. Barton, *Pure Appl. Chem.* 1989, **61**, 563.

90. J. K. Barton, J. M. Goldberg, C. V. Kumar, N. J. Turro, *J. Am. Chem. Soc.* 1986, **108**, 2081.
91. J. K. Barton, A. T. Danishefsky, J. M. Goldberg, *J. Am. Chem. Soc.* 1984, **106**, 2172.
92. A. Yamagishi, *Chem. Commun.* 1983, 572.
93. Ji, Z.; Huang, S. D.; Guadalupe, A. R. *Inorg. Chim. Acta* 2000, **305**, 127.
94. M. T. Murtagh, M. R. Shariari, M. Krihak, *Chem. Mater.*, 1998, **10**, 3862.
95. M. A. Chan, J. L. Lawless, S. K. Lam, D. Lo, *Anal. Chim. Acta*, 2000, **408**, 33.
96. H.-J. Egelhaaf, E. Holder, P. Herman, H. A. Mayer, D. Oelkrug, E. Lindner, *J. Mater. Chem.*, 2001, **11**, 2445.
97. F. Barigelletti, L. Flamigni, *Chem. Soc. Rev.*, 2000, **29**, 1.
98. A. Harriman, R. Ziessel, *Chem. Commun.*, 1996, 1707.
99. V. Balzani, A. Juris, M. Venturi, S. Campagna, S. Serroni, *Chem Rev.*, 1996, **96**, 759.
100. For a series of papers on luminescent chemical sensors based on transition metal complexes, see: *Coord. Chem. Rev.* 2000, **Vol. 205**.

101. D. M. Roundhill, *Photochemistry and Photophysics of Metal Complexes*; Plenum Press: New York, 1994.
102. A. T. Yeh, C. V. Shank, J. K. Mc Cusker, *Science*, 2000, **289**, 935.
103. N. Y. Turro, *Modern Molecular Photochemistry*; Benjamin: Menlo Park, 1978.
104. A. Gilbert, J. Baggot, *Essentials of Molecular Photochemistry*; Blackwell: Oxford, 1991.
105. A. Juris, V. Balzani, F. Barigelletti, S. Campana, P. Belser, A. von Zelewsky, *Coord. Chem. Rev.*, 1988, **84**, 85.
106. K. Kalyanasundaram, *Photochemistry of Polypyridine and Porphyrin Complexes*; Academic Press: London, 1992.
107. D. L. Dexter, *J. Chem. Phys.*, 1953, **21**, 836.
108. H. Laguitton-Pasquier, A. Martre, A. Deronzier, *J. Phys. Chem. B*, 2001, **105**, 4801.
109. H.-B. Kim, N. Kitamura, S. Tazuke, *J Phys. Chem.* 1990, **94**, 7401.
110. H.-J. Egelhaaf, B. Lehr, M. Hof, A. Häfner, M. Fritz, F. W. Schneider, E. Bayer, D. Oelkrug, *J. Fluorescence*, 2000, **10**, 383.

111. D. Garcia–Fresnadillo, M. D. Marazuela, M. C. Moreno–Bondi, G. Orellana, *Langmuir*, 1999, **15**, 6451.
112. C. J. Timpson, C. C. Carter, J. Ohmsted III, *J. Phys. Chem.*, 1989, **93**, 4116.
113. C. T. Kresge, M. E. Leonowicz, W. J. Roth, J. C. Vartuli, and J. S. Beck, *Nature* 1992, **359**, 710.
114. J. S. Beck, J. C. Vartuli, W. J. Roth, M. E. Leonowicz, C. Z. Kresge, K. D. Schmitt, C. T.-W. Chu, D. H. Olson, E. W. Sheppard, S. B. Higgins, and J. L. Schlenker, *J. Am. Chem. Soc.* 1992, **114**, 10834.
115. P. T. Tanev, T. J. Pinnavaia, *Science* 1995, **269**, 865.
116. M. Capka, *Synth. Inorg. Met. Org. Chem.* 1977, **7**, 347.
117. M. D. Greaves, T. H. Galow, and V. M. Rotello, *Chem. Commun.* 1999, 169.
118. C. Sanchez, F. Ribot, *New J. Chem.* 1994, **18**, 1007.
119. U. Schubert, N. Hüsing, A. Lorenz, *Chem. Mater.* 1995, **7**, 2010.
120. D. A. Loy, G. M. Jamison, B.M. Baugher, S. A. Mayers, R. A. Assink, K. J. Shea, *Chem. Mater.* 1996, **8**, 656.

121. S. L. Burkett, S. D. Sims, S. Mann, *Chem. Commun.* 1996, 1367.
122. S. D. Sims, S. L. Burkett, S. Mann, *Mater. Res. Soc. Symp. Proc.* 1996, **431**, 77.
123. D. J. Macquarrie, *Chem. Commun.* 1996, 1961.
124. Q. Huo, D. I. Margolese, G. D. Stucky, *Chem. Mater.* 1996, **8**, 1147.
125. Certificate of Analysis, "SRM 869a Column Selectivity Test Mixture for Liquid Chromatography", Standard Reference Materials Program, National Institute of Standards and Technology, Gaithersburg, MD 20899.
126. L. C. Sander, M. Pursch, S. A. Wise, *Anal. Chem.* 1999, **71**, 4821.
127. J. Wegmann, K. Albert, M. Pursch, L.C. Sander, *Anal. Chem.* 2001, **73**, 1814.
128. J.-B. Pang, K.-Y. Qui, Y. Wie, X-J. Lei, Z.-F. Liu, *Chem. Commun.* 2000, 477.
129. G. Schoetz, O. Trapp, V. Schurig, *Anal. Chem.* 2000, **72**, 2758.
130. D. A. Loy, K. J. Shea, *Chem. Rev.*, 1995, **95**, 1431.

131. R. Veigel, diploma thesis, University Tübingen, 1996.
132. B. P. Sullivan, D. J. Salmon, T. J. Meyer, *Inorg. Chem.* 1978, **17**, 3334.
133. D. P. Rillema, K. B. Mack, *Inorg. Chem.* 1982, **21**, 3849.
134. E. Holder, G. Schoetz, V. Schurig, E. Lindner, *Tetrahedron: Asymmetrie*, 2001, **12**, 2298.

5. Summary

The anchoring of reactive centers, in particular active transition metal complexes to an inert support is a field of increasing interest in terms of academic as well as commercial research. Such materials are able to combine the advantages of homogeneous and heterogeneous catalysis: the catalyst becomes easily separable from the reaction products and can be reused in several runs, but sometimes with an essential loss of activity because of leaching. In addition very often the reactive centers are not well defined and the activities and selectivities decrease. So far these drawbacks prevented a commercial application of heterogenized catalysts.

A versatile approach to reduce or even eliminate the mentioned problems is the introduction of the concept of an interphase. In the presence of a stationary phase (e.g. an anchored organic compound or a transition metal complex) and a mobile phase (solvent, gaseous, liquid, or dissolved organic compound) both phases penetrate on a molecular level. This state is designated as "interphase" since no homogeneous phase is formed.

However, interphases are able to imitate homogeneous conditions providing favorable activities in different types of catalytic reactions without any essential metal leaching. A typical approach for the generation of stationary phases in interphase chemistry is the sol-gel process, which offers a convenient route for the preparation of suitable polysiloxane networks under mild reaction conditions. The co-condensation of T-silyl functionalized metal complexes or ligands with various alkoxysilanes or organosilanes provides materials, in which the reactive centers are nearly homogeneously distributed across a chemical and thermal inert carrier matrix. It was established that the catalytic activity of such systems markedly depends on the mobility of the entire polymer.

The objective of the present work is the synthesis and systematic investigation of stationary phases used in "Chemistry in Interphases". Thereby structural and dynamic parameters were discussed and the rotational mobility as well as the accessibility of reactive centers was probed by a model for catalytic reactions. Also some ordered sol-gel polymers were synthesized and their application for HPLC was improved.

At the beginning of this thesis the rotational mobility of a fluorene label covalently attached on several sol-gel polymers was investigated. First a T-silyl functionalized fluorene label was synthesized and sol-gel processed with the co-condensation agents Me-T, T-C₆-T, and D-C₆-D. Subsequently the non-ordered sol-gel polymers were characterized by ¹³C and ²⁹Si CP/MAS NMR spectroscopy, elemental analyses, and BET measurements. The behavior of the fluorene label was characterized by UV/VIS spectroscopy e.g. fluorescence and fluorescence excitation spectra. To determine the mean fluorescence decay time τ_F steady state fluorescence anisotropies r_{SS} and the mean rotational correlation time τ_R of the sol-gel materials were probed by swelling the materials in cyclohexane, diethyl ether, tetrahydrofuran, dichloromethane, methanol, and water. The sol-gel polymers were also suspended in these solvents to study time resolved fluorescence anisotropy and the accessibility of the reactive centers. The translational mobility of TEA was observed by determining the fluorescence decay curves of an exciplex between the immobilized fluorene and TEA. Both the rotational mobility of fluorene and the translational mobility of TEA are reduced by one

or two orders of magnitude compared to homogeneous solutions, due to diffusion problems. The largest diffusion coefficients are observed in solvents of medium polarity, like dichloromethane, diethyl ether or tetrahydrofuran, because of the good solubility of the fluorescence label in these solvents.

In another part of this thesis a luminescent polypyridylruthenium(II) complex was synthesized as a precursor to obtain a sol-gel processable luminescent material. It was possible to successfully separate this complex into its enantiomers by the use of electrokinetic chromatography if a carboxymethyl- β -cyclodextrin dissolved in a borate buffer was used as chiral mobile phase additive. Enantiomer separation is not well developed in the field of transition metal complexes but is important to control the stereoselectivities of complexation reactions. By the use of EKC a fast analytical method was achieved to improve these stereoselectivity.

In a third chapter the generation of a further luminescent T-silyl functionalized polypyridylruthenium(II) complex and its copolycondensation with Me-T, Ph-T, T-C₆-T, Q, and D-C₆-D was described. The resulting non-ordered materials were characterized

by ^{13}C and ^{29}Si CP/MAS NMR spectroscopy, elemental analyses, BET measurements, and SE micrographs. To get information about the mobility of the transition metal complex, the polymers were swollen in acetonitrile, methanol, acetone, tetrahydrofuran, and dichloromethane. With these interphase systems luminescence and luminescence excitation spectra in the absence and in the presence of dioxygen and anthracene as quencher molecules were recorded. Quenching reactions occur only in the case of close contact between the excited ruthenium complex and the quencher molecule. Investigations of this type serve as a model for the accessibility of sol-gel processed complexes used as catalysts in interphases. Translational mobilities of dioxygen and anthracene in the mentioned polymers were probed by measuring the luminescence decay curves without quencher molecules and in the presence of dioxygen and anthracene. Therefore the rate constants of diffusion and the accessibility factors of the quencher molecules were analyzed. The ruthenium complex in the organically modified polysiloxanes is preferentially solvated by the liquid phase. In the phenyl modified polymer, the degree of solvation strongly depends on the polarity of the employed solvent. Two types of immobilized

ruthenium complexes were found. One type is not accessible for quencher molecules. For other ruthenium complexes the rate constants approach values observed for respective complexes in solution. Due to the larger size of the molecules the accessibility for anthracene is slightly below the accessibility for oxygen. In both cases Q type materials are almost not accessible, but a solution-like accessibility was found in particular hybrid polymers in solvents of low and medium polarity. In polar solvents other polymers provide good accessibilities for both oxygen and anthracene.

If the above mentioned sol-gel process is carried out in the presence of a template molecule like *n*-hexadecylamine ordered structures are obtained. These materials were characterized by several methods: ^{13}C and ^{29}Si CP/MAS NMR spectroscopy, elemental analyses, BET, small angle XRD measurements, and SE micrographs. A further characterization of the materials was carried out by HPLC runs.

In the last chapter of this thesis modified sol-gel layers for some sensing applications in the liquid phase are described. The sol-gel polymer layers were synthesized on gold- and silicon

surfaces. These layers were characterized by light microscope, SEM as well as by static contact angle measurements, and by QCM's. The use of AFM allows the determination of the thickness of the layer. QCM measurements enable the classification of the sol-gel polymers to their solvent affinity. This insight is also important for catalysis in interphases.

Meine Akademische Ausbildung verdanke ich:

K. Albert, E. Bayer, H. Bertagnolli, M. Brendle, D. Christen, H. Eckstein, H.-J. Egelhaaf, G. Gauglitz, W. Göpel, G. Häfelinger, H.-P. Hagenmaier, M. Hanack, D. Hoffmann, V. Hoffmann, G. Jung, S. Kemmler-Sack, W. Koch, D. Krug, E. Lindner, E. Maier, H. A. Mayer, H.-J. Meyer, K. Müller, U. Nagel, W. Nakel, H. Oberhammer, D. Oelkrug, H. Pauschmann, G. Pausewang, E. Plies, H. Pommer, V. Schurig, E. Schweda, F. F. Seelig, Ha. Stegmann, B. Speiser, J. Strähle, W. Voelter, U. Weimar, H.-D. Wiemhöfer, K.-P. Zeller, C. Ziegler.

CURRICULUM VITAE

Personal Data

Elisabeth Holder
born on 30.07.1970 in Lonsingen

Graduate study

Since May 1999

Doctoral thesis "Polysiloxanes with Luminescent Molecular Probes: Synthesis, Characterization and Application of Ordered and Non-Ordered Structures" under the supervision of Prof. Dr. E. Lindner at the Institute of Inorganic Chemistry II of the Eberhard-Karls-University in Tübingen

Industrial Placement

2000

Industrial experience for three months in the field of combinatorial drug research at Bayer AG Pharma Research in Wuppertal-Elberfeld

Interdisciplinary Engagement

Since Oct. 1998

Member of the Graduiertenkolleg "Chemistry in Interphases". Close collaboration with other working groups in the field of "Chemistry in Interphases"

Scientific Employee

Since Oct.1998	Assistant in a tutorial program
Since May 1999	Assistant in the inorganic-quantitative practical course: electrochemical and optical methods

Graduate study / Undergraduate study

Oct. 1998 – April 1999	Diploma thesis "Fluoreszenz- spektroskopische Beweglichkeits-Studien eines T-Silyl-funktionalisierten Fluoren-Derivats in der Interphase" under the supervision of Prof. Dr. E. Lindner
Degree	Diploma in chemistry
Oct. 1998	Diplomhauptprüfung (graduate study)
1994	Diplomvorprüfung (undergraduate study)
Oct. 1992	Commencement of chemistry study at the Eberhard-Karls-Universität of Tübingen

Occupational Activity

1991 – 1992	One year temporary post to support study in various service functions
1988 – 1997	Temporary employment to support education

School Education

1988 – 1991	Secondary school in Reutlingen (A-level)
1987 – 1988	Social year
1981 – 1987	Geschwister-Scholl-secondary school in Bad Urach (level)